

NAVAL POSTGRADUATE SCHOOL
Monterey, California



19980603 028

THESIS

**INVESTIGATION OF BIOMECHANICAL
RESPONSE DUE TO FRAGMENT IMPACT
ON BALLISTIC PROTECTIVE HELMET**

by

Quinten M. King

March 1998

Thesis Advisor:

Young W. Kwon

Approved for public release; distribution is unlimited.

DTIC QUALITY INSPECTED 1

REPORT DOCUMENTATION PAGEForm Approved
OMB No. 0704-0188

Public reporting burden for this collection of information is estimated to average 1 hour per response, including the time for reviewing instructions, searching existing data sources, gathering and maintaining the data needed, and completing and reviewing the collection of information. Send comments regarding this burden estimate or any other aspect of this collection of information, including suggestions for reducing this burden to Washington headquarters Services, Directorate for Information Operations and Reports, 1215 Jefferson Davis Highway, Suite 1204, Arlington VA, 22202-4302, and to the Office of Management and Budget, Paperwork Reduction Project (0704-0188), Washington DC, 20503.

1. AGENCY USE ONLY		2. REPORT DATE March 1998	3. REPORT TYPE AND DATES COVERED Master's Thesis	
4. TITLE AND SUBTITLE Investigation of Biomechanical Response Due to Fragment Impact on Ballistic Protective Helmet			5. FUNDING NUMBERS	
6. AUTHOR(S) King, Quinten M.				
7. PERFORMING ORGANIZATION NAME AND ADDRESS Naval Postgraduate School Monterey, CA, 93943			8. PERFORMING ORGANIZATION REPORT NUMBER	
9. SPONSORING/MONITORING AGENCY NAME AND ADDRESS			10. SPONSORING/MONITORING AGENCY REPORT NUMBER	
11. SUPPLEMENTARY NOTES The views expressed in this report are those of the authors and do not reflect the official policy or position of the Department of Defense or the U.S. Government				
12a. DISTRIBUTION/AVAILABILITY STATEMENT Approved for public release; distribution is unlimited			12b. DISTRIBUTION CODE	
12. ABSTRACT <i>(Maximum of 200 words)</i> Technology has increased dramatically over the last 25 years. It has allowed the development of personnel body armor capable of preventing penetration of fragments traveling in excess of 2000 ft/s (609 m/s). However, these strides have also exposed the body to greater impact energies without a lethal penetration. The objective of this research was to examine how the body in particular the Head-Neck Complex responds to these impacts. A finite element model was developed to characterize the behavior of this biomechanical system. This model was then validated against existing experimental work from the automotive industry. The validated model was then subjected to impacts at different positions to induce different load cases. Each set of results were then compared to the Head Injury Criteria (HIC), Abbreviated Injury Scale (AIS), and the Injury Assessment Reference Values (IARVS) for evidence of injury potential. Disc stiffness was found to be proportional to the injury potential. Rupture of the disc was considered likely for 5 of the 6 cases examined. Fracture of the vertebral body was considered likely in 3 of the 6 cases. Suggestions for future research are included in the hopes to furthering research into this area.				
14. SUBJECT TERMS Finite Element Method, Biomechanics, Body Armor, Material Properties			15. NUMBER OF PAGES 132	
			16. PRICE CODE	
17. SECURITY CLASSIFICATION OF REPORT Unclassified	18. SECURITY CLASSIFICATION OF THIS PAGE Unclassified	19. SECURITY CLASSIFICATION OF ABSTRACT Unclassified	20. LIMITATION OF ABSTRACT UL	

NSN 7540-01-280-5500

Standard Form 298 (Rev2-89)
Prescribed by ANSI Std Z39-18

Approved for public release; distribution is unlimited

**INVESTIGATION OF BIOMECHANICAL RESPONSE
DUE TO FRAGMENT IMPACT ON BALLISTIC
PROTECTIVE HELMET**

Quinten M. King
Lieutenant, United States Navy
B.S., Renssaeler Polytechnic Institute, 1990

Submitted in partial fulfillment of the
requirements for the degree of

MASTER OF SCIENCE IN MECHANICAL ENGINEERING

from the

**NAVAL POSTGRADUATE SCHOOL
March 1998**

Author: Quinten M King
Quinten M. King

Approved by: Young W. Kwon
Young W. Kwon, Thesis Advisor

Terry R. McNelley
Terry R. McNelley, Chairman
Department of Mechanical Engineering

ABSTRACT

Technology has increased dramatically over the last 25 years. It has allowed the development of personnel body armor capable of preventing penetration of fragments traveling in excess of 2000 ft/s (609 m/s). However these strides have also exposed the body to greater impact energies without a lethal penetration. The objective of this research was to examine how the body in particular the Head-Neck Complex responds to these impacts. A finite element model was developed to characterize the behavior of this biomechanical system. This model was then validated against existing experimental work from the automotive industry. The validated model was then subjected to impacts at different positions to induce different load cases. Each set of results were then compared to Head Injury Criteria (HIC), Abbreviated Injury Scale (AIS), and the Injury Assessment Reference Values (IARVS) for evidence of injury potential. Disc stiffness was found to be proportional to the injury potential. Rupture of the disc was considered likely for 5 of the 6 cases examined. Fracture of the vertebral body was considered likely in 3 of the 6 cases. Suggestions for future research are included in the hopes to furthering research into this area.

TABLE OF CONTENTS

I.	INTRODUCTION	1
II.	BACKGROUND	5
	A. ANATOMY OF THE SPINE	5
	B. EARLY EFFORTS TO MODEL THE SPINE	8
	C. PRASAD AND KING'S MODEL	9
	D. BELYTSCHKO'S THREE DIMENSIONAL MODELS OF THE HUMAN SPINE	10
	E. SURVEY OF ADDITIONAL WORK IN THE FIELD	12
III.	FINITE ELEMENT MODEL	15
	A. FRAGMENT	15
	B. PROTECTIVE HELMET	17
	C. BODY	19
	1. Head	19
	2. Spine	20
IV.	INJURY ASSESSMENT	23
	A. MATERIAL PROPERTY VARIATION	23
	B. HEAD INJURY CRITERIA (HIC)	25
	C. INJURY ASSESSMENT REFERENCE VALUES (IARVS)	27
	D. OTHER PUBLISHED CRITICAL INJURY VALUES	29

V.	RESULTS	31
A.	MODEL VERIFICATION	31
B.	FRONT IMPACT	35
1.	Case 1	35
2.	Case 2	36
3.	Case 3	37
C.	BACK IMPACT	64
D.	TOP IMPACT	75
E.	SIDE IMPACT	87
VI.	CONCLUSIONS	101
	APPENDIX	107
	LIST OF REFERENCES	109
	INITIAL DISTRIBUTION LIST	113

LIST OF FIGURES

Figure 2.1. Occipital-Atlantal Joint connecting the skull to the spine.....	5
Figure 2.2. Spinal motion segment showing vertebra, disc, facet joint, and structurally significant ligaments.....	6
Figure 2.3. Belytschko's hydrodynamic element.....	11
Figure 3.1. Entire finite element model.....	16
Figure 3.2. Model of helmet created from geometrical data..	18
Figure 3.3. Anatomical view of cervical spine.....	21
Figure 3.4 Model of cervical spine.....	22
Figure 4.1. Risk of brain injury as a function of HIC based on a 15 ms acceleration period.....	26
Figure 4.2. IARV for axial tensile forces acting on the neck.....	28
Figure 4.3. IARV for axial compressive forces acting on the neck.....	28
Figure 4.4. IARV for shearing forces at the junction of the head and neck.....	29
Figure 5.1. View of spinal model attached to rigid wall for validation case.....	32
Figure 5.2. Comparison of relative displacements between experiment (Ewing, 1978) and model.....	33

Figure 5.3. Comparison of the acceleration of the head between experiment (Ewing, 1978) and model.....	34
Figure 5.4. Relative position of fragment to helmet before impact.....	39
Figure 5.5. Effective stress induced in helmet 1 ms after impact.....	39
Figure 5.6. Effective stress induced in helmet 10 ms after impact.....	40
Figure 5.7. Effective stress induced in helmet 30 ms after impact.....	40
Figure 5.8. Effective stress induced in helmet 200 ms after impact.....	41
Figure 5.9. Acceleration profile used to calculate HIC for Case 1.....	42
Figure 5.10. Axial force on the Occipital Condyle for Case 1.....	43
Figure 5.11. Shear force on the Occipital Condyle for Case 1.....	44
Figure 5.12. Bending moment on C4 vertebra for Case 1.....	45
Figure 5.13. Bending moment on C7 vertebra for Case 1.....	46
Figure 5.14. Bending moment on C3-C4 disk for Case 1.....	47
Figure 5.15. Shear force acting on facet joints of cervical spine for Case 1.....	48

Figure 5.16.	Torsional moment acting on facet joints of cervical spine for Case 1.....	49
Figure 5.17.	Acceleration profile used to calculate HIC for Case 2.....	50
Figure 5.18.	Axial force on the Occipital Condyle for Case 2.....	51
Figure 5.19.	Shear force on the Occipital Condyle for Case 2.....	52
Figure 5.20.	Bending moment on C5 vertebra for Case 2....	53
Figure 5.21.	Bending moment on C3-C4 disk for Case 2....	54
Figure 5.22.	Shear force acting on facet joints of cervical spine for Case 2.....	55
Figure 5.23.	Torsional moment acting on facet joints of cervical spine for Case 2.....	56
Figure 5.24.	Acceleration profile used to calculate HIC for Case 3.....	57
Figure 5.25.	Axial force on the Occipital Condyle for Case 3.....	58
Figure 5.26.	Shear force on the Occipital Condyle for Case 3.....	59
Figure 5.27.	Bending moment on C6 vertebra for Case 3....	60
Figure 5.28.	Bending moment on C3-C4 disk for Case 3....	61

Figure 5.29. Shear force acting on facet joints of cervical spine for Case 3.....	62
Figure 5.30. Torsional moment acting on facet joints of cervical spine for Case 3.....	63
Figure 5.31. View of helmet and fragment prior to rear impact.....	65
Figure 5.32. Von Mises stress induced in helmet after 1 ms.....	66
Figure 5.33. Von Mises stress induced in helmet after 10 ms.....	66
Figure 5.34. Von Mises stress induced in helmet 30 ms after rear impact.....	67
Figure 5.35. Von Mises stress induced in helmet after 200 ms.....	67
Figure 5.36. Acceleration profile used to calculate HIC for rear impact case.....	68
Figure 5.37. Axial force on the Occipital Condyle for rear impact case	69
Figure 5.38. Shear force on the Occipital Condyle for rear impact case.....	70
Figure 5.39. Bending moment on C3 vertebra for rear impact case.....	71

Figure 5.40. Bending moment on C4-C5 disk for rear impact case.....72

Figure 5.41. Shear force acting on facet joints of cervical spine during rear impact case.....73

Figure 5.42. Torsional moment acting on facet joints of cervical spine during rear impact case.....74

Figure 5.43. View of helmet prior to top impact.....75

Figure 5.44. Von Mises stress induced in helmet 1 ms after impact.....77

Figure 5.45. Von Mises stress induced in helmet 10 ms after impact.....77

Figure 5.46. Von Mises stress induced in helmet 30 ms after impact.....78

Figure 5.47. Von Mises stress induced in helmet 200 ms after impact.....78

Figure 5.48. Acceleration profile used to calculate HIC for top impact case.....79

Figure 5.49. Axial force on the Occipital Condyle for top impact case.....80

Figure 5.50. Shear force on the Occipital Condyle for top impact case.....81

Figure 5.51. Axial force on C1 vertebra for top impact case.....82

Figure 5.52. Bending moment on C5 vertebra for top impact case.....	83
Figure 5.53. Bending moment on C4-C5 disk for top impact case.....	84
Figure 5.54. Shear force acting on facet joints of cervical spine for top impact case.....	85
Figure 5.55. Torsional moment acting on facet joints of cervical spine for top impact case.....	86
Figure 5.56. View of helmet before side impact.....	88
Figure 5.57. Von Mises stress induced in helmet 1 ms after side impact.....	89
Figure 5.58 Von Mises stress induced in helmet 10 ms after side impact.....	89
Figure 5.59. Von Mises stress induced in helmet 30 ms after side impact.....	90
Figure 5.60 Von Mises stress induce in helmet 200 ms after side impact.....	90
Figure 5.61. Acceleration profile used to calculate HIC for side impact case.....	91
Figure 5.62. Axial force on occipital condyle during side impact.....	92
Figure 5.63. Shear force on occipital condyle during side impact.....	93

Figure 5.64. Lateral bending moment of C4 during side impact.....	94
Figure 5.65. Bending moment of C7 vertebra during side impact.....	95
Figure 5.66. Lateral bending moment on C4-C5 disc during side impact.....	96
Figure 5.67. Bending moment on C4-C5 disc during side impact.....	97
Figure 5.68. Shear force action on facet joints of cervical spine during side impact.....	98
Figure 5.69. Torsion moment action on facet joints of cervical spine during side impact.....	99
Figure 6.1. Comparison of HIC values for each test case...	103
Figure 6.2. Comparison of results with critical values..	103
Figure 6.3. Comparison of vertebral compression for top impact case.....	104
Figure 6.4. Comparison of vertebral lateral bending for side impact case.....	104
Figure A.1. Stress-strain curve for PASTG helmet.....	107
Figure A.2. View of linear region of stress-strain curve for PASTG helmet.....	108

ACKNOWLEDGMENT

The author would like to thank his family, Sandra and Jonathan King, for their patience, understanding, support, and assistance with this investigation. The author would also like to thank Professor Kwon for his guidance and assistance in performing this investigation.

I. INTRODUCTION

The advent of increasing technology has exposed the human body to loading situations beyond its natural capacity to withstand. This has spurred a vast amount of research over the last 50 years into the mechanics of the human body and its ability to dissipate these loads. Physicians have teamed with engineers from all fields to design systems to aid the body to withstand these ever increasing forces.

Helmets have been used for centuries to protect from serious injury, among the systems developed were ballistic helmets. The ballistic helmets used during the Vietnam War were not much different in design and function than the helmets worn by knights 1000 years earlier. The "steel pots", as they were affectionately known, provided only the most rudimentary protection against fragment penetration.

Materials science and composite engineering during the 1970's led to the first technological approach to helmet design. Dupont developed the Personnel Armor System for Ground Troop (PASGT) Helmet that replaced the "steel pot" during the late 1970's in the United States Army. This helmet not only reduced the weight of the helmet, but also increased the ballistic limit, V_{50} , to 2000 ft/s (Dupont, 1997). This translates to protection from penetration of a one gram fragment traveling up to 609 m/s at least 50% of the time.

This breakthrough in protection resulted from the use of aramid fibers (Kevlar-29) in a layered composite of 19 effective plies. A reduced weight PASTG Helmet is scheduled to replace this helmet over the next several years (Dupont, 1997). This helmet will make use of a new fiber (Kevlar-KM2) to reduce the weight of the helmet by 15% while increasing the protection to $V_{50} = 2150$ ft/s (655 m/s). The new helmet will have 34 effective plies.

Increases in the ballistic limits have increased the impact energy incident on the helmet before penetration. These higher energy levels are transmitted to the body via the helmet's harness. The head-neck complex will be subjected to complex loading conditions as the energy is dissipated by the soft tissues and joints of the body.

Even without penetrating the impact energy delivered by these fragments can cause serious, even life threatening, injuries. These injuries include head trauma, fractures of the vertebra, ruptured ligaments, and soft tissue damage. To determine the injury potential of these impacts an effort must be made to characterize the following:

1. Mechanical behavior of the head-neck complex.
2. Characteristics and energy associated with the fragment.
3. Interaction between the two.

Determining this experimentally for the various cases presents several challenges. The human body comes in a wide range of shapes and sizes. Each of these has its own particular material properties. This makes it very difficult to establish the proper controls for comparative experiments. Another significant challenge is cost. The costs associated with the instrumentation, controls, and actual cadavers add up quickly for the number of runs required to produce meaningful results.

Finite element analysis provides a more attractive solution. Careful construction and validation of a model provides a method of repeatable results. The model also provides complete flexibility in establishing controls and varying the constraints to simulate several different cases. The costs associated with this method are small after an initial outlay for computer hardware and software.

It is the objective of this research to develop a simplified model capable of accurately portraying the behavior of the head-spine system. The model will then be validated using available experimental data. The validated model will be subjected to several impacts to determine the injury potential from each. This potential will be based on several criteria discussed in Chapter IV.

II. BACKGROUND

A. ANATOMY OF THE SPINE

A brief anatomical review of the major structural components of the spinal system would seem prudent. Familiarity with the anatomy of the head precludes mentioning it in detail here. The head is attached to the spine by the occipital condyle, the atlas (C1) and the axis (C2). Figure 2.1 shows how these three fit together to form the occipital-atlantal joint.

The spine is divided into four distinct regions: cervical, thoracic, lumbar and sacral. The cervical spine is made up of seven vertebra including the atlas and axis described above. It descends from the head to the bottom of the neck. The thoracic spine is made up of 12 vertebra and

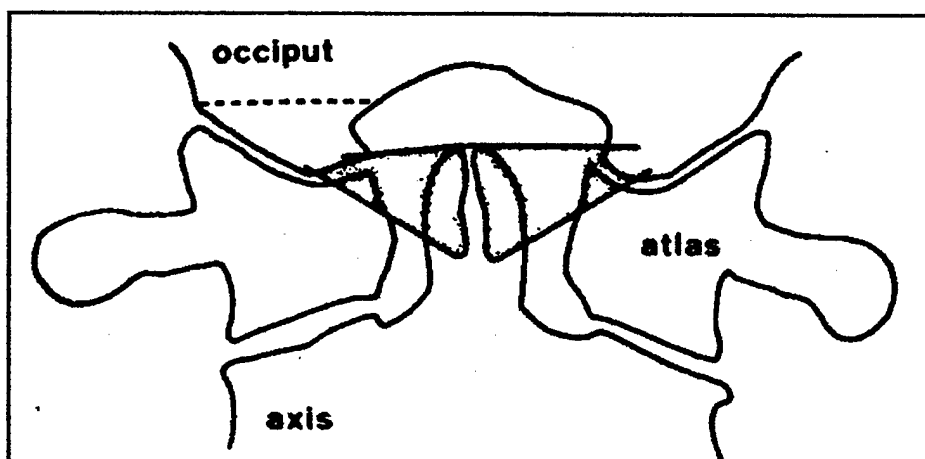


Figure 2.1. Occipital-Atlantal Joint connecting the skull to the spine (From White and Panjabi, 1978).

combines with the rib cage to form the chest cavity. The five lumbar vertebra are the largest individual vertebra and descend through the lower back. The sacral region contains five fused vertebra that transition into the pelvis. Individual vertebra are connected and aligned by intervertebral discs, ligaments, and facet joints.

Perhaps the best method of describing the vertebra and their interactions is by examining them as a spinal motion segment as seen in Figure 2.2. This method has been suggested by Mow and Hayes (1997), as well as Schultz, et al, 1979 and

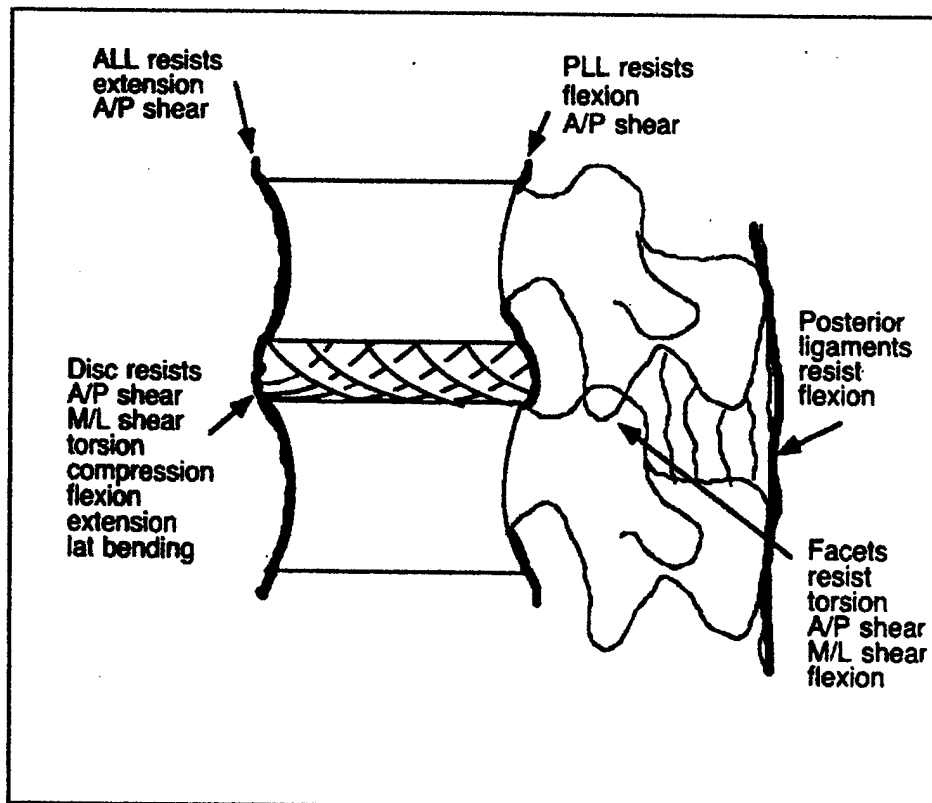


Figure 2.2. Spinal motion segment showing vertebra, disc, facet joint, and structurally significant ligaments (Tencer, A F, and Johnson, K D, 1994).

Berkeson, et al (1979), among others.

It shows the superior (top) and inferior (bottom) vertebral bodies separated by an intervertebral disc. This disc is much softer than the vertebra. This allows it to aid not only in the flexibility of motion, but also to aid in dampening impulse types of loading. It resists Anterior/Posterior (A/P)¹ shear, Medial/Lateral (M/L)² shear, torsion, compression, lateral bending, flexion,³ and extension.⁴ "The disc contains two regions, the inner nucleus pulposus and the outer annulus fibrosus... the normal disc behaves as a thick walled, deformable annulus, which until degenerate, contains fluid under pressure. (Mow and Hayes, 1997)" When subjected to a load, the disc pressure increases to stiffen the disc proportionately.

The major ligaments and the motions they resist are also shown in Figure 2.2. These ligaments run the length of the spine connecting with each vertebral body. The main function is to limit excessive motion of the segments and help maintain alignment (Mow and Hayes, 1997).

-
- ¹ Anterior/Posterior describes a front to back motion
 - ² Medial/Lateral describes a side to side motion
 - ³ Flexion is a bending of the neck forward
 - ⁴ Extension is a bending of the neck backward

"The main role of the facet joints is to limit excessive intervertebral shear and torsion motions of the intervertebral segment (Mow and Hayes, 1997)." This is accomplished by the superior and inferior faces meeting at an angle off that of the main vertebral body. This provides a load bearing surface off axis to resist shearing motions.

B. EARLY EFFORTS TO MODEL THE SPINE

Early mathematical efforts to model the spine followed two paths. The first was a lumped parameter treatment of the system; and the second was a continuum model. Latham developed one of the earliest lumped parameter models to study pilot ejections. This model was modified by Payne to include damping effects. The Dynamic Response Index (DRI) grew out of this effort (Kleinberger, 1993). Other models have been developed to examine specific loading conditions by McElhaney, et al (1976), Sances, et al (1984), and Reber and Goldsmith (1979).

Hess and Lombard developed the first continuum spinal model in 1958. This model treated the spine as a straight homogeneous elastic beam that was free at the top. It was modified by others in subsequent years to include spinal curvature, viscoelasticity, head mass (Kleinberger, 1993). As computing power increased in the 1970's, continuum models gave

way to the more powerful finite element analysis. Many early models were two dimensional and sought to characterize the properties of the various spinal components, i.e. vertebra, discs, and ligaments.

C. PRASAD AND KING'S MODEL

Prasad and King (1974) developed one of these early models. Their model was the first to explore some critical parameters of realistic spinal behavior. The first of these important parameters was to incorporate the curvature of the spine. They showed the importance of the curvature by conducting identical experiments with the spine in its natural shape and in a hyper extended⁵ condition. The hyper extended spine displayed significantly different behavior from the normal spine under identical loading conditions. These differences could also be predicted using their model and helped it to become one of the earliest experimentally verified models.

Earlier in 1974, they had published a paper along with Ewing describing for the first time the existence of a load path across the articular facet joints. This off axis loading

⁵ Hyper extension is placing a tensile force on the spine to diminish the overall curvature so as to approximate a straight beam.

surface was able to explain failure behavior that was being observed clinically but had yet to be predicted by the early models.

Prasad and King treated the vertebra as rigid bodies constrained to move in the mid-sagittal plane. The intervertebral discs were treated as a combination of spring-mass damper pairs. A pair was assigned to each translational and rotational degree of freedom (DOF). Facet interaction was modeled by springs connected to the vertebral body by a massless rigid rod.

D. BELYTSCHKO'S THREE DIMENSIONAL MODELS OF THE HUMAN SPINE

Belytschko developed a three dimensional model in 1976. This treats vertebra as solid elements. Discs, ligaments, and muscles are modeled as spring elements. Belytschko also introduced a new type of element called a hydrodynamic element. This pentahedron shaped element, shown in Figure 2.3, is used to model the behavior of the facet joints.

The triangular top and bottom faces are considered to be rigid. "The force deflection characteristics of this element are obtained from a linear pressure-dilation relationship... the resistance tends to be directed through a line of action connecting the centroids of the two triangular surfaces. (Belytschko, et al, 1976)" This resistance attribute is

appropriate for modeling the behavior of the articular facets because they exert their kinematic resistance perpendicular to the opposite faces of each motion segment.

Belytschko working with Privitzer, Williams, and others continued to improve this basic model by adding complexity and verifying against different loading conditions (Belytschko, et al, 1976, Belytschko, et al, 1978, Belytschko and Privitzer, 1978, Williams and Belytschko, 1983). This work led to several versions. The Simplified Spine Model (SSM) was based on the stiffness data to approximate the force deformations. This does not include ligaments, viscera, or other dampening

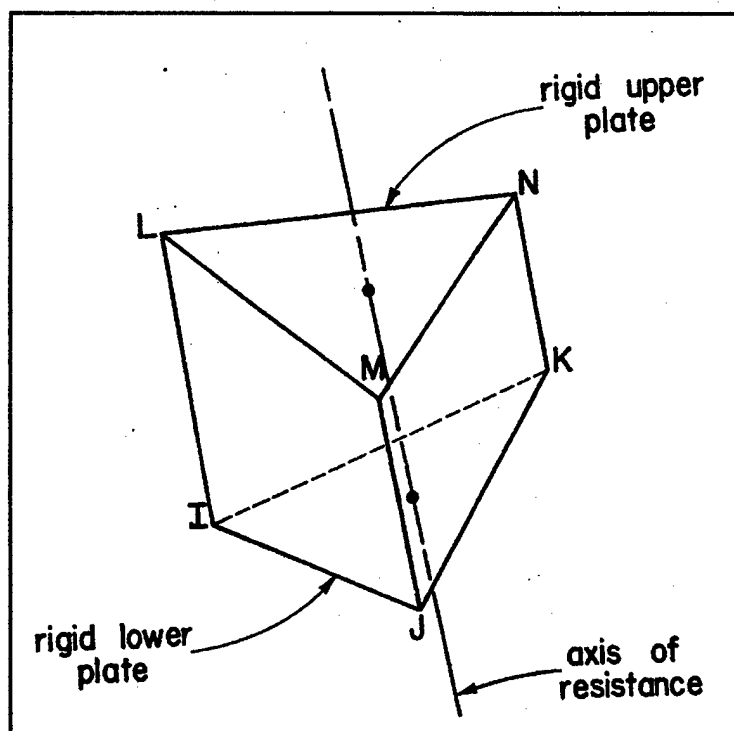


Figure 2.3 Belytschko's hydrodynamic element (from Belytschko, et al, 1976)

effects. The Isolated Ligamentous Spine Model (ILSM) incorporates ligament and viscera data for the torso. This addition of some inertial aspects of the body leads to a more realistic whole body response. The Complex Spine Model (CSM) built upon this by including aspects of the rib cage, refinement of the inertial by assignment to the torso vice the spine, and allowing a separate load path through the viscera.

Williams and Belytschko (1983) describe one additional model that is a combination of those above. It provides a detailed treatment of the cervical spine with a simplified lower spine as described in Belytschko and Privitzer (1978). "This is useful when the details of the lower spine response are not of interest, because it provides realistic boundary conditions for C7, which are essential for good simulations of the head-neck response. (Williams and Belytschko, 1983)" It is felt this model has potential as a guide for examination of the ballistic impact problem.

E. SURVEY OF ADDITIONAL WORK IN THE FIELD

Other investigators have conducted experimental, as well as analytic, analyses of the head and spine. Soni, 1982, conducted an experimental investigation (Part 1 of 2) of the kinematics of a motion segment of the lumbar spine. Patwarden, 1982, developed a finite element model (Part 2) to

simulate the segment motions observed above. This model represented the vertebra as rigid bodies, while modeling the intervertebral discs and ligaments as elastic elements. The articular facets were modeled as two springs. The first spring is set perpendicular to the facet face with a stiffness. The second spring provides a lower stiffness parallel with the face.

Tencer and Mayer, 1983, studied intervertebral and facet joints of the lumbar spine. Their efforts concentrated on characterizing the geometry and function of the soft tissues and facet face interactions. Strains of these elements were also examined.

Li, 1991, performed a quasi-static analysis of the cervical spine in both extension and compression. This work also examined failure loads for the vertebral bodies, spinous processes, and anterior longitudinal ligaments. These failure loads are grouped by age groups. This is done to differentiate between bone and disc strength variations with age.

Nightingale, 1991, examined the effect of the end condition on injury probability. This research showed that whether the head was fixed or free to rotate had a significant impact on the potential of injury.

Yogandan and Pintar, 1997, studied the cervical spine

under inertial loading. This effort concentrated on identifying the effect of non-contact inertial loads had on injury potential. These experiments determined some of these inertial properties of the cervical spine by subjecting it to two different velocities.

Huston and Sears, 1981, investigated the effect of protective helmets on head-neck dynamics from the perspective of motorcycle riders. It identified the detrimental effect which the additional mass of the helmet contributes to the motion and rotation of the system. To help alleviate the problem, it also suggested wearing a restraining collar around the neck to help dampen those motions.

Perry and Buhrman, 1996, established the Standard Inertial Weight (SIW) to aid their research into the effects of helmets on head-neck dynamics. This non-dimensional parameter offered a method of examining parametric changes of helmet mass without biasing the results due to the corresponding change in the center of gravity of the system. Using the SIW, they plotted the effect of helmet weight on the compression, shear and torque loads on the occipital condyle. Their efforts calculated loads induced with varying helmet mass during a +10g ejection motion.

III. FINITE ELEMENT MODEL

A simplified Finite Element Model (FEM) has been developed to analyze the complex interactions involved when a bullet or other high velocity fragment impacts the PASTG Helmet being worn by a soldier during combat. The commercial finite element analysis program, LS-Dyna-3D version 936 (Livermore Software Technology Corporation, 1995), was utilized as the processor for this analysis. The accompanying LS-Taurus software was used as the post-processor to display the results of the computations. This analysis focused on the biomechanical responses of the spine and head due to the impact of the bullet/fragment on the surface of the helmet. The initial geometry of this model is shown in Figure 3.1. This system required the construction of three significant parts: the fragment, the protective helmet, and the body.

A. FRAGMENT

The choice of an fragment was based on the ballistic limit of the PASTG helmet. Using this criterion provided a reasonable limit to the energy delivered without considering fragment penetration of the head. The ballistic limit, however, does not preclude higher velocity fragments striking the helmet without penetration. Rather, it establishes a probability of penetration as 50%. This model did not

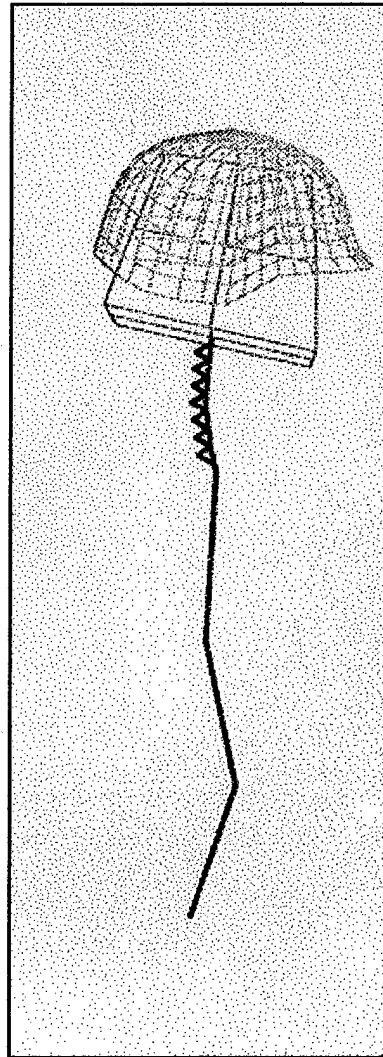


Figure 3.1. Entire Finite Element Model

consider the penetrating capabilities of the bullet or similar projectiles. Rather it was generalized as a high velocity fragment capable of delivering a known energy to the protective helmet.

A simple cubic shape was chosen for the geometry of the fragment. The properties used for the fragment, which was

treated as a rigid body, are defined in Table 3.1. By not allowing for deformation of the bullet, we ensure maximum energy transfer to the protective helmet. The relative position of the fragment to the helmet was varied to different positions to induce the different loading conditions.

Table 3.1. Properties of Fragment

PROPERTY	VALUE
Mass	3.62 grams
Density	5000 Kg/M ³
Elastic Modulus	29.9 M Pa
Poisson's Ratio	0.3

B. PROTECTIVE HELMET

This model was designed to simulate the PASTG Helmet currently in use as protective head gear for United States combat troops. The PASTG helmet has 19 effective plies of Kevlar-29 composite material (MIL-C-44050A). It has been designed to stop small fragment penetration up to a ballistic limit of $V_{50} = 2000$ ft/s (609.5 m/s) (Dupont, 1997). Mechanical testing was performed on samples cut from the helmet to determine the elastic modulus, E, in compression. The results of the testing are included in Appendix A. The other material properties are included in Table 3.2.

The geometrical coordinates for the helmet were measured using a Mitutoyo coordinate machine. These coordinates were then inputted into the PATRAN pre-processor. The surface of the helmet was generated based on this data. The helmet is shown in Figure 3.2. PATRAN was also used to automatically generate the finite element mesh. Four noded shell elements were used with the exception of 2 three noded shell elements at the top of the helmet to maintain continuity.

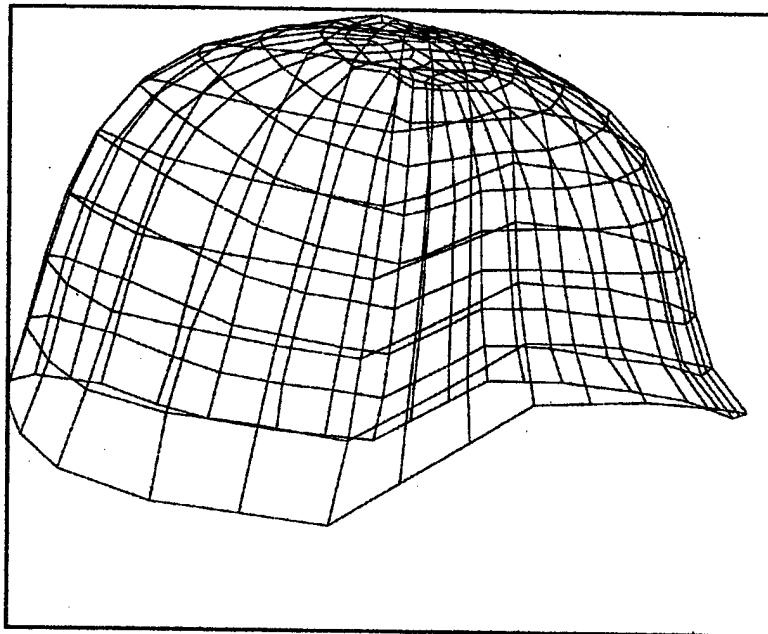


Figure 3.2. Model of helmet created from geometrical data.

Table 3.2. Properties of the Helmet

PROPERTY	VALUE
Mass	1.5 Kg
Density	500 Kg/M ³
Elastic Modulus	689 MPA
Poisson's Ratio	0.2

C. BODY

The objective of this research was to investigate the biomechanical response of the human head and spine when subjected to specific impact loading. To accomplish this, a system of beam and solid elements were combined to represent both the head and spine.

1. Head

The head was modeled by 8 eight noded solid elements. The shape is approximately correct, but more important for the research was attaining the proper mass, center of gravity, and moments of inertia. The center node of this volume has been adjusted to coincide with the center of gravity of the head. This adjustment allowed for ease in computation of the Head Injury Criterion (HIC). These values will be used in the Chapter V to estimate the injury potential to the head and brain.

2. Spine

This simplified model strives to mirror the behavior of a very complex biological system, the cervical spine shown in Figure 3.3. A series of one dimensional beams were used to simulate the spine similar to the model proposed by Belytschko and Privityzer (1978). This model utilizes a series of simple beams to model the thoracolumbar vertebra. Although very basic, it provides realistic boundary conditions to the lower cervical spine without unnecessarily complicating the model. This is useful when the details of the lower spine are not of interest.

Each cervical vertebra has been modeled by 2 one dimensional beams. Between each vertebra is a vertebral disc that has been modeled by a single beam. The facet joint is a load bearing surface that mainly serves to help restrict excessive motions and maintain vertebra alignment. This joint has been modeled by 2 beams extending from the midpoints of adjoining vertebra as shown in Figure 3.4. Where these 2 beams meet, a discrete beam is defined to maintain connectivity between them.

The discrete beam is an element in the LS-DYNA code that allows for the definition of a beam that takes up no space. The advantage of this element is it allows for the specification of a specific stiffness in each Degree Of

Freedom (DOF). This replaces defining six separate springs (1 for each DOF) between each vertebra.

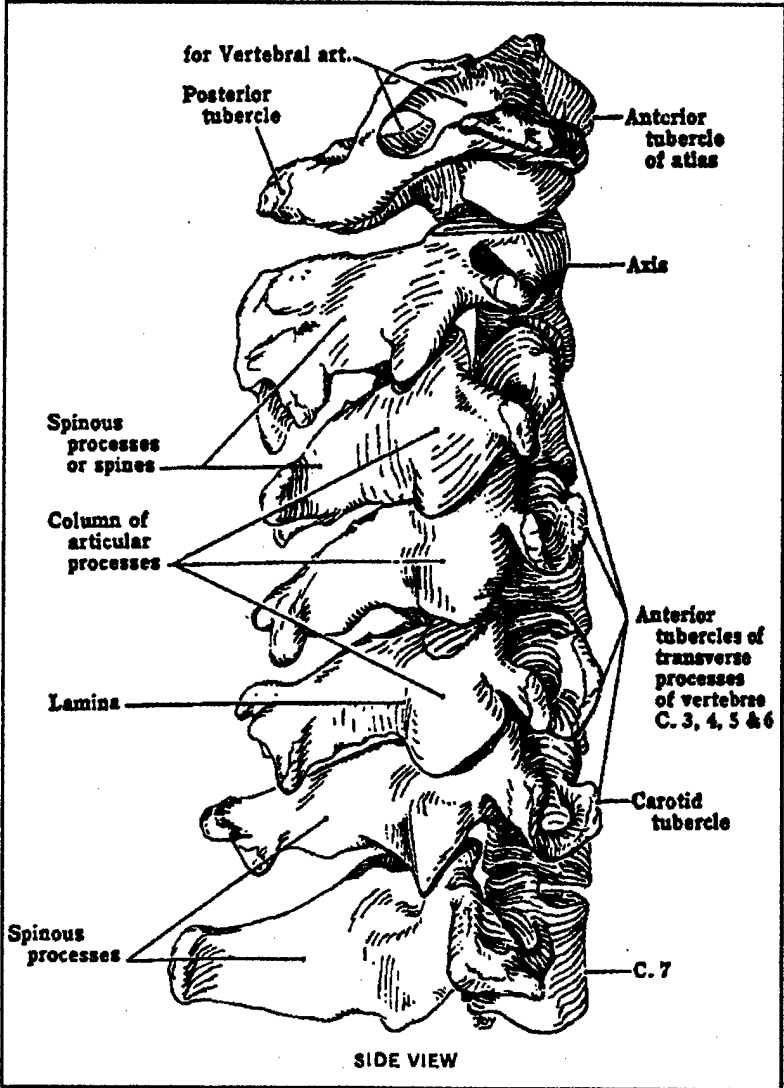


Figure 3.3. Anatomical view of cervical spine (from Nahum and Melvin, 1993)

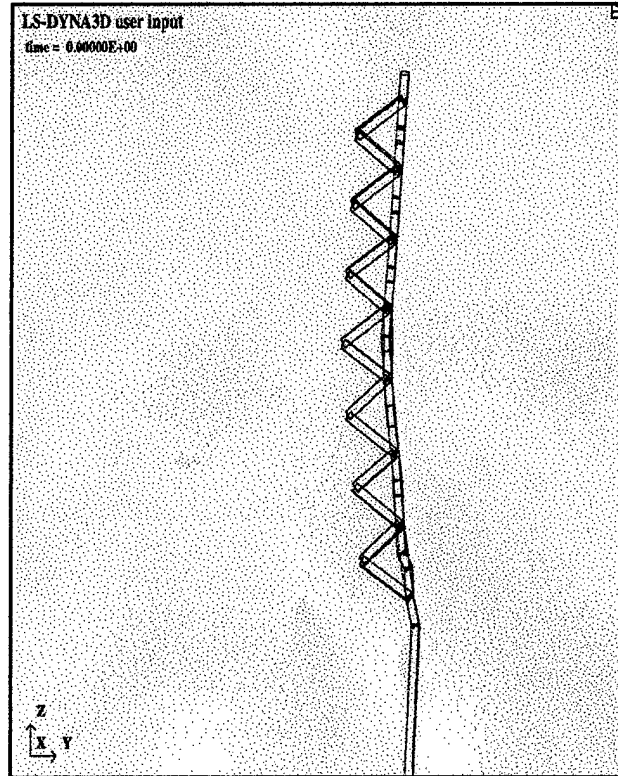


Figure 3.4. Model of cervical spine

There are numerous ligaments and other connective tissue surround the cervical spine. For the purposes of this model they have been reduced to a single ligament running from C1 to C7. The ligament was modeled using a cable element that only provides a resistance to tensile forces. Muscles and other soft tissue were not included in this model; however, a damper system was added to the cervical spine to simulate the inherent dampening capabilities these tissues provide to the biological system.

IV. INJURY ASSESSMENT

A. MATERIAL PROPERTY VARIATION

Evaluation of the injury potential for a given activity is a difficult proposition. The first of many difficulties is wide variation of properties between individuals. This is particularly true of spinal properties. Vertebra are constructed of two types of bone. The cortical bone forms a hard thin shell around the trabecular bone which makes up the majority of the structure. Cortical bone is made up of several subunits called osteons, that form concentric sheaths of the bone. The orientation of these sheaths determines the strength of the individual bone (Nahum and Melvin, 1993).

"Trabecular bone is a highly anisotropic structure composed of a large number of rods, plates, or beams (Nahum and Melvin, 1993)." It has a much greater porosity than cortical bone which increases its susceptibility to weaknesses associated with the aging process and certain diseases. "The structural anisotropy or orientation of trabecular bone also varies with location, being nearly isotropic in regions such as the center of the femoral head, while highly oriented in the vertebral bodies....Variations as high as two orders of magnitude have been found within individual metaphyses (Nahum and Melvin, 1993)." This high degree of anisotropy has led to

wide variations of properties measured by investigators as shown in Table 4.1.

Table 4.1. Spinal material property variations

Material	Property	Source
Trabecular Vertebra	7.35×10^5 Pa	Belytschko, et al, 1976
Cortical Vertebra (Shell)	1.50×10^8 Pa	Belytschko, et al, 1976
Trabecular Vertebra	1.00×10^7 Pa - 4.28×10^8 Pa	Nahum and Melvin, 1993 (from Struhl, et al, 1987)
Trabecular Vertebra	1.58×10^8 Pa - 3.78×10^8 Pa	Nahum and Melvin, 1993 (from Ashman, et al, 1986)
Whole Vertebra	2.08×10^5 Pa	Kleinberger, 1993
Disc	6.00×10^5 Pa - 2.84×10^6 Pa	Belytschko, et al, 1976
Disc	3.5×10^5 Pa - 20.0×10^5 Pa	Williams and Belytschko, 1983
Disc	3.4×10^3 Pa	Kleinberger, 1993
Facet Joints	1.5×10^4 Pa	Belytschko, et al, 1976
Facet Joints	0.5×10^5 Pa - 10.0×10^5 Pa	Williams and Belytschko, 1983
Facet Joints	3.4×10^3 Pa	Kleinberger, 1993
Ligaments (Ligamentum Flavum)	1.00×10^8 Pa - 2.00×10^6 Pa	Nahum and Melvin, 1993
Ligaments	1.5×10^4 N/m	Belytschko, et al, 1976
Ligaments	2.04×10^4 N/m - 3.30×10^4 N/m	Kleinberger, 1993

B. HEAD INJURY CRITERIA (HIC)

Many criterions have been established over the years to try to predict injury. However, none of these can be considered a threshold or certainty of injury due to the wide variation between individuals. Perhaps the best indicator of head injury is the Head Injury Criteria (HIC). This is a measure of the acceleration the head experiences during the impact. It is calculated using Equation 4.1:

$$\text{HIC} = \left[\frac{1}{(t_2 - t_1)} \int a \, dt \right]^{2.5} (t_2 - t_1) \quad \text{Equation 4.1}$$

where a = acceleration of center of mass of head in Gs
 t_1 = time at beginning of period of interest in sec
 t_2 = time at end of period of interest in sec

The United States Department of Transportation has regulated a tolerance limit of $\text{HIC} = 1000$ (Mohan, et al, 1979). Figure 4.1. shows not only the 1000 level, but also an injury risk curve based on experimental work to show the probability of Abbreviated Injury Scale (AIS) brain injury of 4 or greater (AGARD, 1996). The AIS levels are shown in Table 4.2.

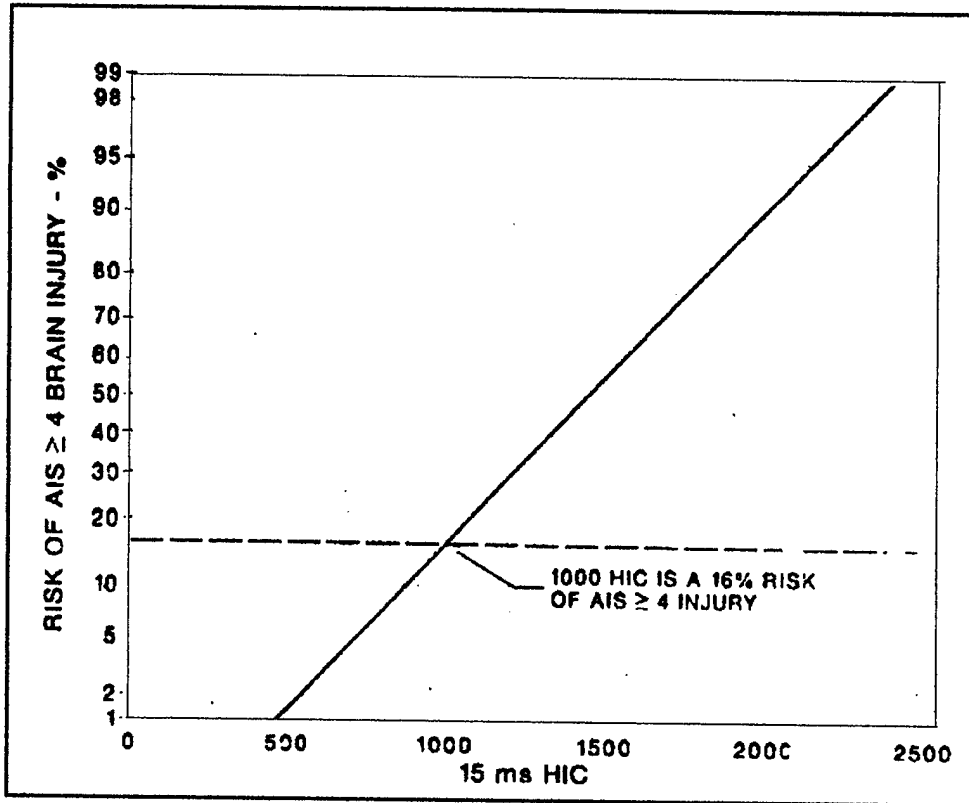


Figure 4.1. Risk of brain injury as a function of HIC based on a 15 ms acceleration period (from AGARD, 1996).

Table 4.2. Abbreviated Injury Scale (AIS)

AIS	Severity of Injury
0	Not injured
1	Minor
2	Moderate
3	Serious
4	Severe
5	Critical
6	Maximum
7	Injured but Severity Not Known

C. INJURY ASSESSMENT REFERENCE VALUES (IARVS)

Injury Assessment Reference Values (IARVS) were developed by the General Motors Corporation to help assess the potential for injury from the data collected from Hybrid III 50th percentile anthropomorphic dummies (AGARD, 1996). "They noted that each IARV refers 'to a human response level below which a specified significant injury is considered unlikely to occur for a given individual'. However, they cautioned that being below all of the IARVS does not assure that significant injury would not occur (AGARD, 1996)." Likewise, it is pointed out that exceeding a given IARV does not guarantee an injury. These should be considered injury potentials vice thresholds. Table 4.3 lists IARVS for three adult body types: small female, mid-size male, and large male.

Table 4.3. IARVS for Hybrid III Dummies (from AGARD, 1996)

Injury Assessment Criteria	Small Female	Mid-Size Male	Large Male
Head : HIC ($t_2 - t_1 \leq 15$ ms)	1113	1000	957
Head/Neck: Flexion Moment (Nm)	104	190	258
Extension Moment (Nm)	31	57	78
Axial Tension (N)	Figure 5.2	Figure 5.2	Figure 5.2
Axial Compression (N)	Figure 5.3	Figure 5.3	Figure 5.3
Fore/Aft Shear (N)	Figure 5.4	Figure 5.4	Figure 5.4

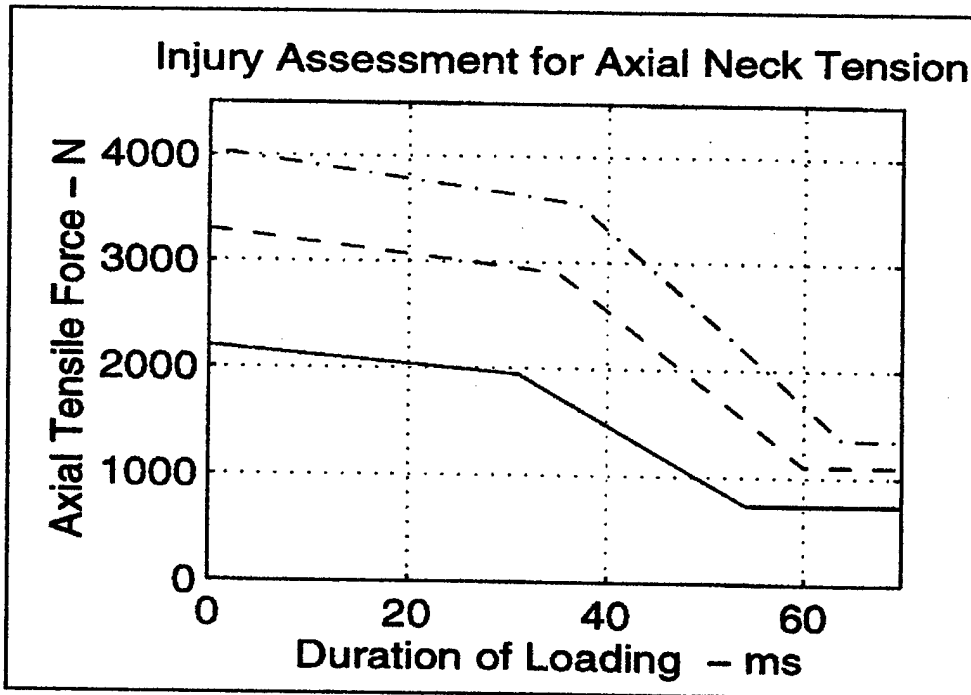


Figure 4.2. IARV for axial tensile forces acting on the neck (from AGARD, 1996). The solid line represents the case of female. The dashed line a mid-size male. The dashed and dotted line represents a large male.

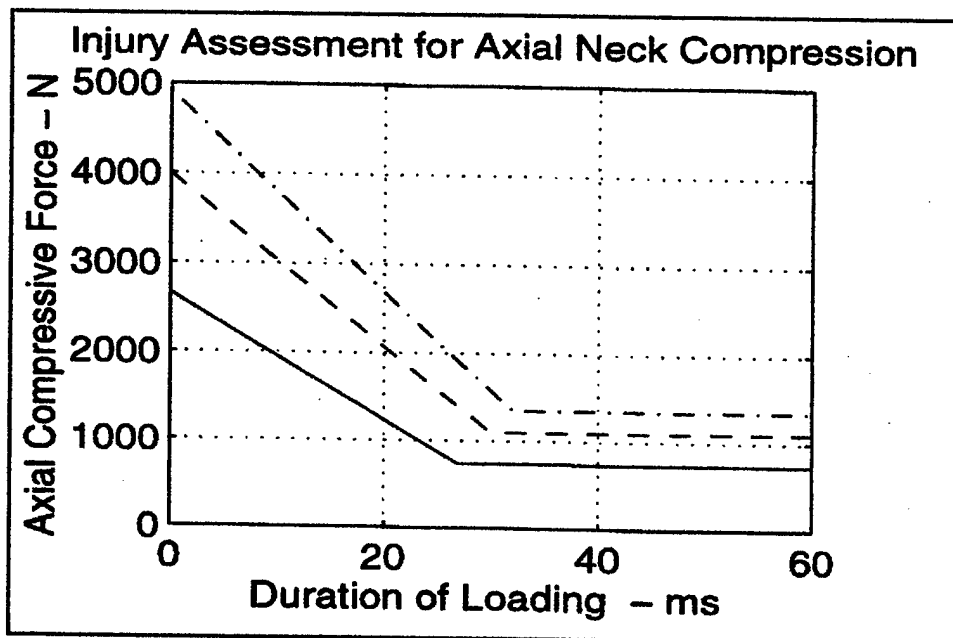


Figure 4.3. IARV for axial compressive forces acting on the neck (from AGARD, 1996)

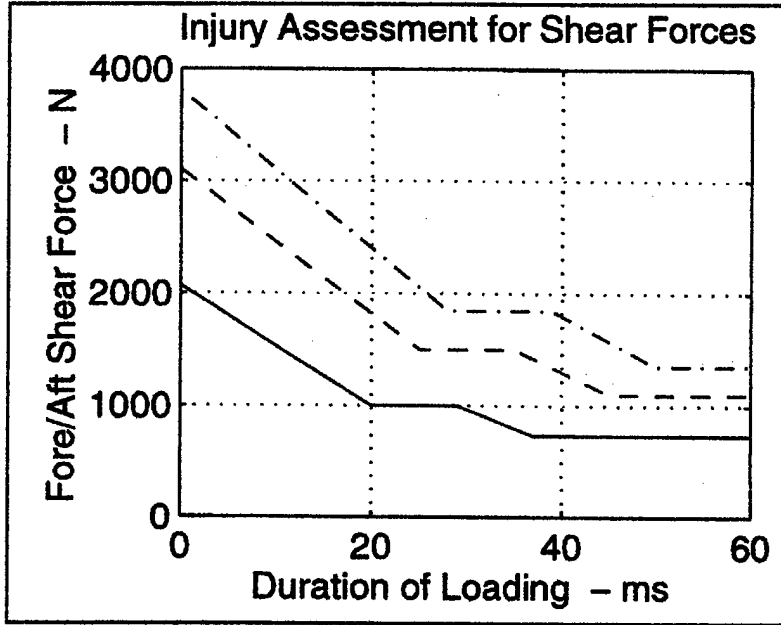


Figure 4.4. IARV for shearing forces at the junction of the head and neck (from AGARD, 1996). The solid line represents a female. The dashed line is the case of the mid-size male. The dashed and dotted line represents a large male.

D. OTHER PUBLISHED CRITICAL INJURY VALUES

Several authors have reported using other criteria to determine injury potentials for the head and head/neck complex. The limits suggested by these sources are not as complete as those above or accepted as industry standards. They are included in Table 4.4 for completeness.

Table 4.4. Critical Injury Values Reported by Other Authors

Type of Loading	Critical Value	Source
Vertebral Compression	10140 N	Tencer and Johnson, 1994
	.06 - 15 x 10 ⁶ Pa	Struhl, et al, 1987 (from Nahum and Melvin 1993)
	3620 N	Belytschko, et al, 1976
Flexion Bending Moment	154 Nm	Tencer and Johnson, 1994
	189 Nm 59.4 Nm for pain threshold	Nahum and Melvin, 1993
Extension Bending Moment	105 Nm	Tencer and Johnson, 1994
Disc Bending Moment	4 - 11 Nm	Belytschko, et al, 1976
Torsional Moment	4 - 11 Nm	Belytschko, et al, 1976
Ligament Injury Due to Bending Moment	56.7 Nm	Mertz and Patrick, 1971 (from Nahum and Melvin, 1993)

V. RESULTS

A. MODEL VERIFICATION

This model was validated against the experimental work of Ewing, 1978. He measured the displacements and accelerations experienced by volunteers during a horizontal sled acceleration. The sled was linearly accelerated from rest to a maximum at 14.2 ms. Then was allowed to decelerate linearly back to rest at 340 ms. The head and neck were not constrained during the testing. Ewing, 1978, repeated this procedure varying the magnitude of the acceleration profile to produce maximum acceleration magnitudes ranging from 3 G to 10 G.

The test used for comparison fixed the finite element model of the spine and head to a rigid wall with three linear springs ($k = 1 \times 10^5$ N/m), shown in Figure 5.1. The wall was then accelerated along a profile similar to the one described above. The resulting displacement and acceleration of the center of gravity of the head was compared with the results of Ewing, 1978.

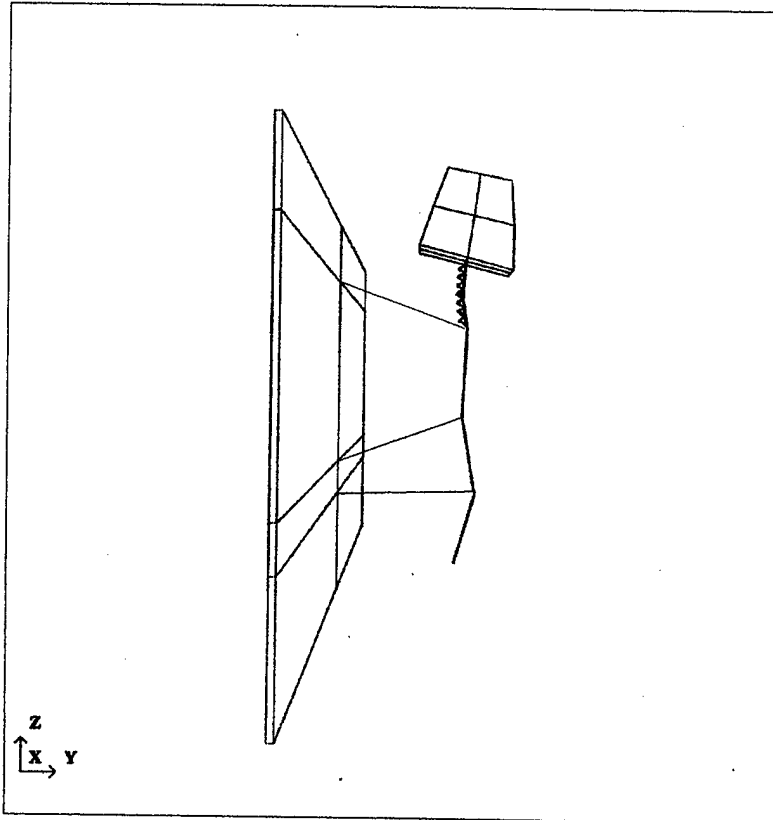


Figure 5.1. View of spinal model attached to rigid wall for validation case. The 3 springs attaching the model to the wall represent the sled's restraint system.

Figure 5.2 shows the displacement of the head relative to the first thoracic vertebra (T1). The model slightly underestimates the peak displacements measured by Ewing, 1978. The resulting horizontal acceleration is shown in Figure 5.3. The model predicts the first negative peak of the experiment, but with a 20 ms time delay. The model fails to predict the second negative peak of the experiment which occurs at 120 ms.

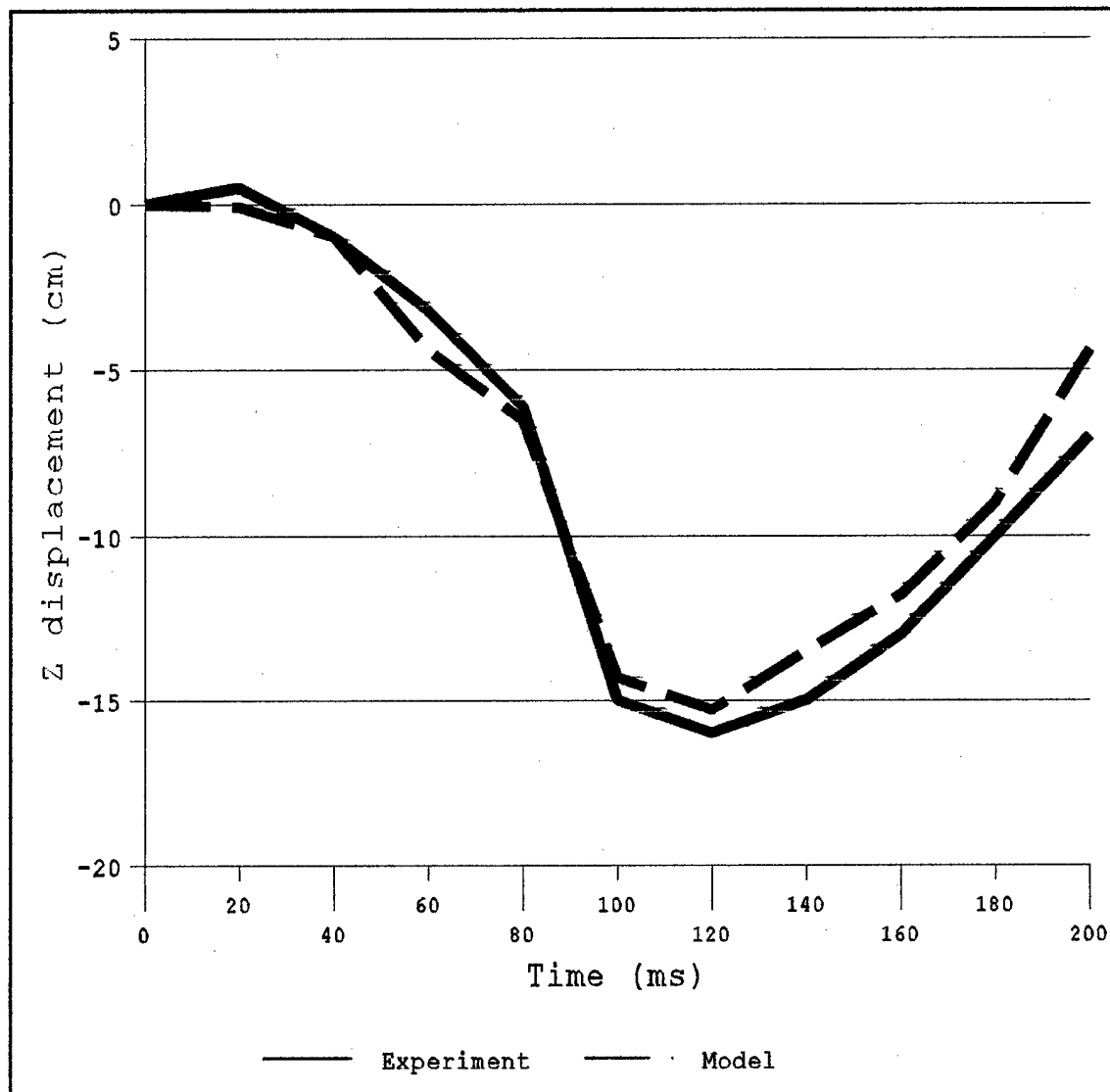


Figure 5.2. Comparison of relative displacements between experiment (Ewing, 1978) and model. The displacement is measure of the vertical distance between T1 and the center of gravity of the head.

The model does predict the final peak of the experiment which occurs at 160 ms. The differences between the model and the experiment are likely due to the model's simplistic treatment of the sled and restraint system as a rigid wall and series of three springs. Additional sources for differences could

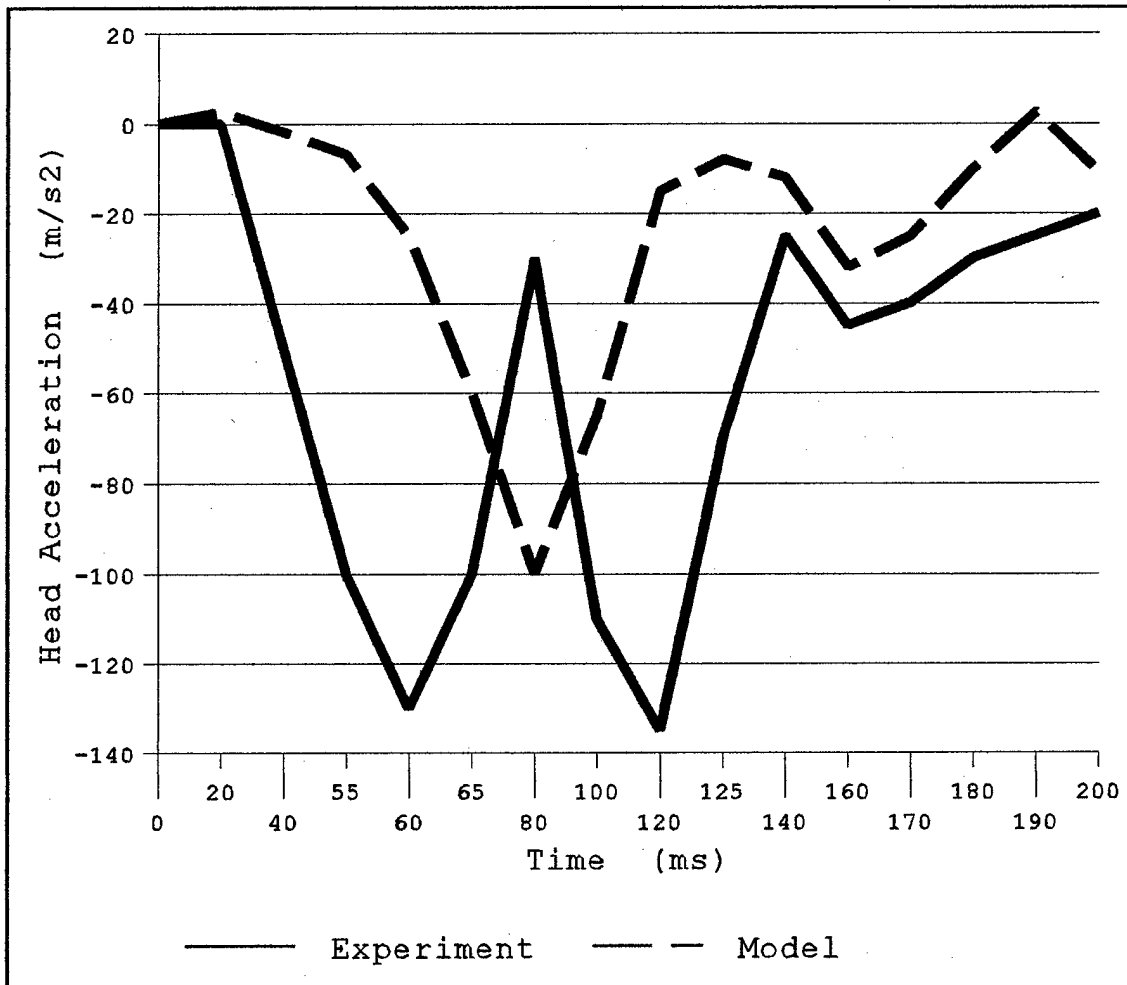


Figure 5.3. Comparison of the acceleration of the head between experiment (Ewing, 1978) and model. The acceleration is measured at the head's center of gravity.

result from the wide variation of properties between individuals.

B. FRONT IMPACT

Three runs were conducted with a frontal impact to try to determine the effect of disc stiffness on spinal behavior. The stiffness of the vertebral discs was varied from 3.4×10^3 Pa to 5×10^5 Pa. This matched the range of values summarized in Table 4.1. All other values for the model were held constant.

The position of the fragment relative to the helmet before impact is shown in Figure 5.4. The history of the stress field induced by the collision is shown in Figure 5.5 through Figure 5.8. The stress is a maximum right after impact of 1.42×10^6 Pa. This stress slowly decays but is still greater than 1.83×10^4 Pa after 200 ms. The interaction of the fragment and the helmet is not dependent on the varying value of the intervertebral disc. Therefore, this energy transfer is unchanged for each of the three following cases:

- Case 1: Young's Modulus of disc = 3400 Pa
- Case 2: Young's Modulus of disc = 34000 Pa
- Case 3: Young's Modulus of disc = 500000 Pa

1. Case 1

This case covered the least stiff case examined. Figure 5.9 shows the total acceleration of the center of gravity of

the head for the first 15 ms after impact. The area under this curve was used to calculate an HIC value of 1.28. The maximum axial force acting on the occipital condyle, shown in Figure 5.10, is 68.2 N. Figure 5.11 shows the maximum shear force acting on the occipital condyle to be 24.9 N. The maximum bending moment for C4 and T1 vertebra, shown in Figures 5.12 and 5.13, respectively, are 6.25 Nm and 10.7 Nm. Figure 5.14 shows the maximum bending moment for vertebral discs of 1.12 Nm to occur at the C4-C5 level. The ability of the facet joints to resist shearing and torsional moments are shown in Figures 5.15 and 5.16. The shearing force is 29.7 N and the torsional moment 8.78 Nm.

The vertebral bending moment is 34.5% of the IARV listed in Table 4.3. While the possibility of severe injury is unlikely, minor strains and pains are still possible. These minor injuries could lead to reduced productivity and loss of mobility in a battlefield environment.

2. Case 2

Figure 5.17 shows the total acceleration of the center of gravity of the head for the first 15 ms after impact. The area under this curve was used to calculate an HIC value of 144.1. The maximum axial on the occipital condyle, shown in Figure 5.18, is 217.25 N. Figure 5.19 shows the maximum shear forces acting on the occipital condyle to be 71.9 N. The

maximum bending moment for the vertebra occurs at C5. It is shown to be 16.5 Nm in Figures 5.20. Figure 5.21 shows the maximum bending moment for the discs to occur at C4-C5. It is 10.7 Nm. The ability of the facet joints to resist shearing and torsional moments are shown in Figures 5.22 and 5.23. The shearing force is 65.2 N and the torsional moment is 11.5 Nm.

The vertebral bending moment is 53.2% of the IARV value listed in Table 4.3. The likelihood of severe injury is increased but still not probable. Minor injuries will increase both in frequency and severity.

The bending moment of the disc surpasses the critical value from Table 4.4 reported by Belytschko, et al, 1976. This potential for disc injury most likely will manifest itself as rupture of the disk. This is caused when the disc is compressed. The compression increases the pressure of the disc fluid. This pressure finds a weak point in the disc wall and erupts into the spinal column.

3. Case 3

This case covered the stiffest case examined. Figure 5.24 shows the total acceleration of the center of gravity of the head for the first 15 ms after impact. The area under this curve was used to calculate an HIC value of 138.7. The maximum axial force acting on the occipital condyle, shown in Figure 5.25, is 221.9 N. Figure 5.26 shows the maximum shear

force acting on the occipital condyle to be 82.3 N. The maximum bending moment for the vertebra, shown in Figure 5.27, is 48.9 Nm and occurs at C6. Figure 5.28 shows the maximum bending moment for vertebral discs occurs at C3-C4. It is 40.1 Nm. The ability of the facet joints to resist shearing and torsional moments are shown in Figures 5.29 and 5.30. The shearing force is 59.5 N. The torsional moment is 12.5 Nm.

The IARV for bending moment in extension is surpassed by C3, C4, C5, C6, and C7 with the maximum occurring in C6. This suggests a high probability of severe injury (AIS 4 or greater). This injury is likely to appear as a burst fracture of the vertebral body. The critical value for the disc from Table 4.4 is surpassed by discs C3-C4, C4-C5, and C5-C6 with the maximum occurring at C3-C4. These injuries may appear as a disc rupture, which was described above, or a collapse of the disk around one of the many nerves surrounding the spinal column.

As the torsional moment on the cervical spine increases it becomes more likely that the facet joints will become displaced. This means the superior face of the facet joint slides up and over the inferior face and locks into that position.

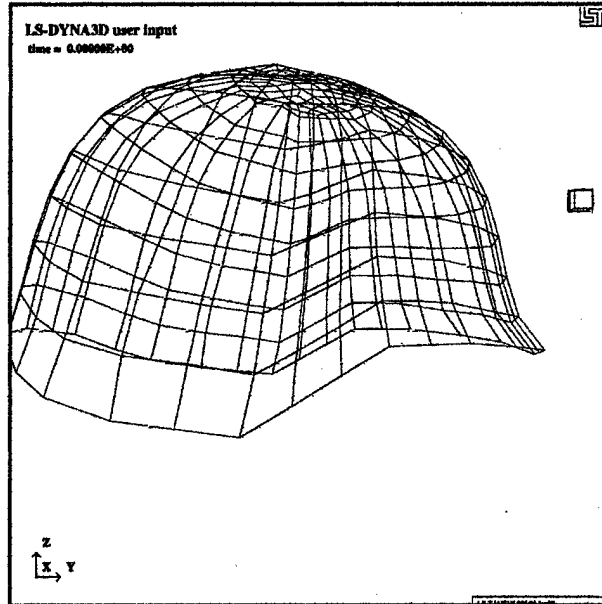


Figure 5.4. Relative position of fragment to helmet before impact

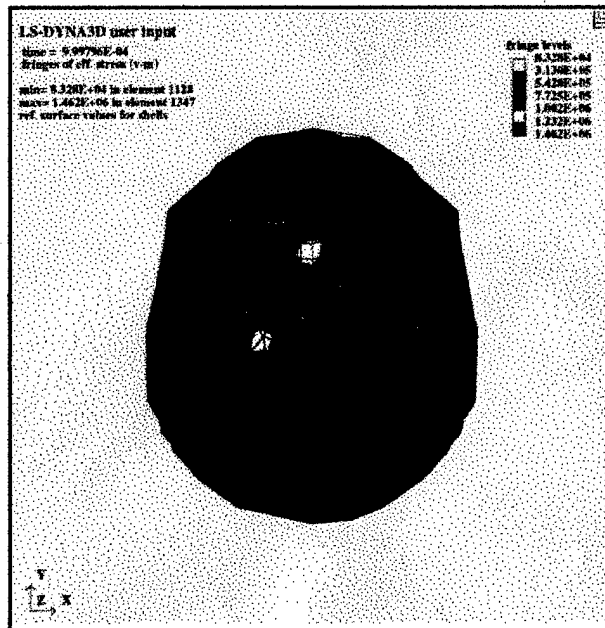


Figure 5.5. Effective stress induced in helmet 1 ms after impact



Figure 5.6. Effective stress induced in helmet 10 ms after impact



Figure 5.7. Effective stress induced in helmet 30 ms after impact

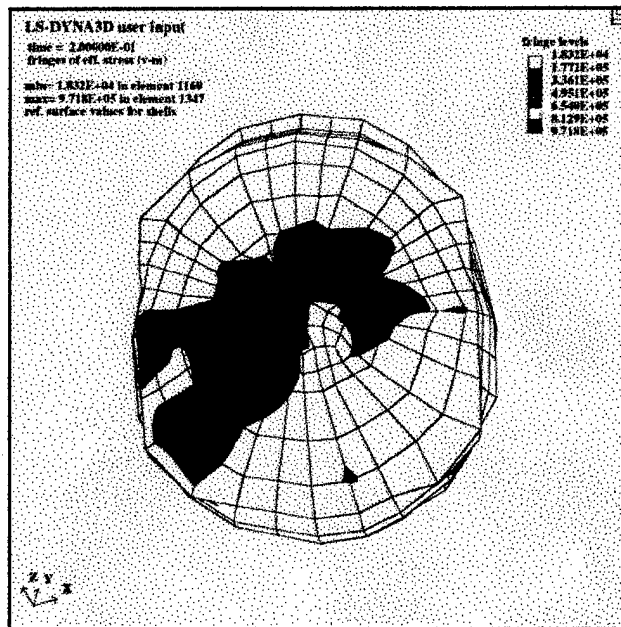


Figure 5.8. Effective stress induced in helmet 200 ms after impact.

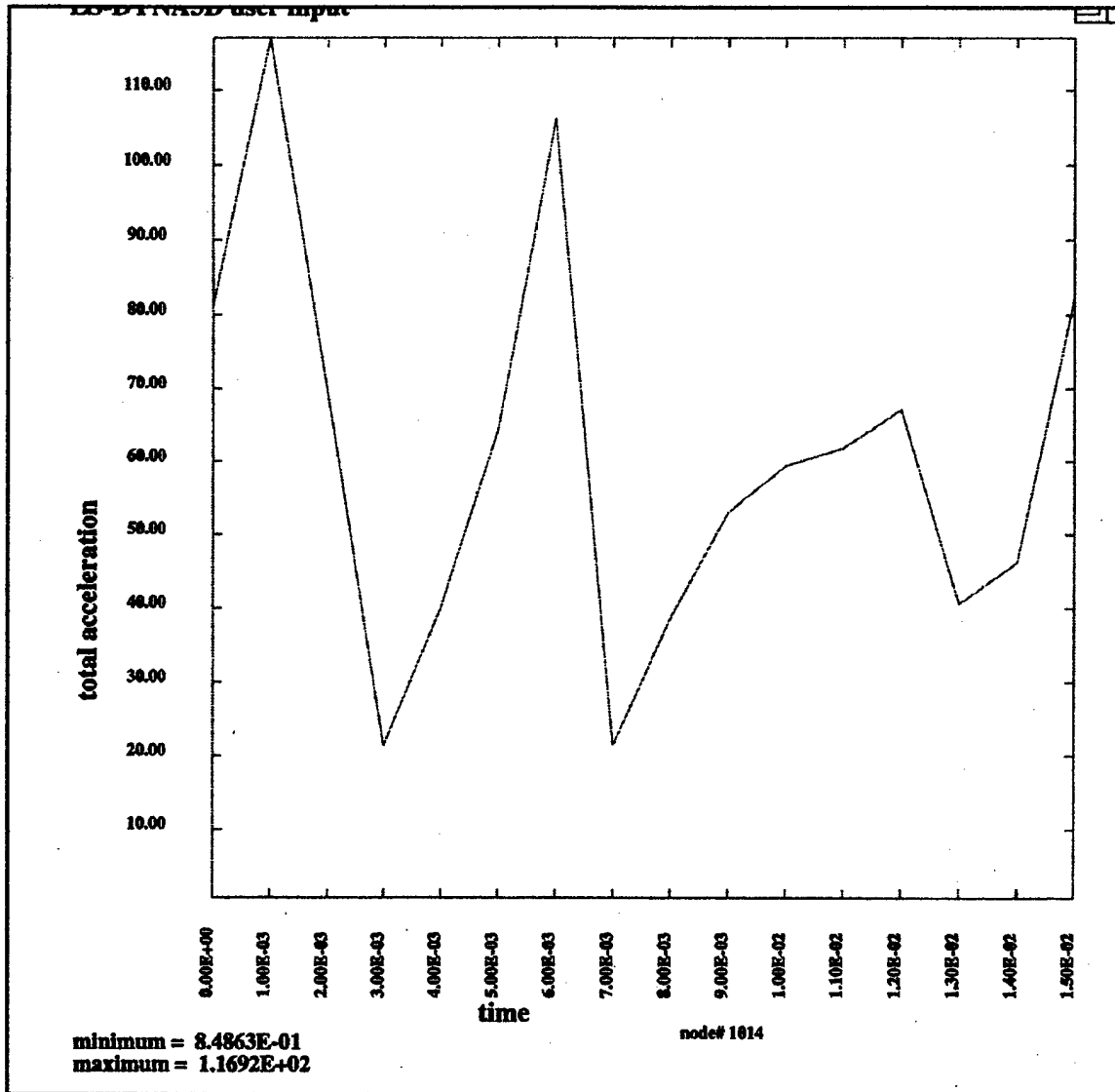


Figure 5.9. Acceleration profile used to calculate HIC for Case 1

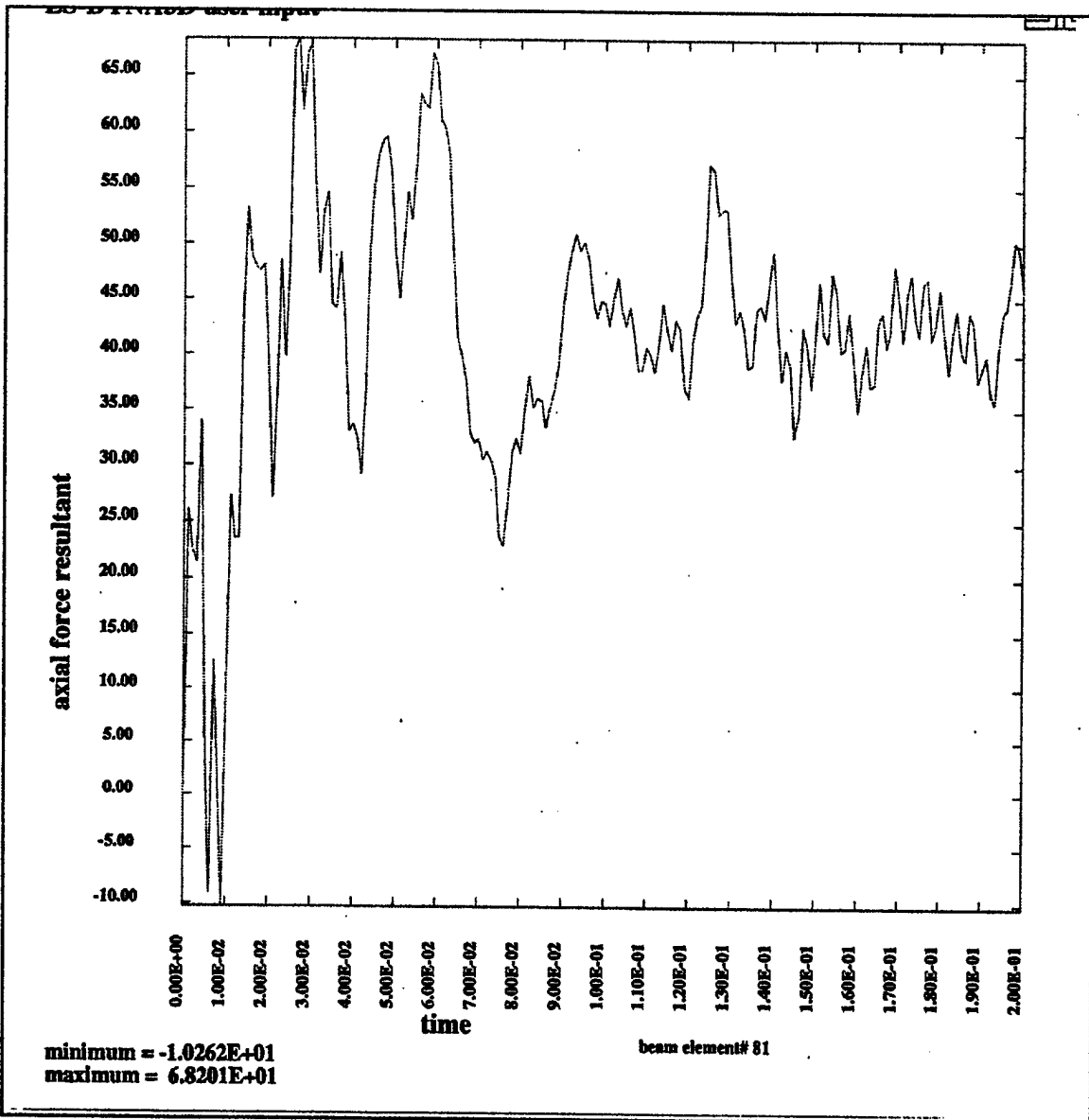


Figure 5.10. Axial force on the occipital condyle for Case 1

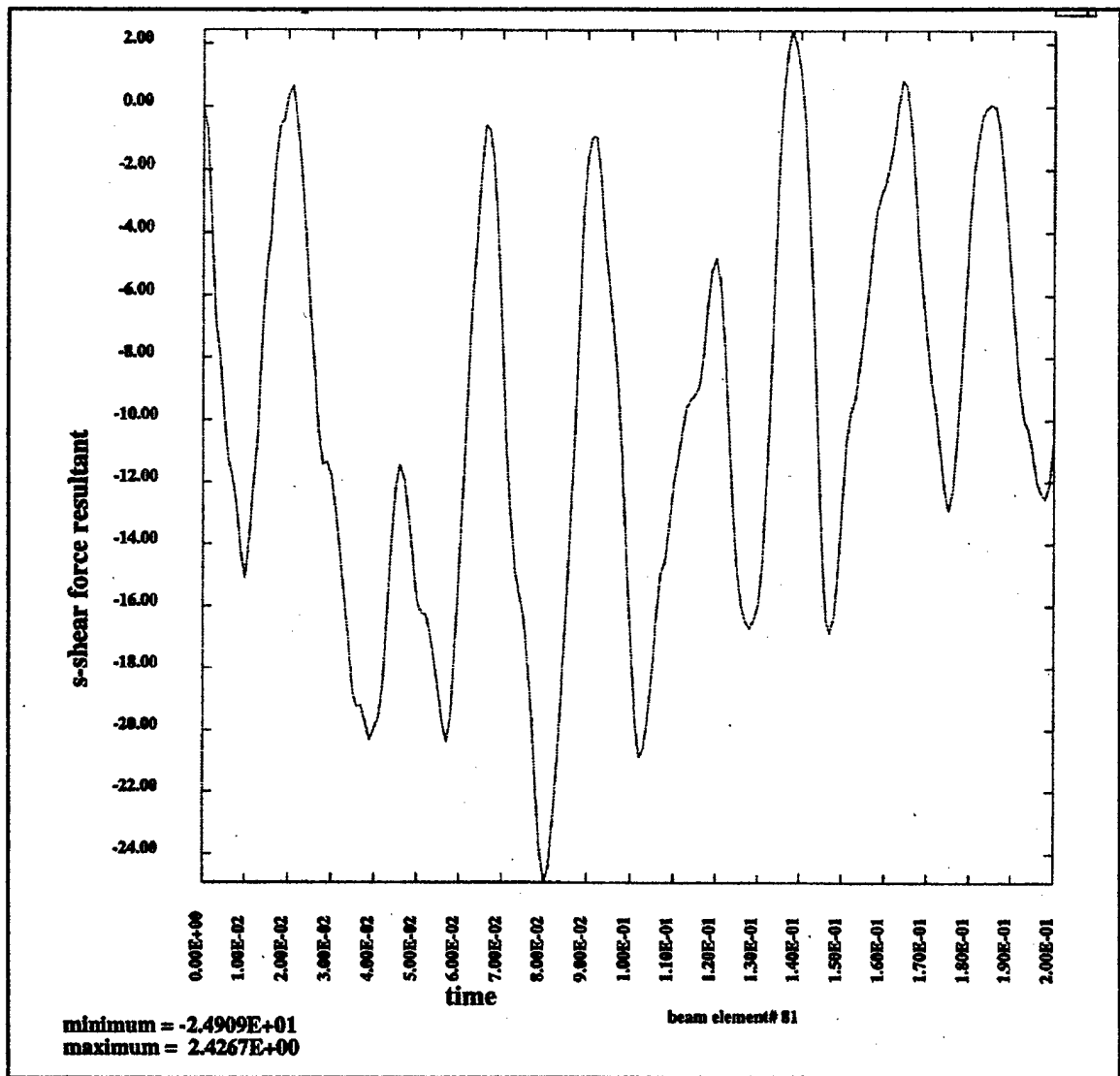


Figure 5.11. Shear force on the occipital condyle for Case 1

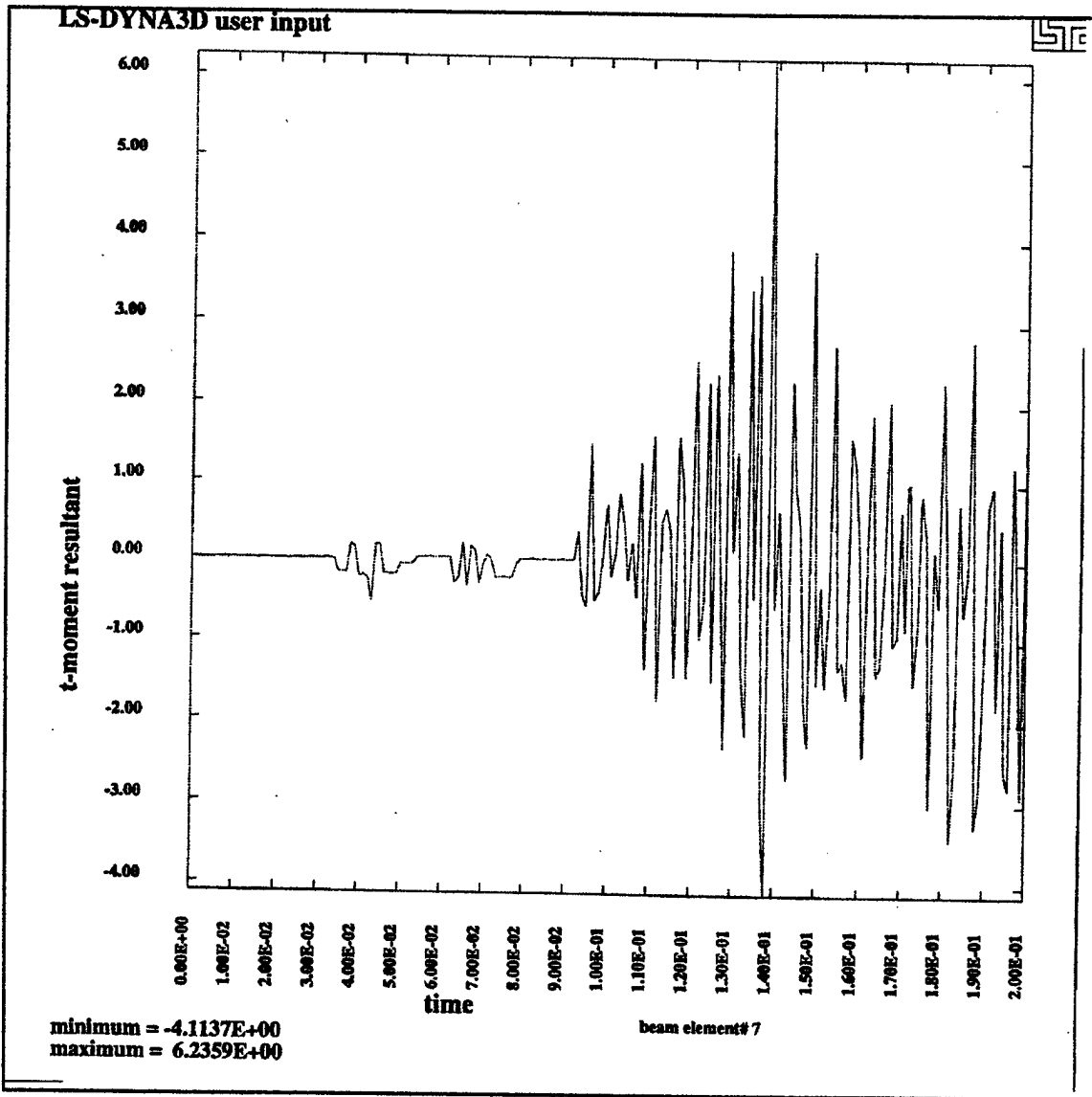


Figure 5.12. Bending moment on C4 vertebra for Case 1

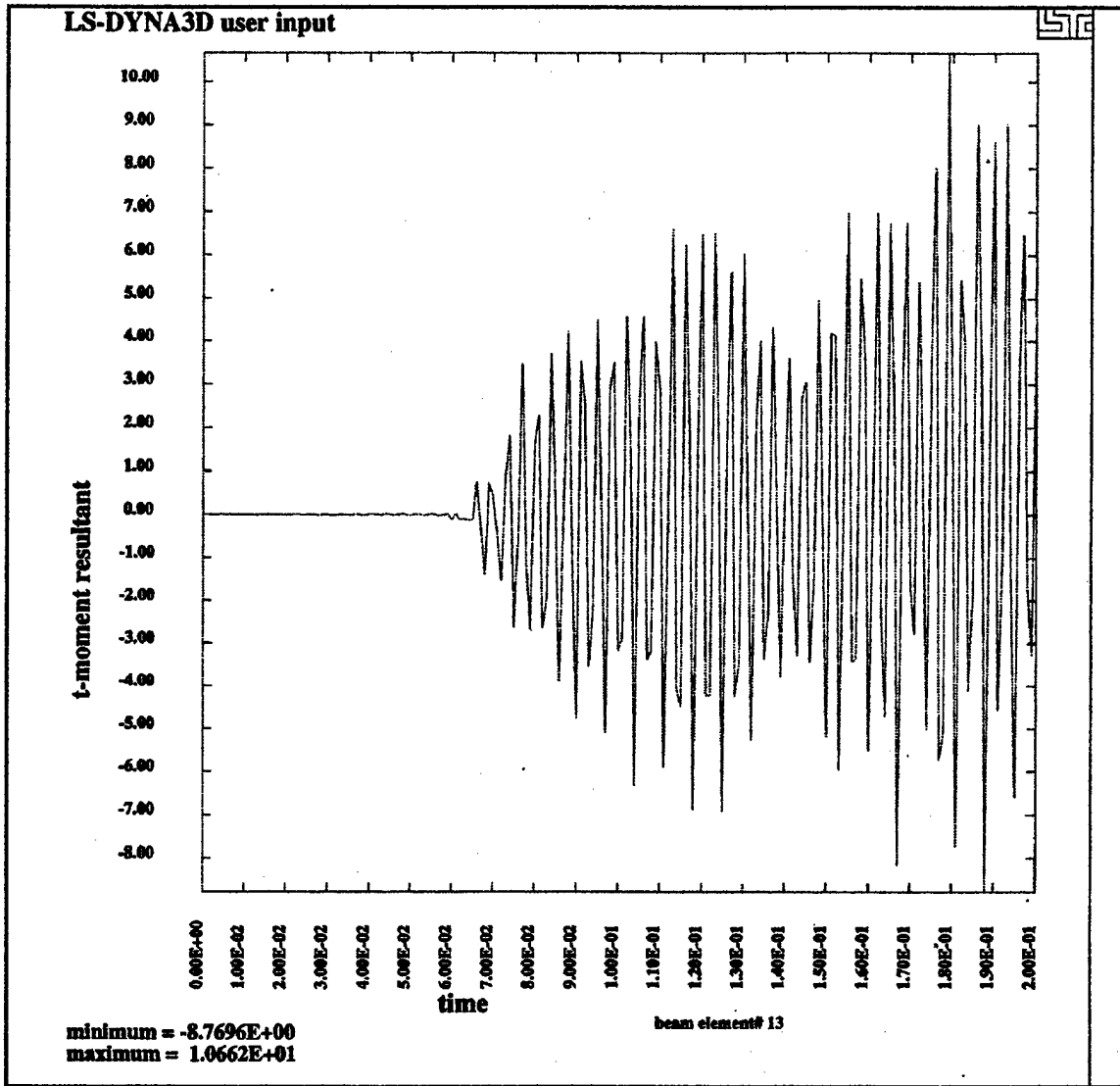


Figure 5.13. Bending moment on C7 vertebra for Case 1

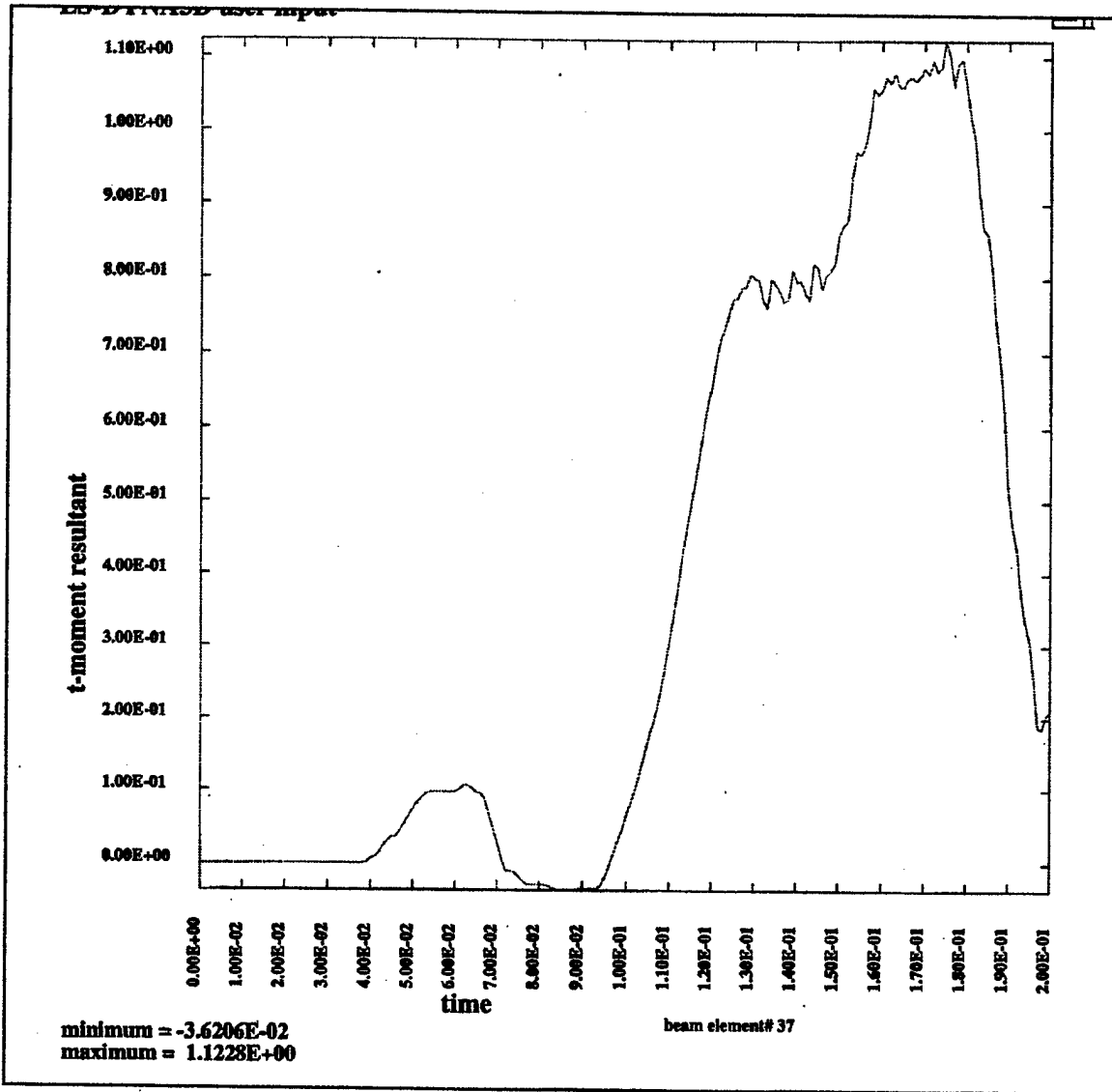


Figure 5.14. Bending moment on C3-C5 disc for Case 1

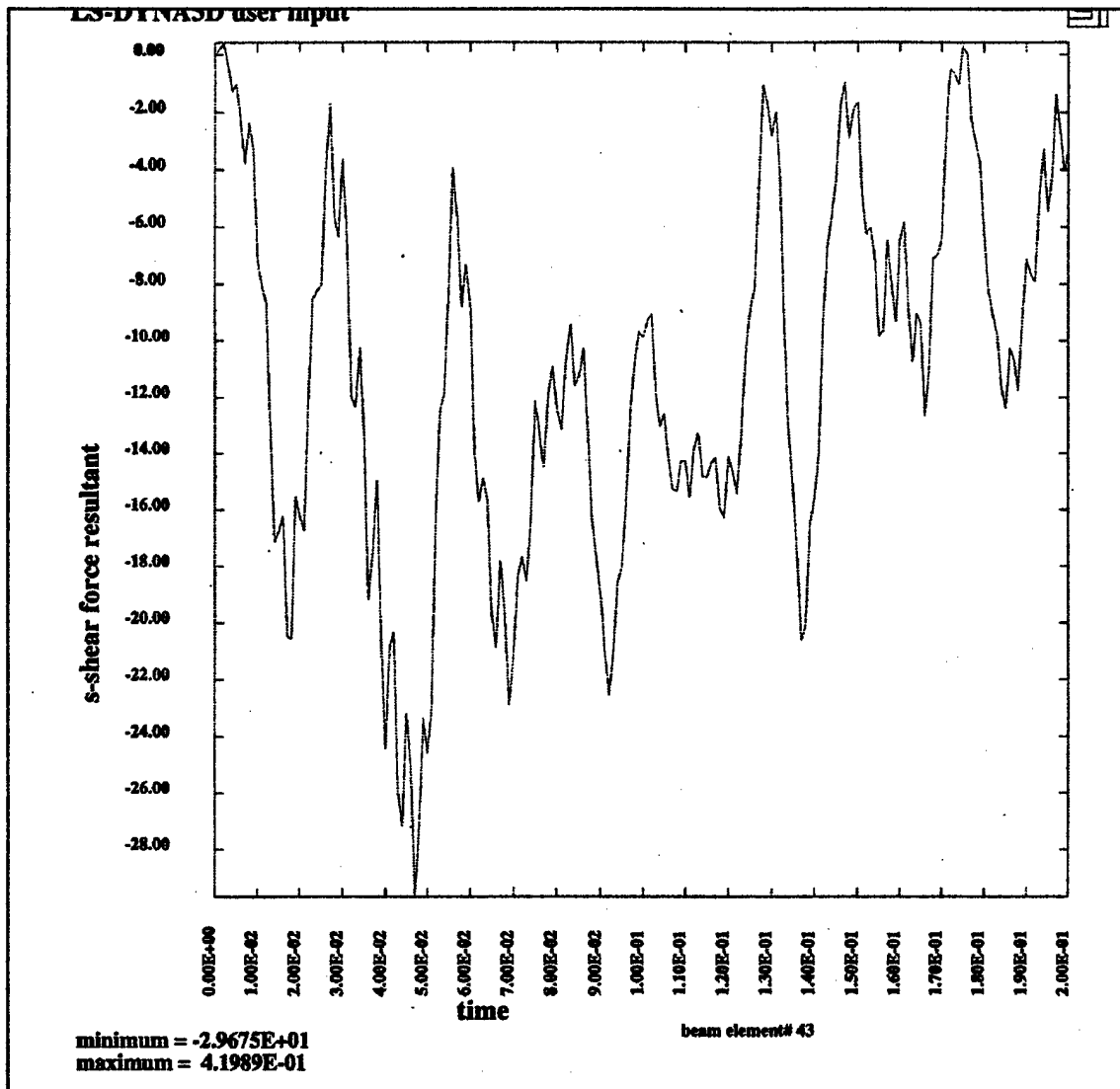


Figure 5.15. Shear force acting on facet joints of cervical spine for Case 1

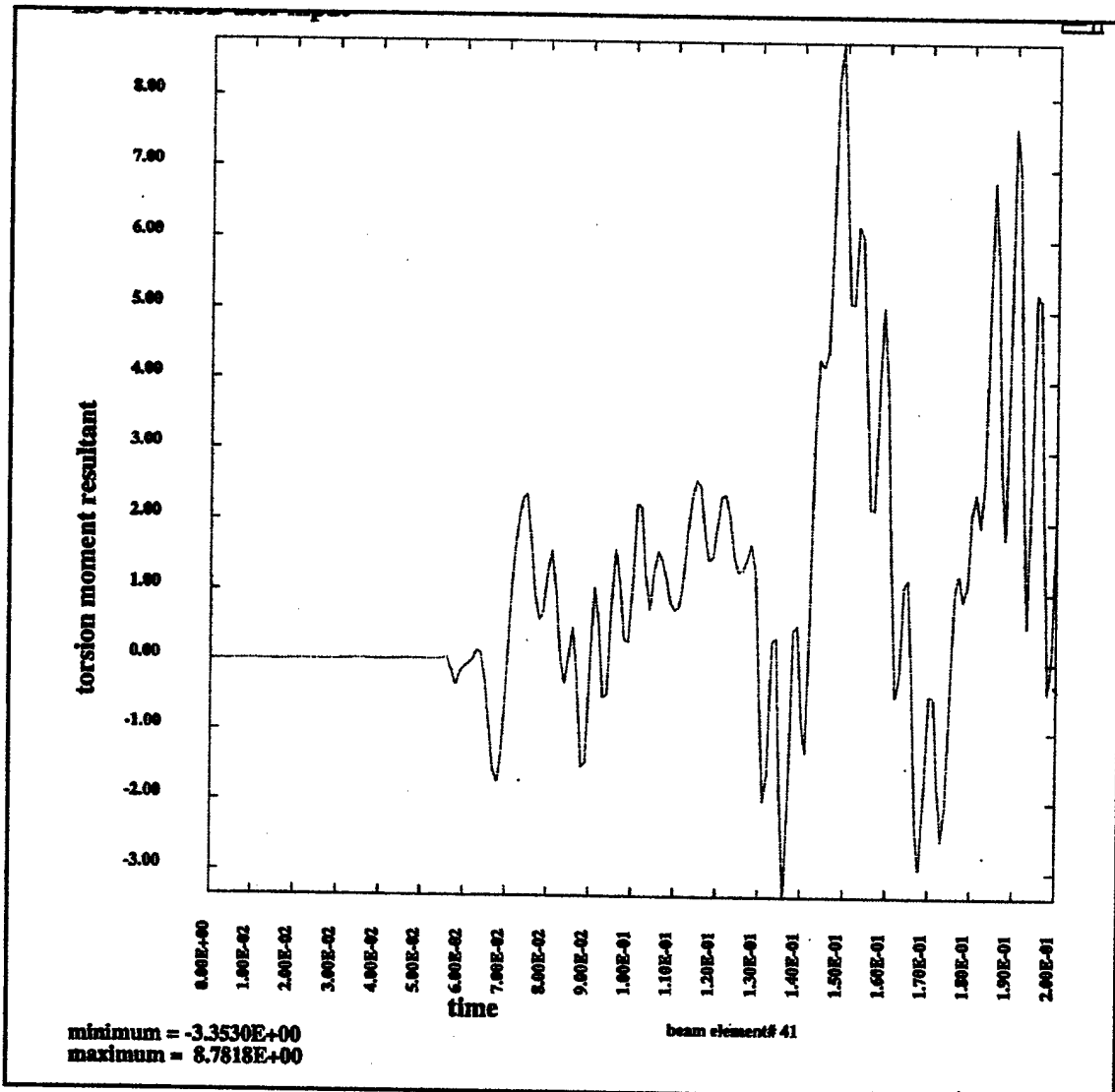


Figure 5.16. Torsional moment acting on facet joints of cervical spine for Case 1

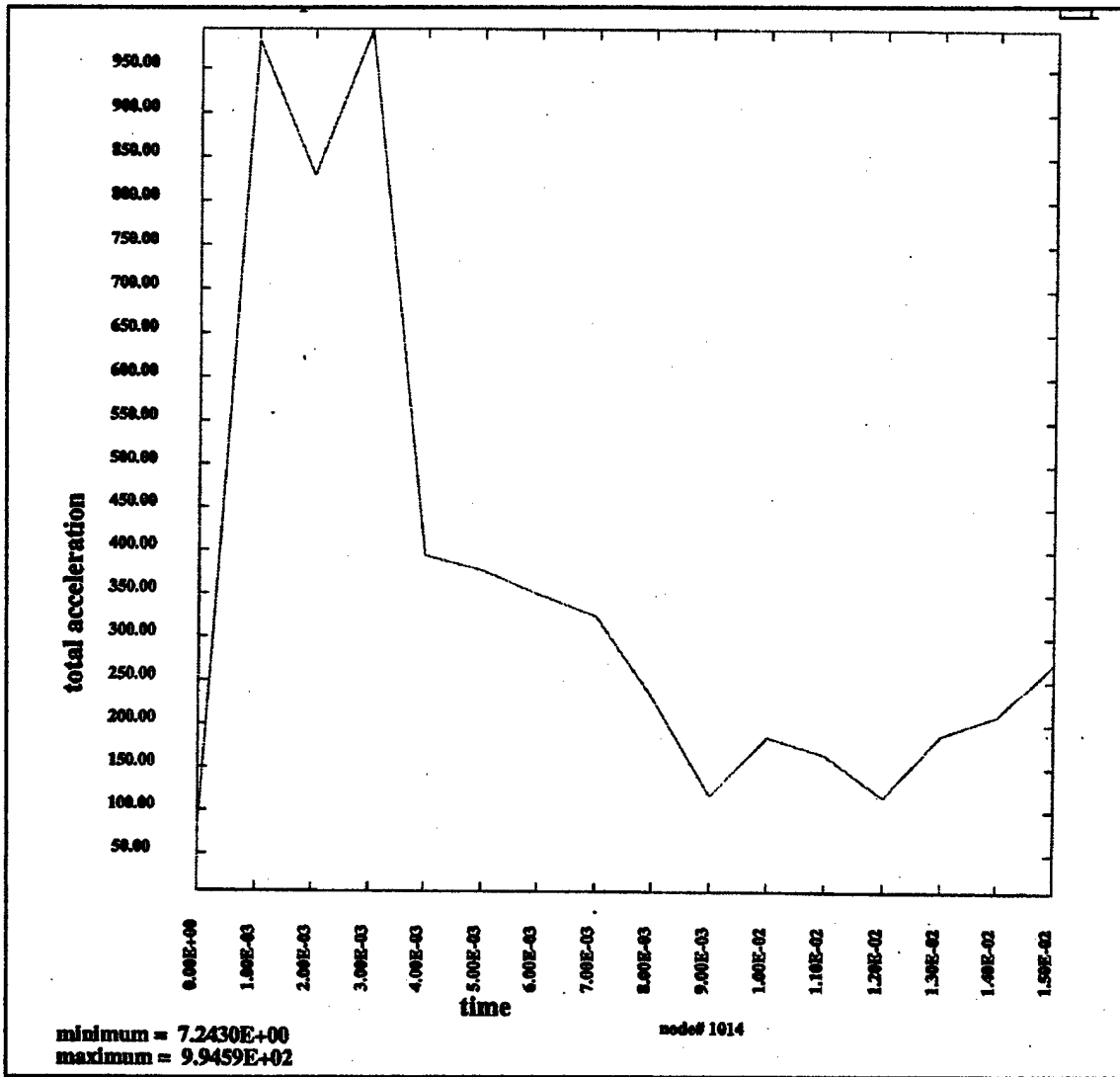


Figure 5.17. Acceleration profile used to calculate HIC for Case 2

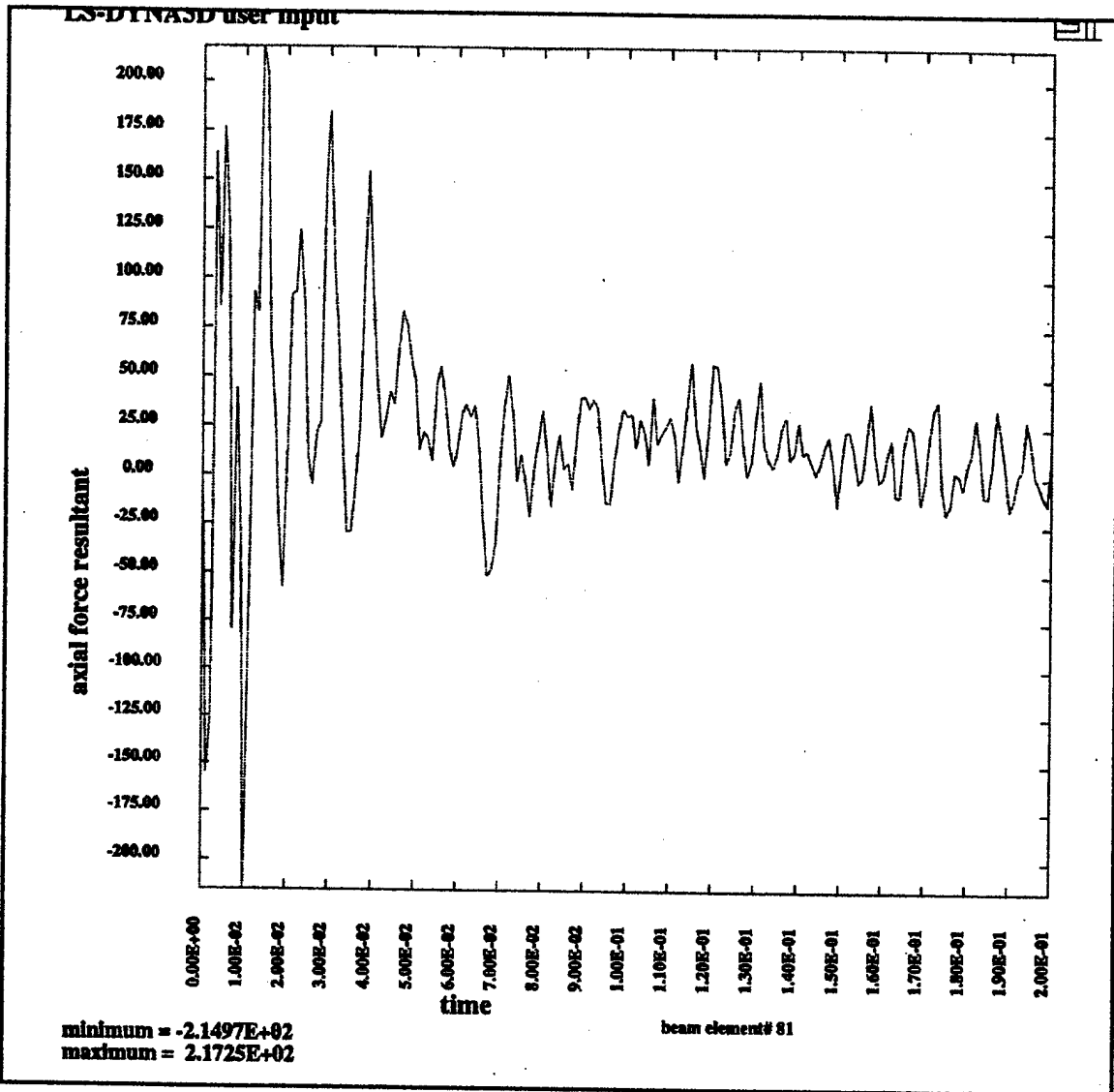


Figure 5.18. Axial force on the occipital condyle for Case 2

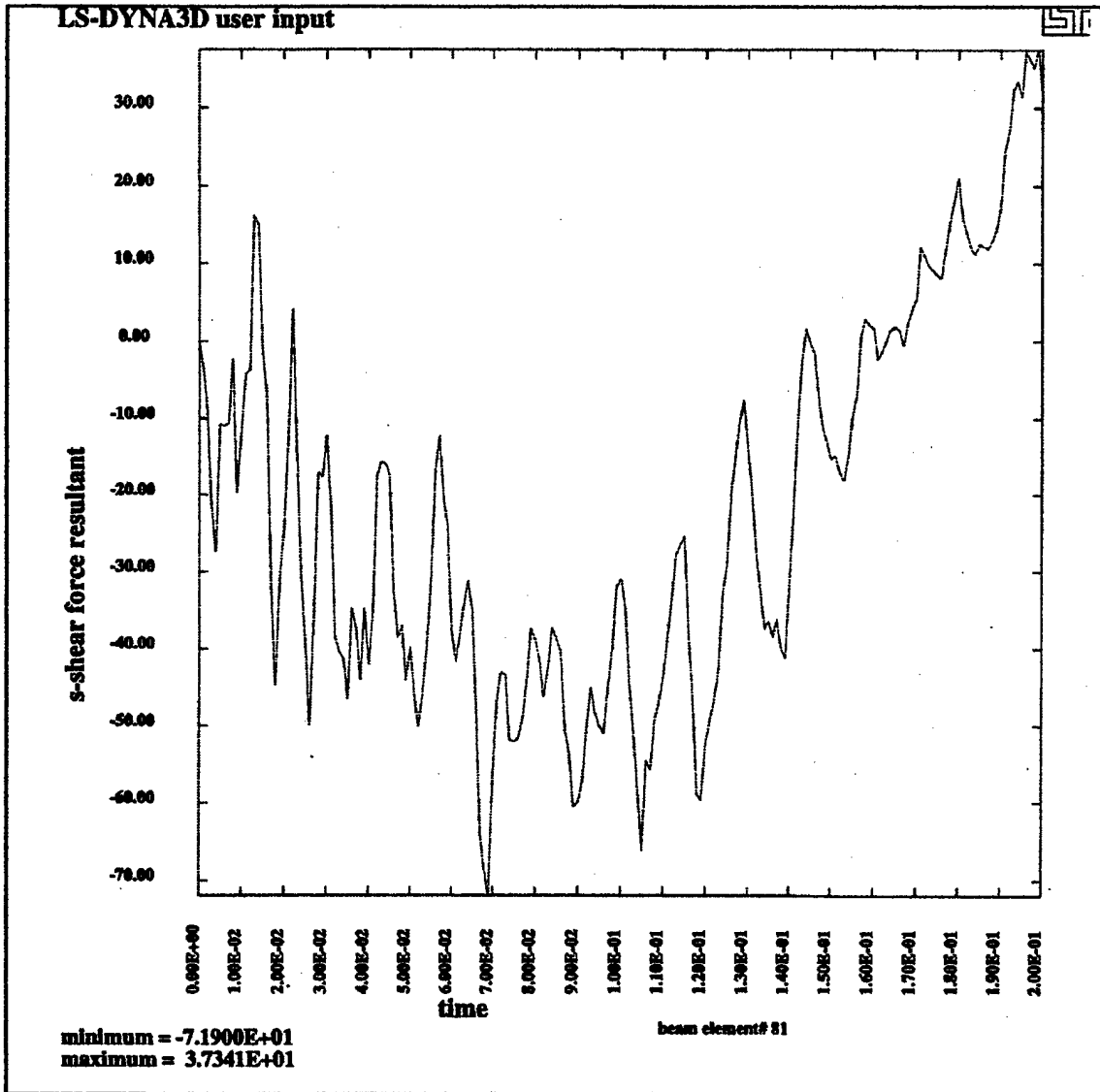


Figure 5.19. Shear force on the occipital condyle for Case 2

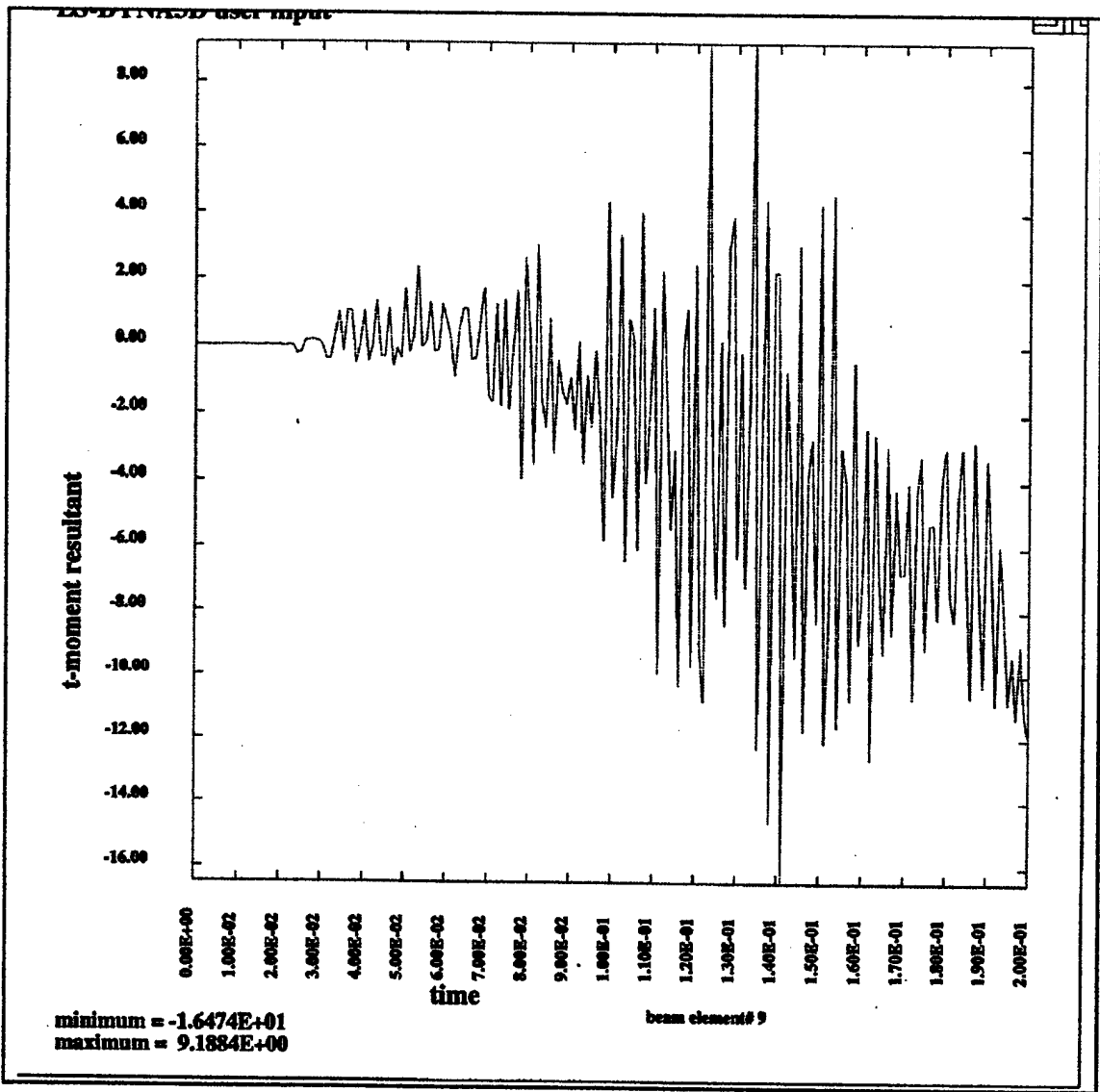


Figure 5.20. Bending moment on C5 vertebra for Case 2

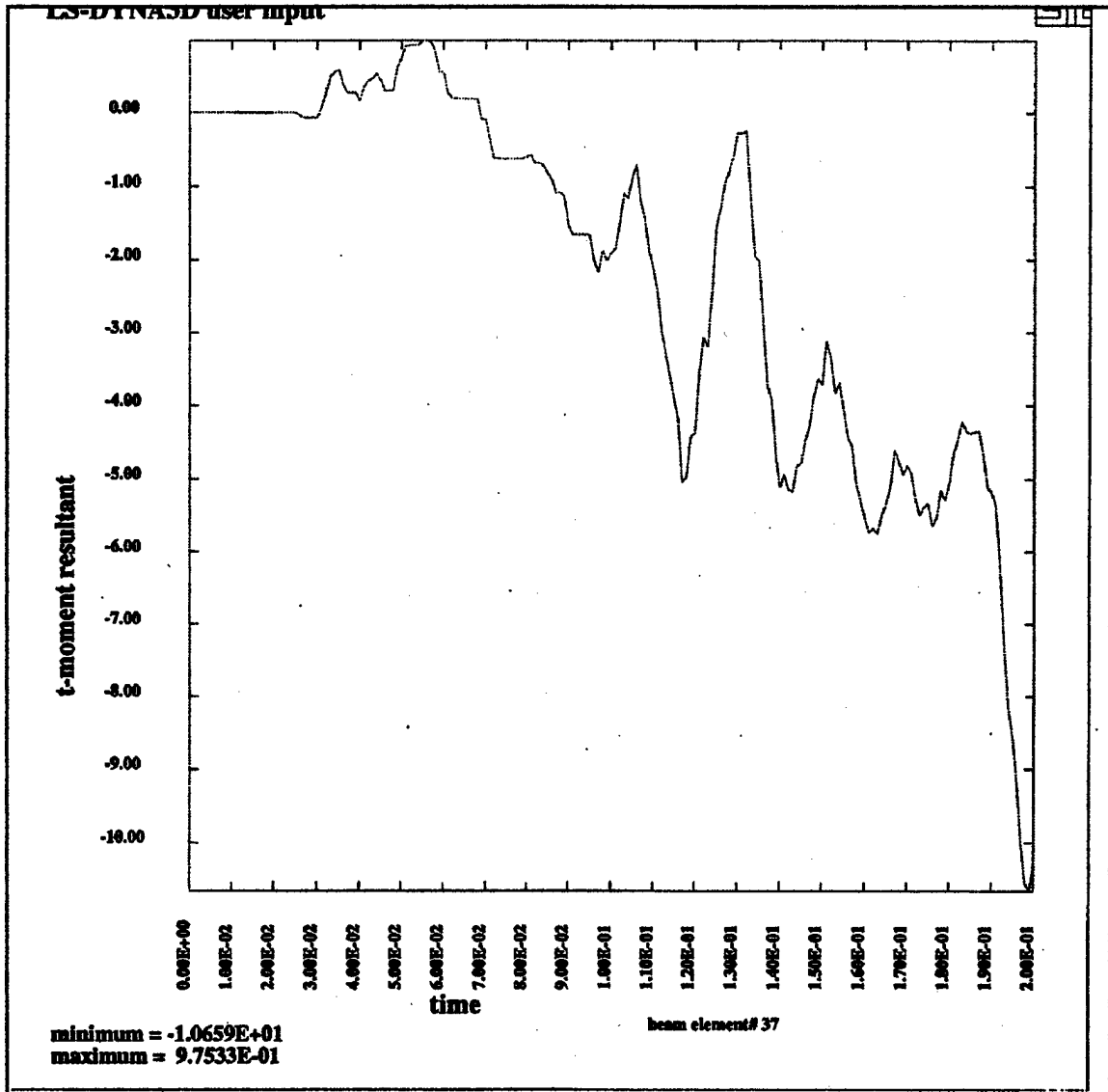


Figure 5.21. Bending moment on C3-C4 disc for Case 2

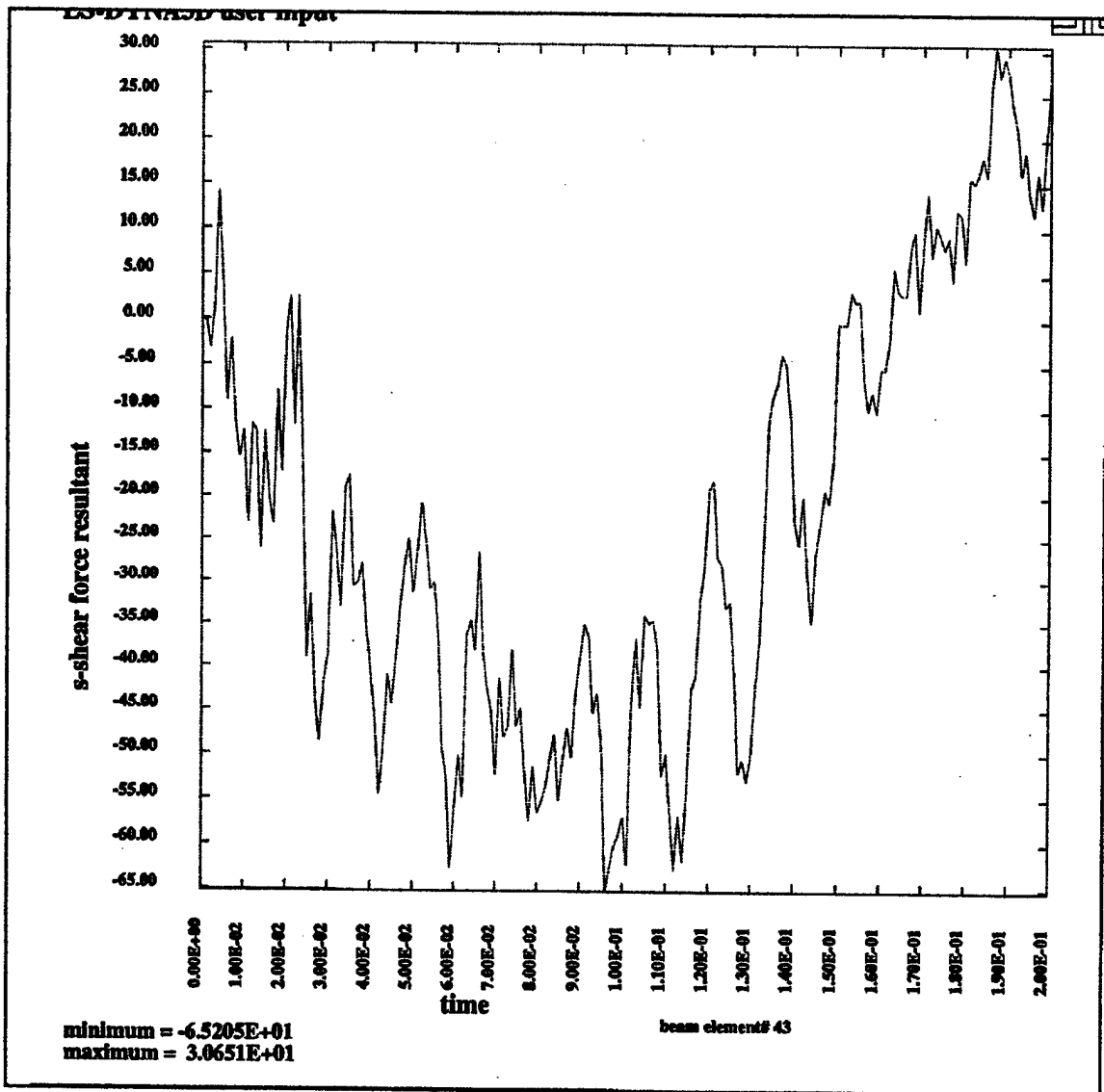


Figure 5.22 Shear force acting on facet joints of cervical spine for Case 2

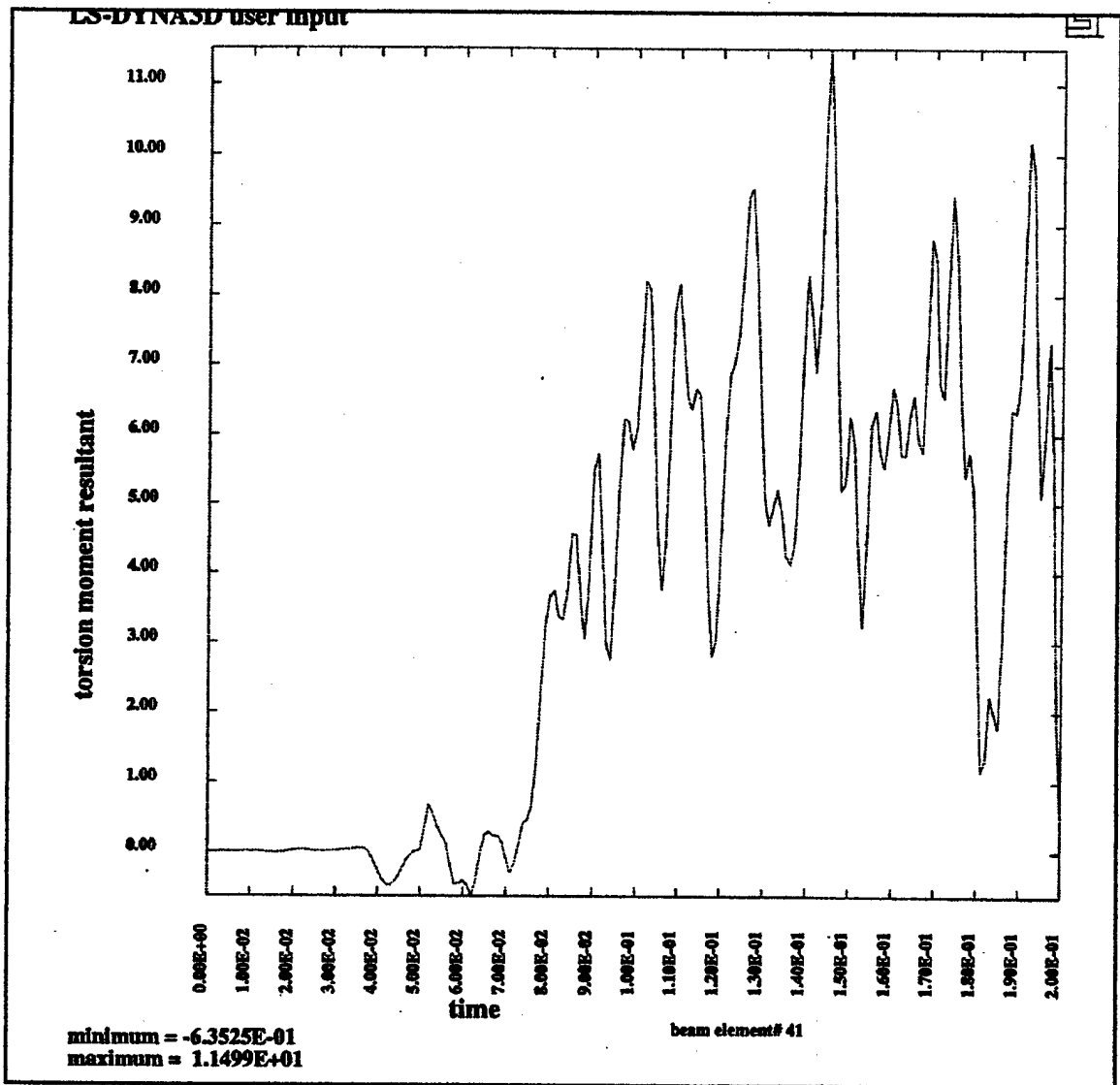


Figure 5.23. Torsional moment acting on facet joints of cervical spine for Case 2

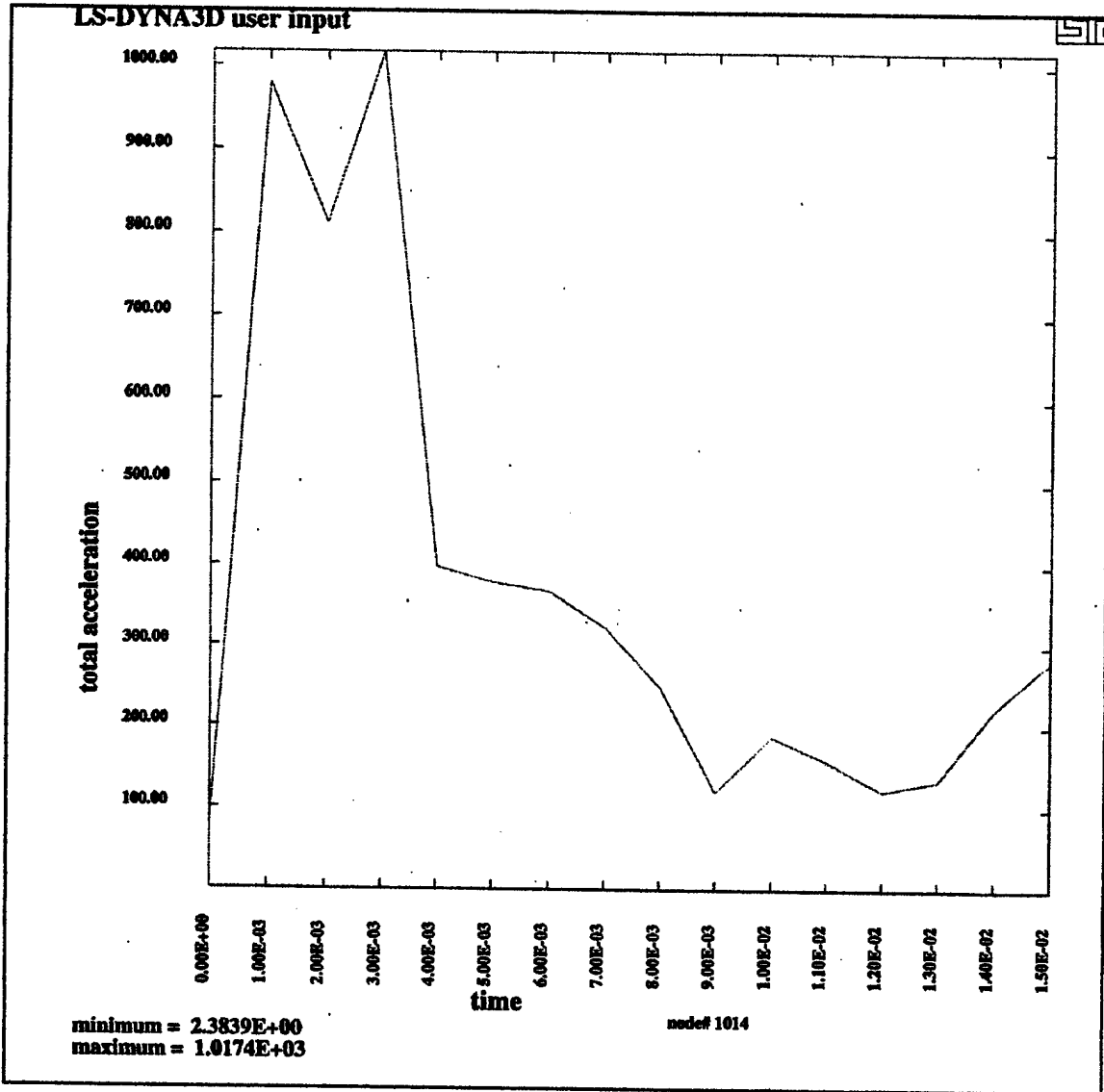


Figure 5.24. Acceleration profile used to calculate HIC for Case 3

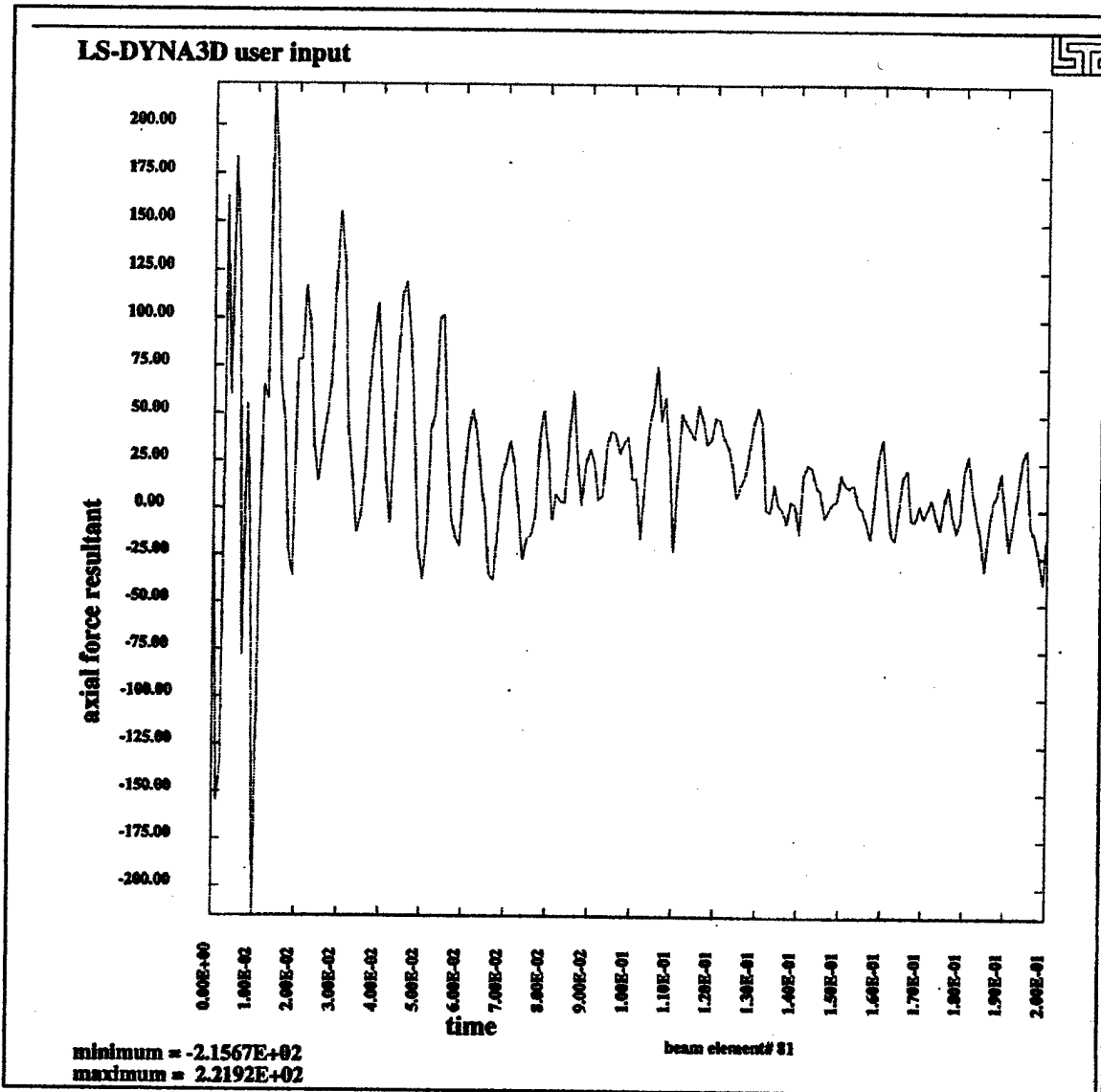


Figure 5.25. Axial force on occipital condyle for Case 3

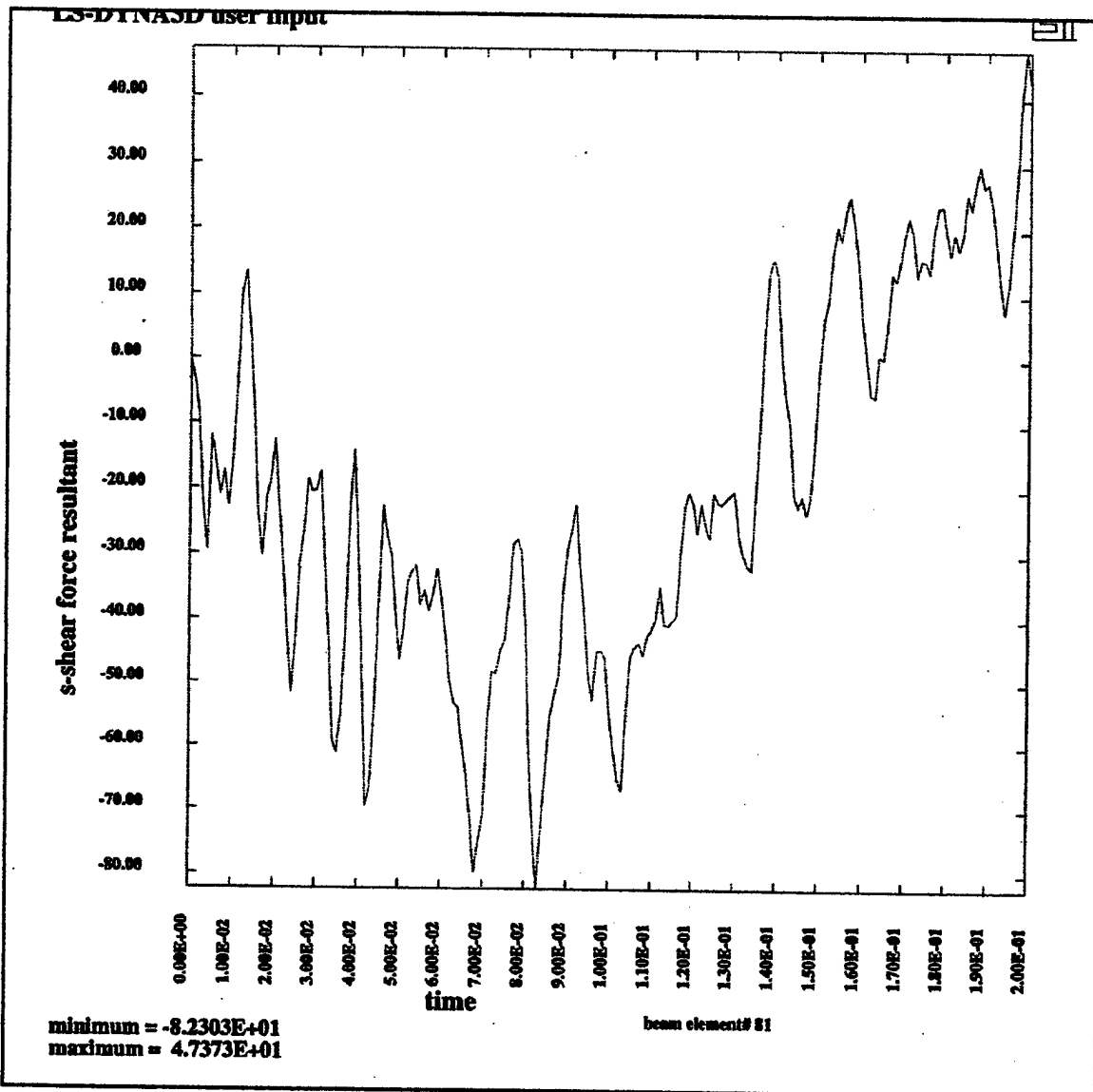


Figure 5.26. Shear force on occipital condyle for Case 3

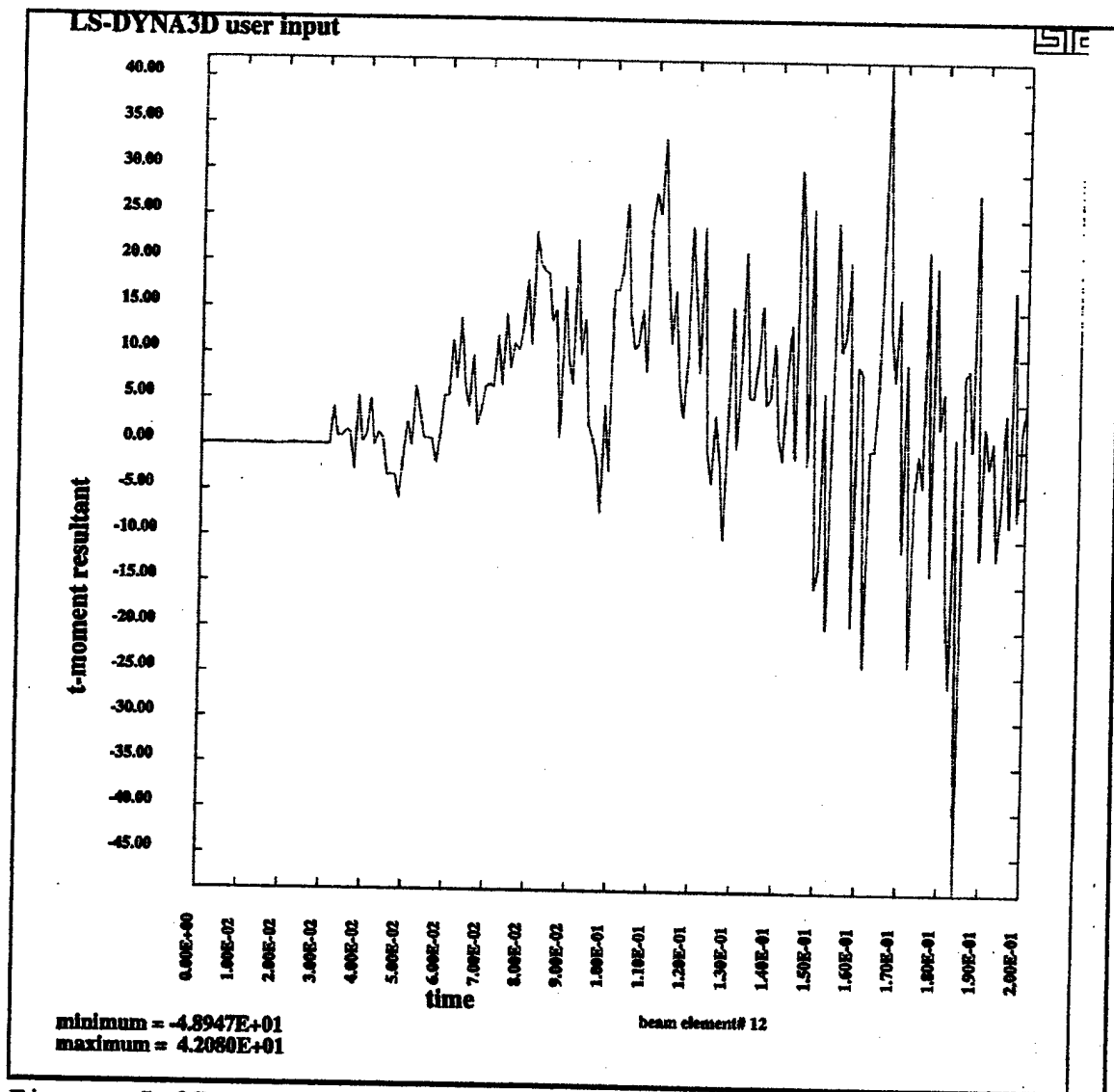


Figure 5.27. Bending moment on C6 vertebra for Case 3

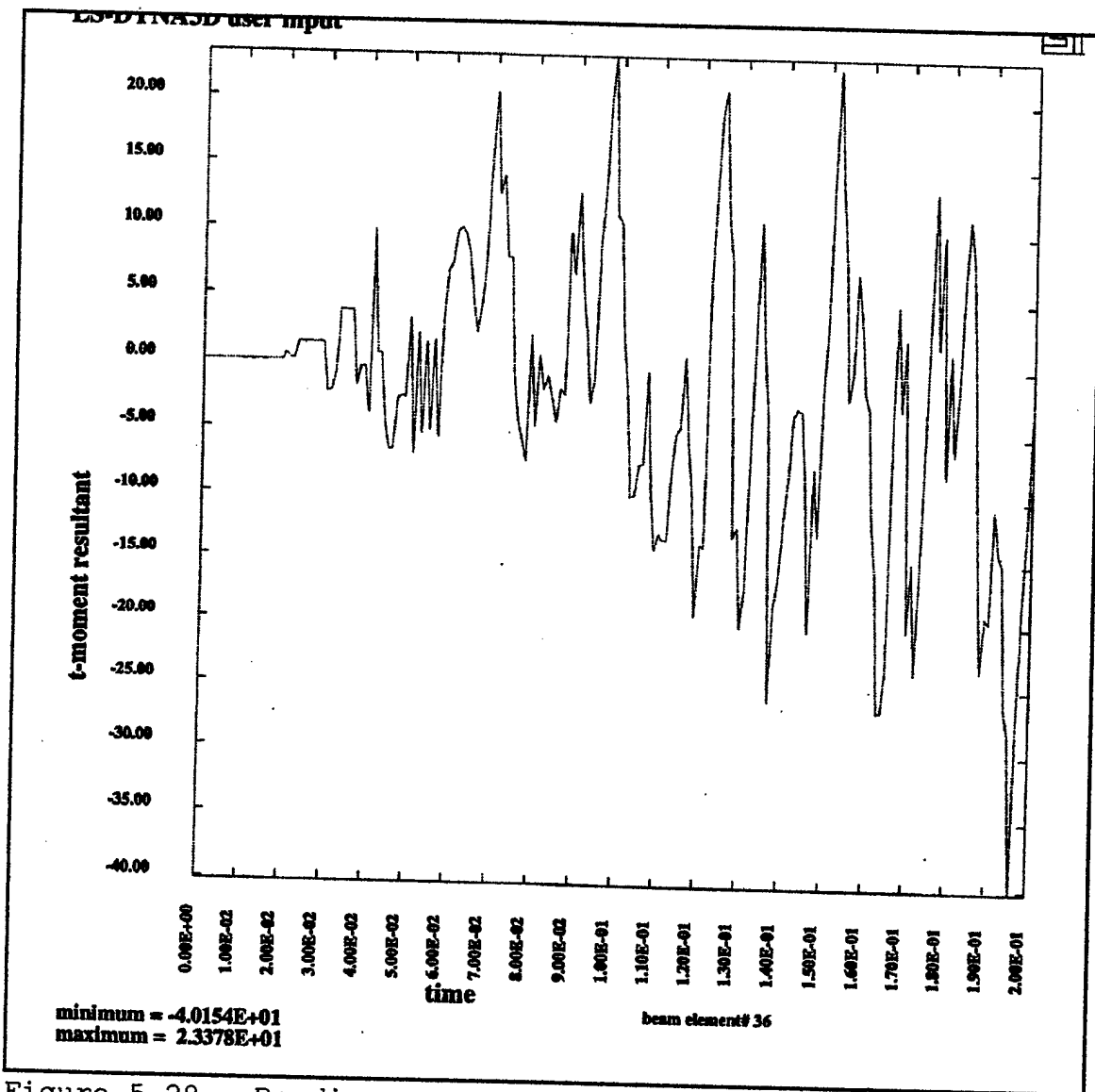


Figure 5.28. Bending moment of C3-C4 disc for Case 3

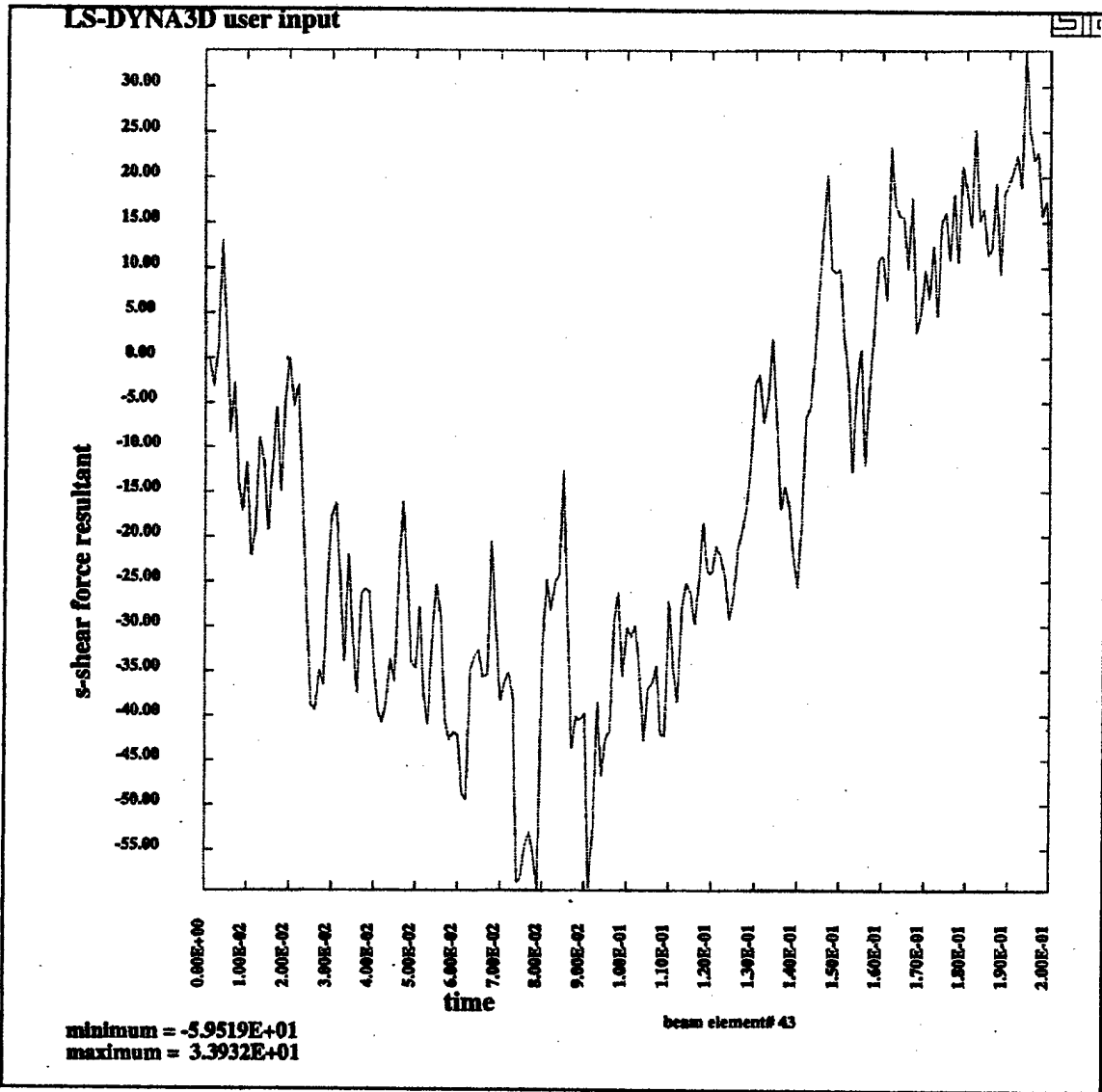


Figure 5.29. Shear moment acting on facet joints of cervical spine for Case 3

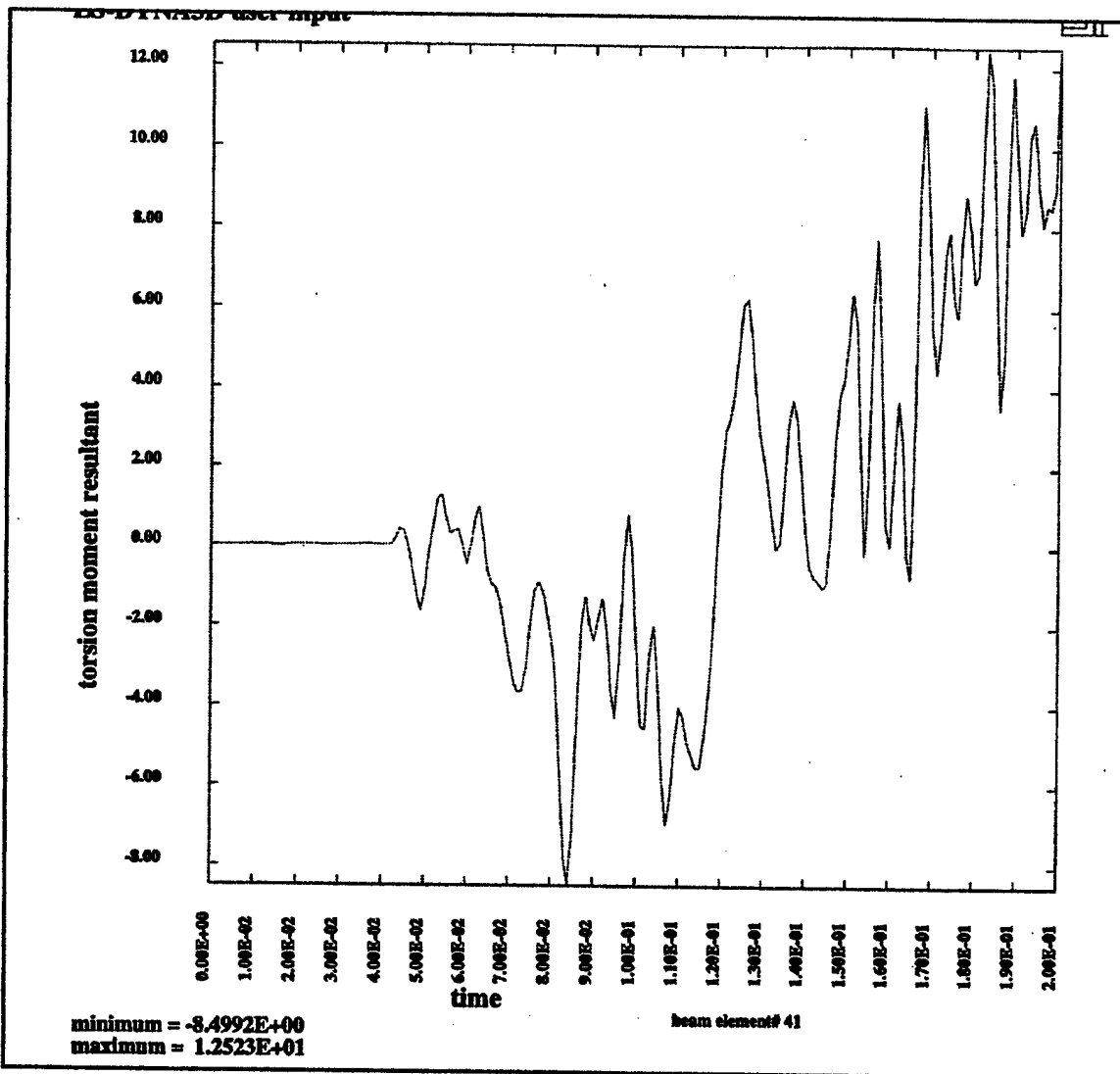


Figure 5.30. Torsion moment acting on facet joints of cervical spine for Case 3

C. BACK IMPACT

Additional runs were made using the material properties from Case 3 to examine the loading conditions from different directions. The next case to be explored is a fragment impact to the back of the helmet. This induces a flexion moment in the cervical spine. The position of the fragment relative to the helmet before impact is shown in Figure 5.31. The history of the stress field induced by the collision is shown in Figure 5.32 through Figure 5.35. The stress is a maximum right after impact of 1.01×10^6 Pa. This stress slowly decays but is still greater than 7.66×10^3 Pa after 200 ms.

Figure 5.36 shows the total acceleration of the center of gravity of the head for the first 15 ms after impact. The area under this curve was used to calculate an HIC value of 64.0. The maximum axial force acting on the occipital condyle, shown in Figure 5.37, is 336.1 N. Figure 5.38 shows the maximum shear force acting on the occipital condyle to be 360.0 N. The maximum bending moment for the vertebra, shown in Figure 5.39, is 36.0 Nm and occurs at C3. Figure 5.40 shows the maximum bending moment for vertebral discs occurs at C4-C5. It is 28.9 Nm. The ability of the facet joints to resist shearing and torsional moments are shown in Figures 5.41 and 5.42. The shearing force is 27.5 N. The torsional moment is 13.3 Nm.

The maximum bending moment is 34.6% of the flexion IARV listed in Table 4.3 and 60.6% of the pain threshold listed in Table 4.4. These values are unlikely to cause severe damage, but may lead to the type of minor injuries described above.

The bending moment acting on the discs is a maximum at the C4-C5 level and exceeds the critical value listed in Table 4.4. This is likely to cause a severe rupture of that disk. Disc C3-C4 also exceeded the critical value and faces a probable rupture as well.

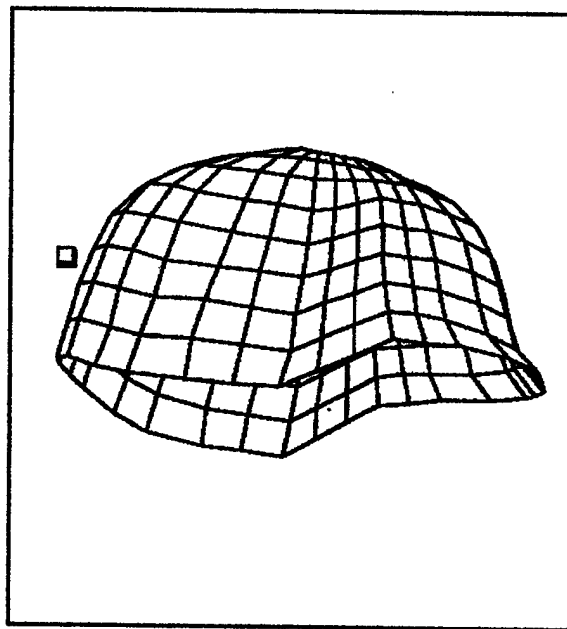


Figure 5.31. View of helmet and fragment prior to rear impact



Figure 5.32. Von Mises stress induced in helmet after 1 ms



Figure 5.33. Von Mises stress induced in Helmet after 10 ms

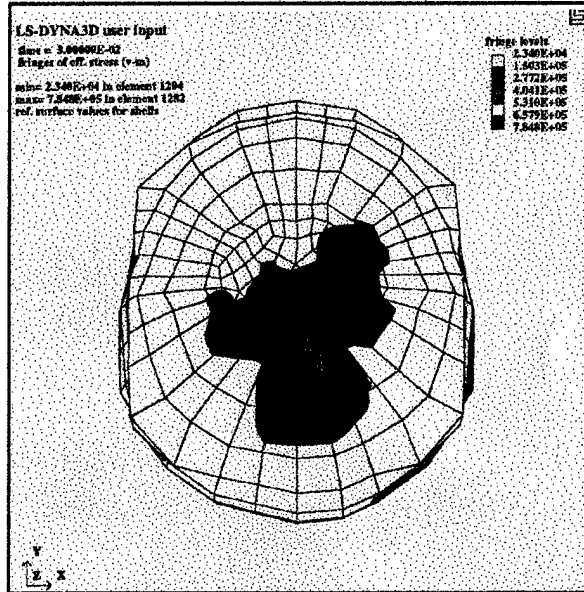


Figure 5.34. Von Mises stress induced in helmet 30 ms after rear impact

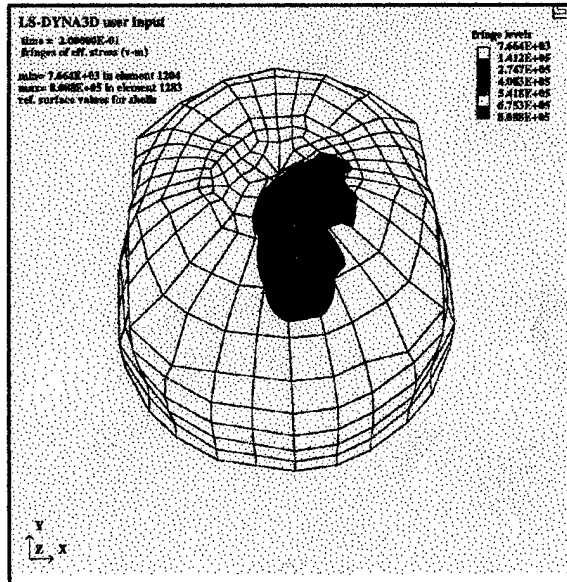


Figure 5.35. Von Mises stress induced in helmet after 200 ms

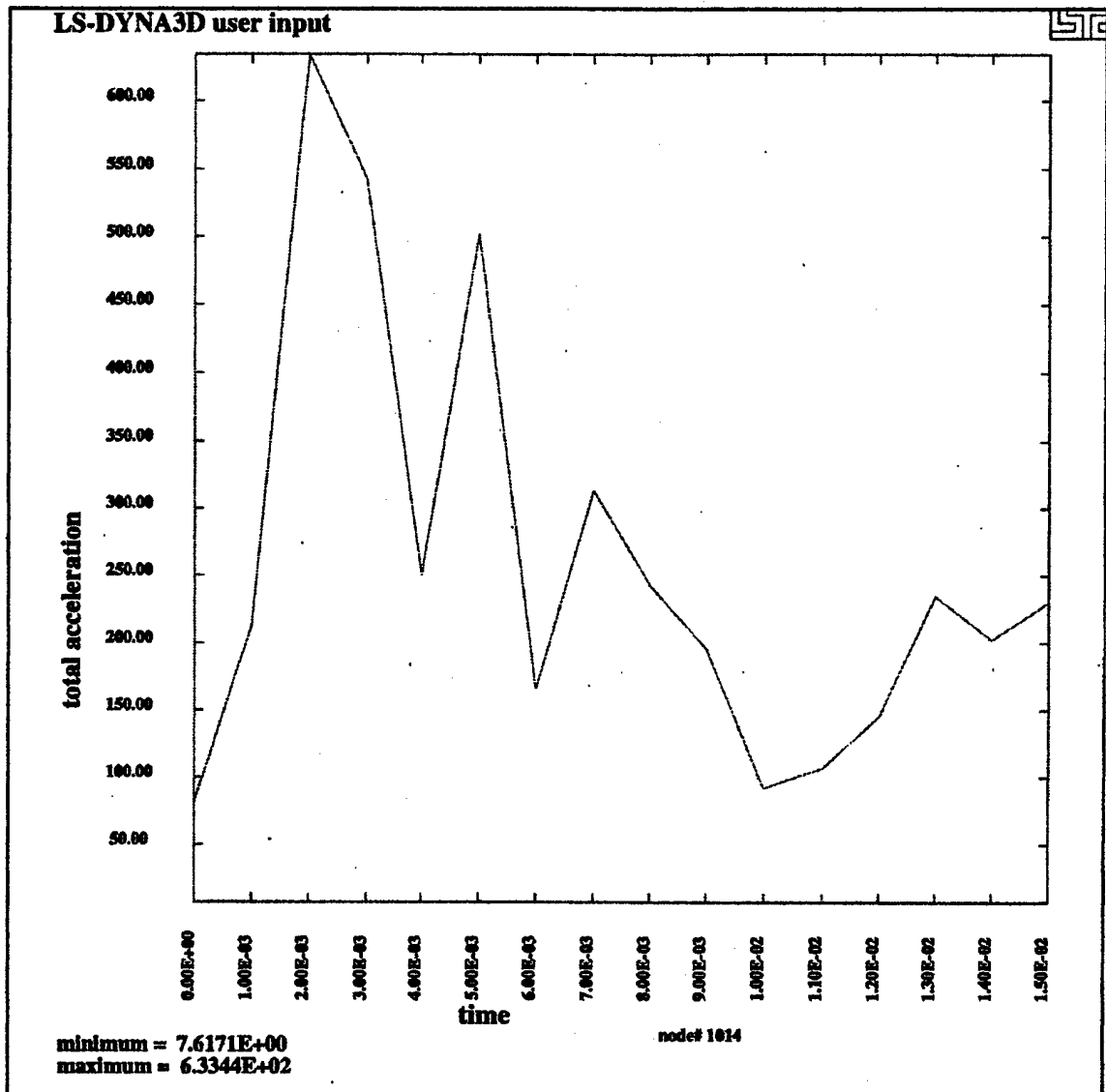


Figure 5.36. Acceleration profile used to calculate HIC for rear impact case

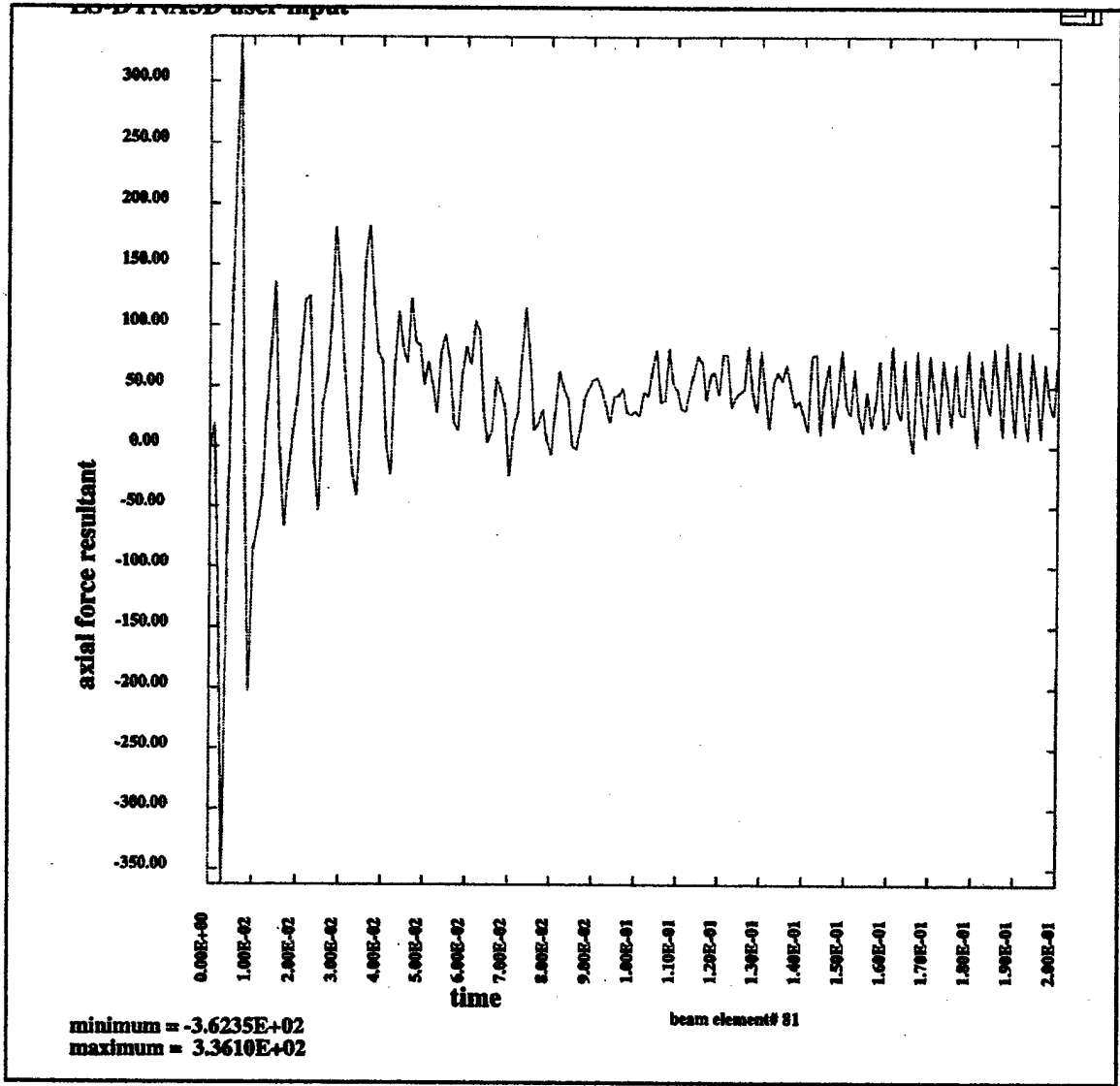


Figure 5.37. Axial force on occipital condyle for rear impact case.

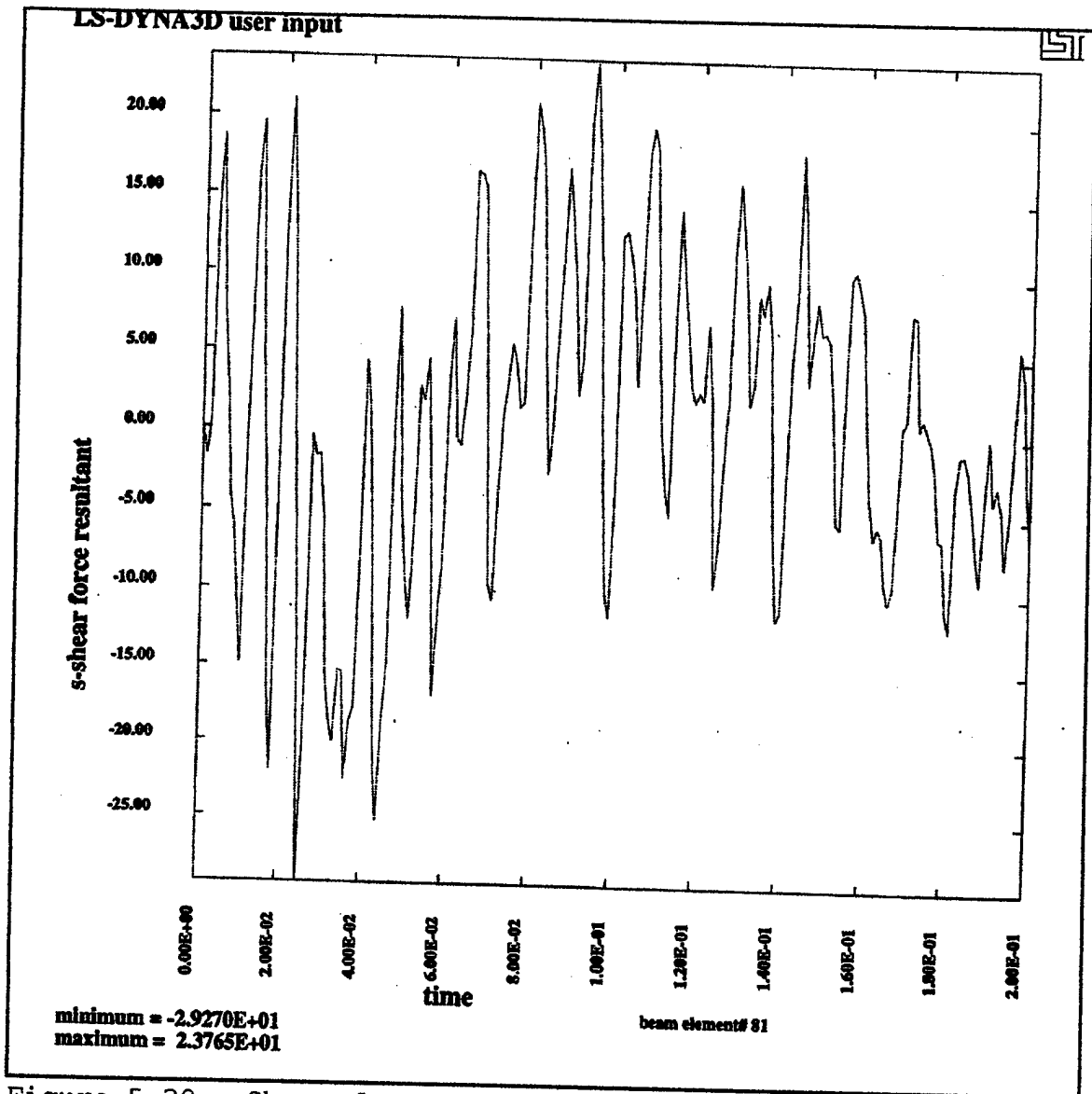


Figure 5.38. Shear force on occipital condyle for rear impact case

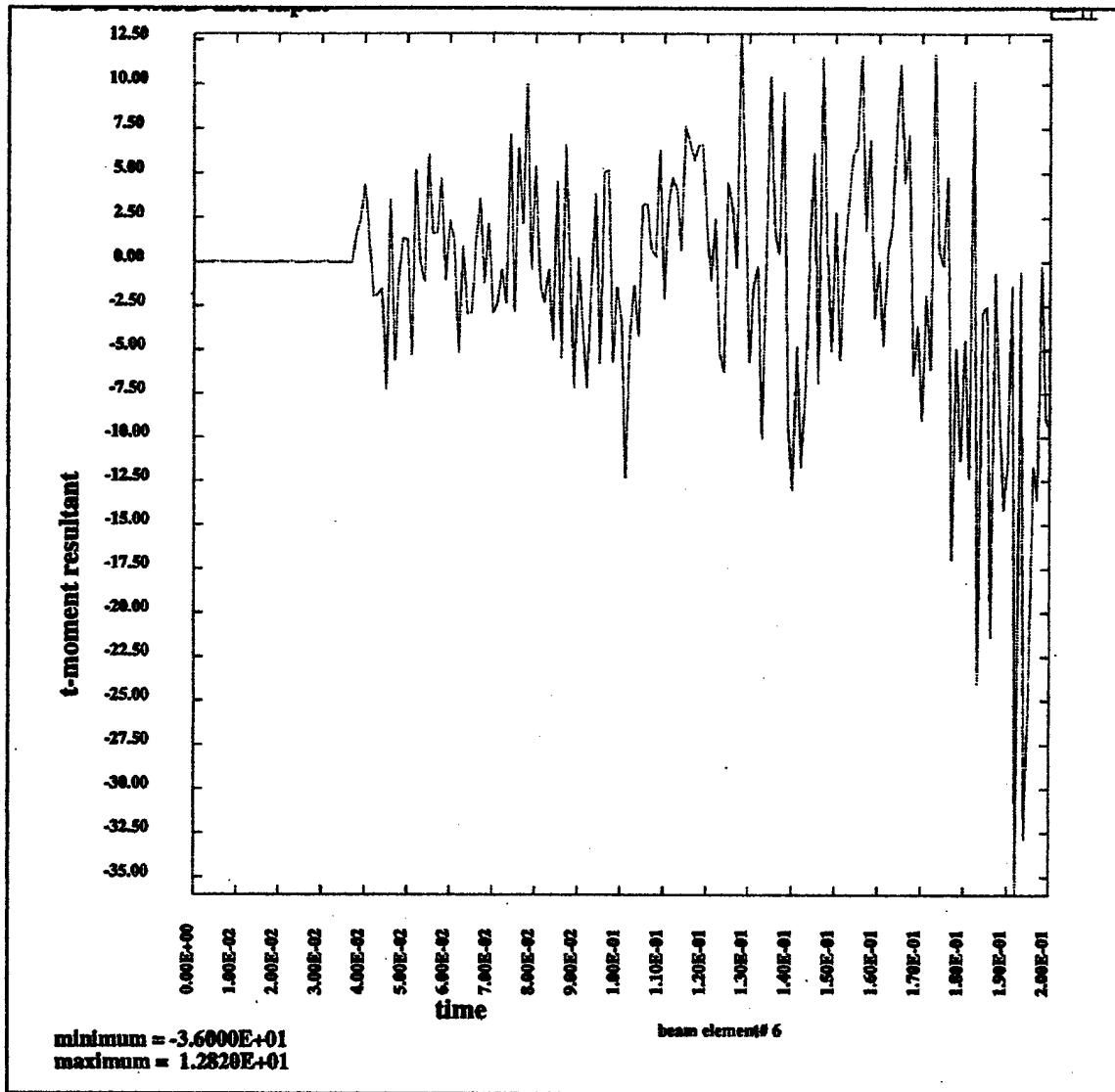


Figure 5.39. Bending moment on C3 vertebra for rear impact case

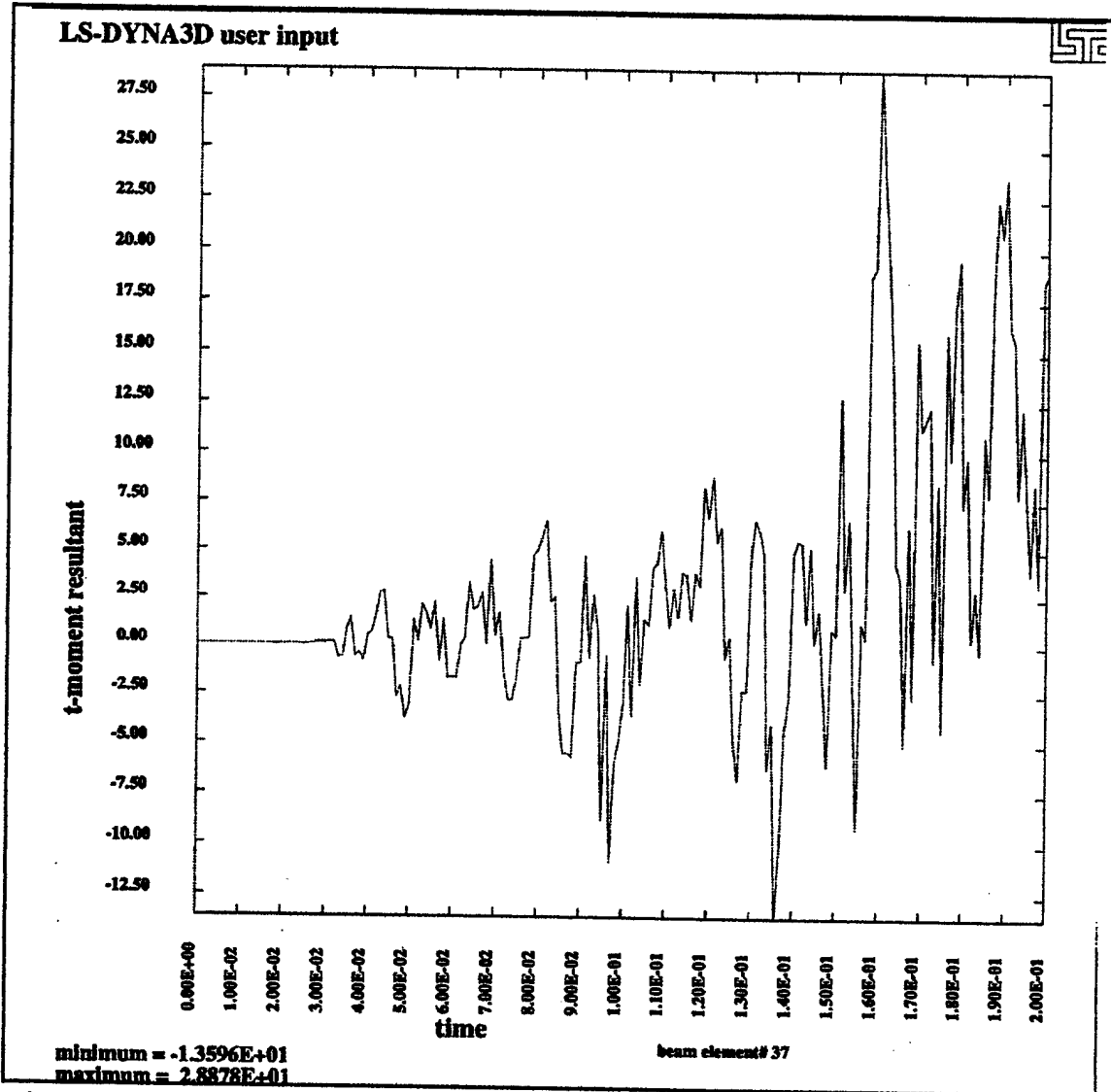


Figure 5.40. Bending moment on C4-C5 disc for rear impact case

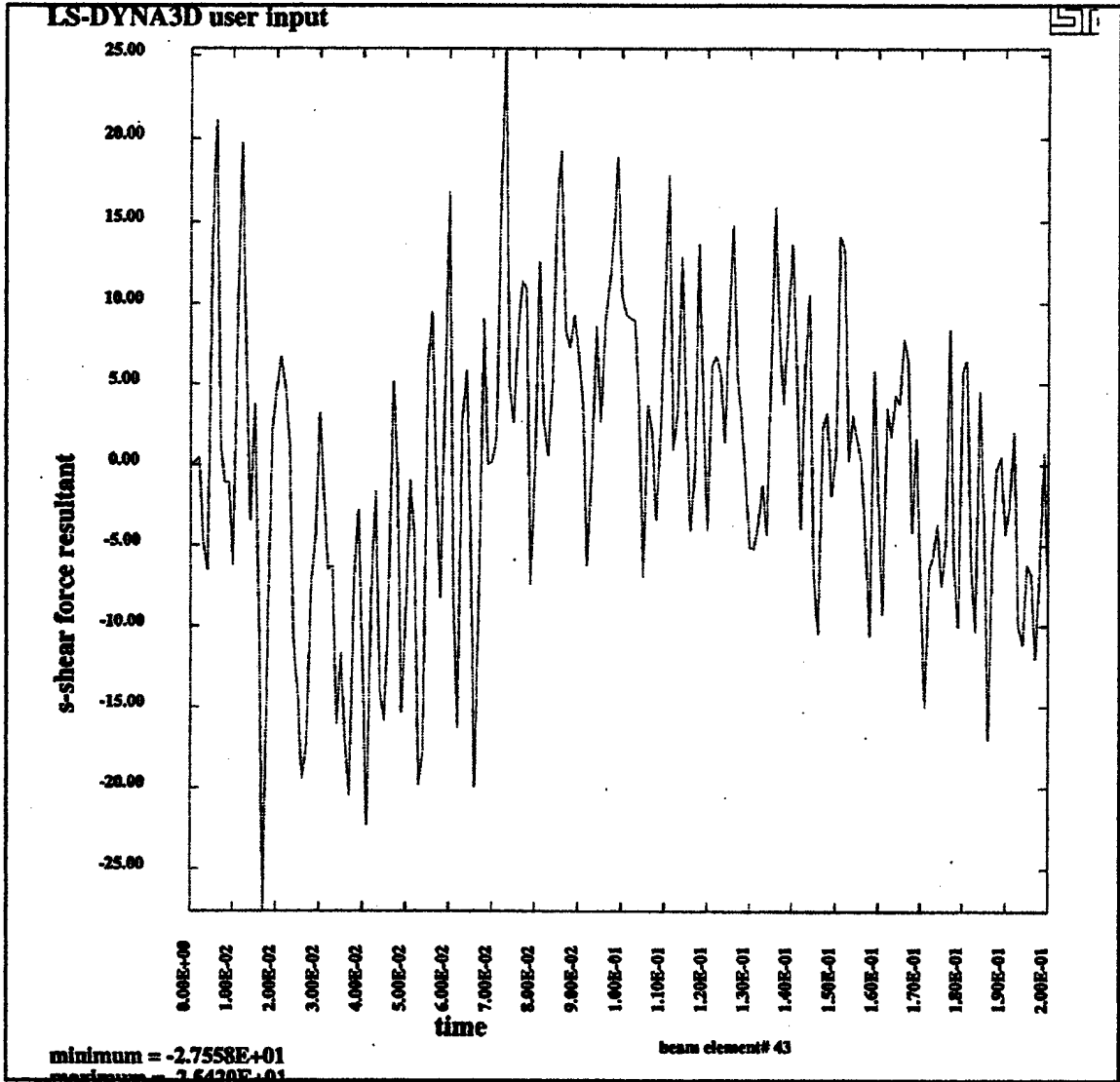


Figure 5.41. Shear force acting on facet joints of cervical spine during rear impact

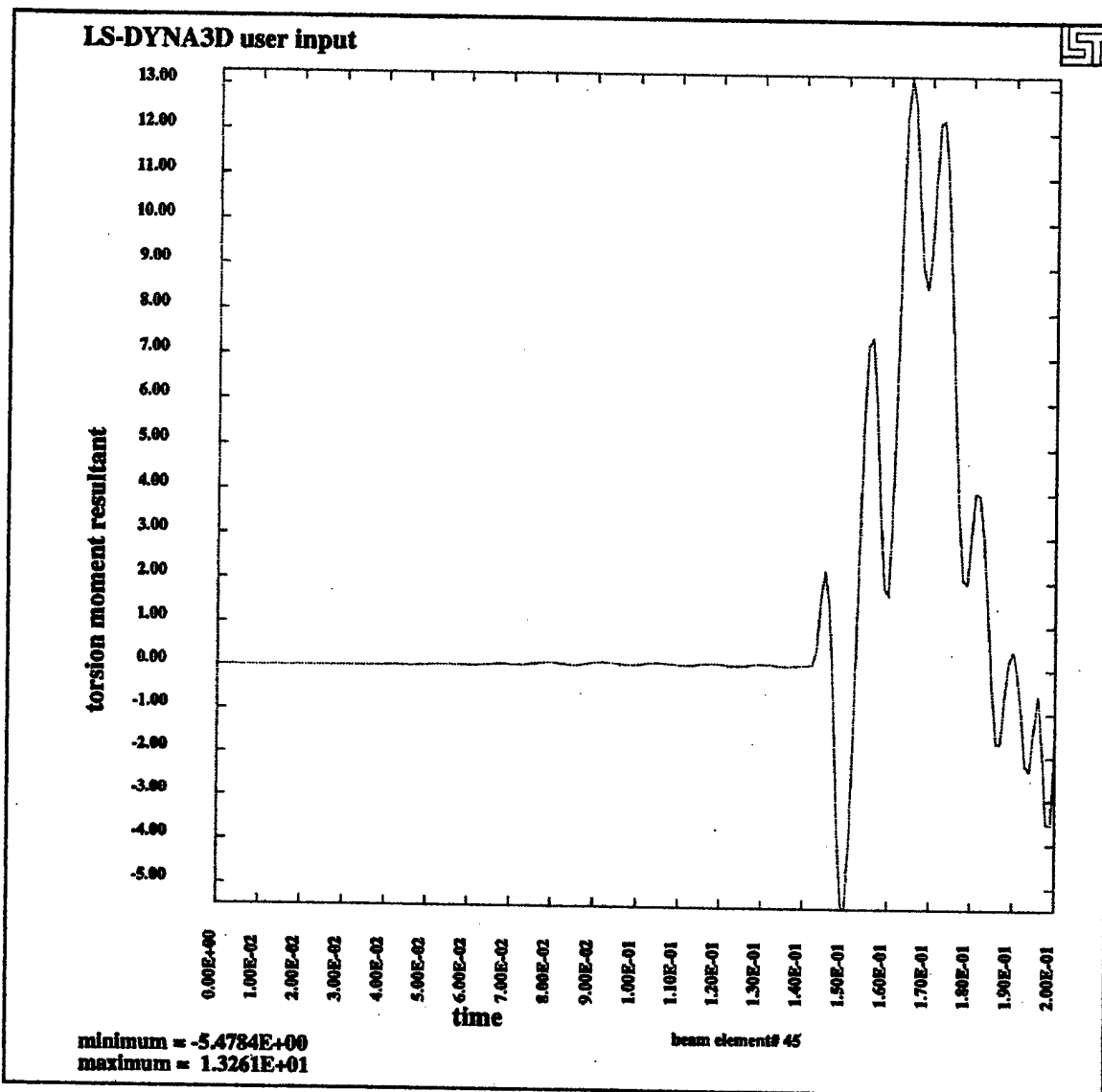


Figure 5.42. Torsion moment acting on the facet joints of cervical spine during rear impact case

D. TOP IMPACT

The next case to be explored is a fragment impact to the top of the helmet. This creates a combination loading condition by inducing an extension moment in addition to the expected compression load. The position of the fragment relative to the helmet before impact is shown in Figure 5.43. The history of the stress field induced by the collision is shown in Figure 5.44 through Figure 5.47. The stress is a maximum right after impact of 2.99×10^6 Pa. This stress slowly decays but is still greater than 1.43×10^4 Pa after 200 ms.

Figure 5.48 shows the total acceleration of the center of gravity of the head for the first 15 ms after impact. The area under this curve was used to calculate an HIC value of 143.1. The maximum axial force acting on the occipital condyle, shown

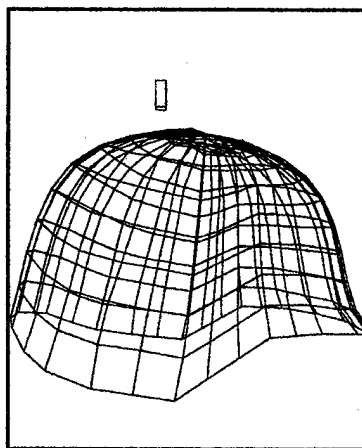


Figure 5.43 View of helmet prior to top impact

in Figure 5.49, is 253.4 N. Figure 5.50 shows the maximum shear force acting on the occipital condyle to be 73.8 N. The maximum compressive force on the vertebra is 42.4 N, shown in Figure 5.51, and occurs at C1. The maximum bending moment for the vertebra, shown in Figure 5.52, is 47.9 Nm and occurs at C5. Figure 5.53 shows the maximum bending moment for vertebral discs occurs at C4-C5. It is 31.8 Nm. The ability of the facet joints to resist shearing and torsional moments are shown in Figures 5.54 and 5.55. The shearing force is 64.5 N. The torsional moment is 17.3 Nm.

The compressive force is well below the potential values listed in Tables 4.3 and 4.4. However, the impact also induces an extension moment in the cervical spine. The IARV potential value from Table 4.3 is exceeded by vertebra C2, C4, C5, and C6 with the maximum occurring at C5. Varying degrees of fractures can be expected at each vertebra.

The critical value for the discs listed in Table 4.4 is exceeded by C3-C4, C4-C5, and C5-C6 with the maximum occurring at the C4-C5 level. This will probably result in severe disc injury. This injury may be in the form of a disc rupture, collapse around a nerve, or other injury.



Figure 5.44. Von Mises stress induced in helmet 1 ms after impact

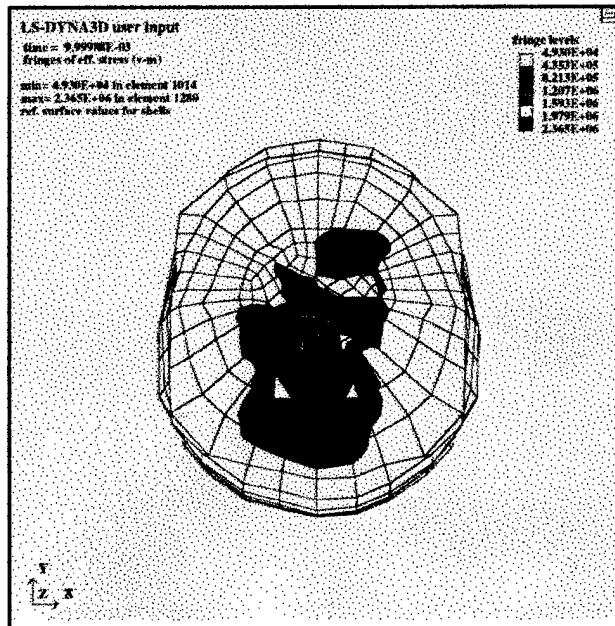


Figure 5.45. Von Mises stress induced in helmet 10 ms after impact

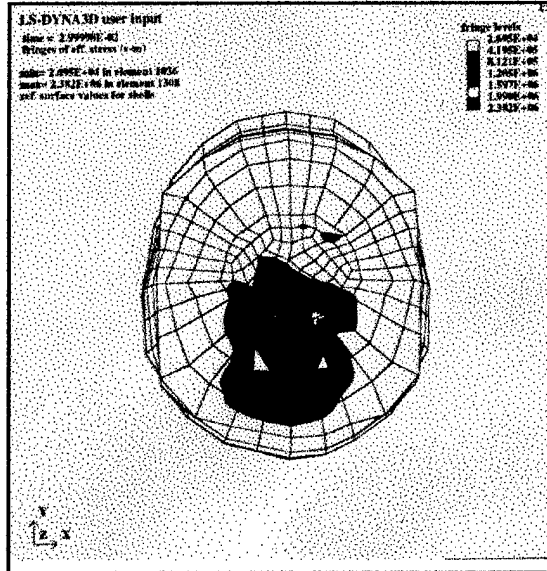


Figure 5.46. Von Mises stress induced in helmet 30 ms after impact

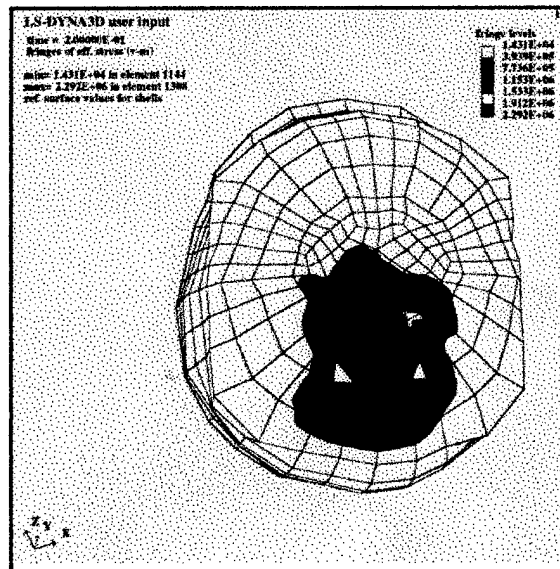


Figure 5.47. Von Mises stress induced in helmet 200 ms after impact

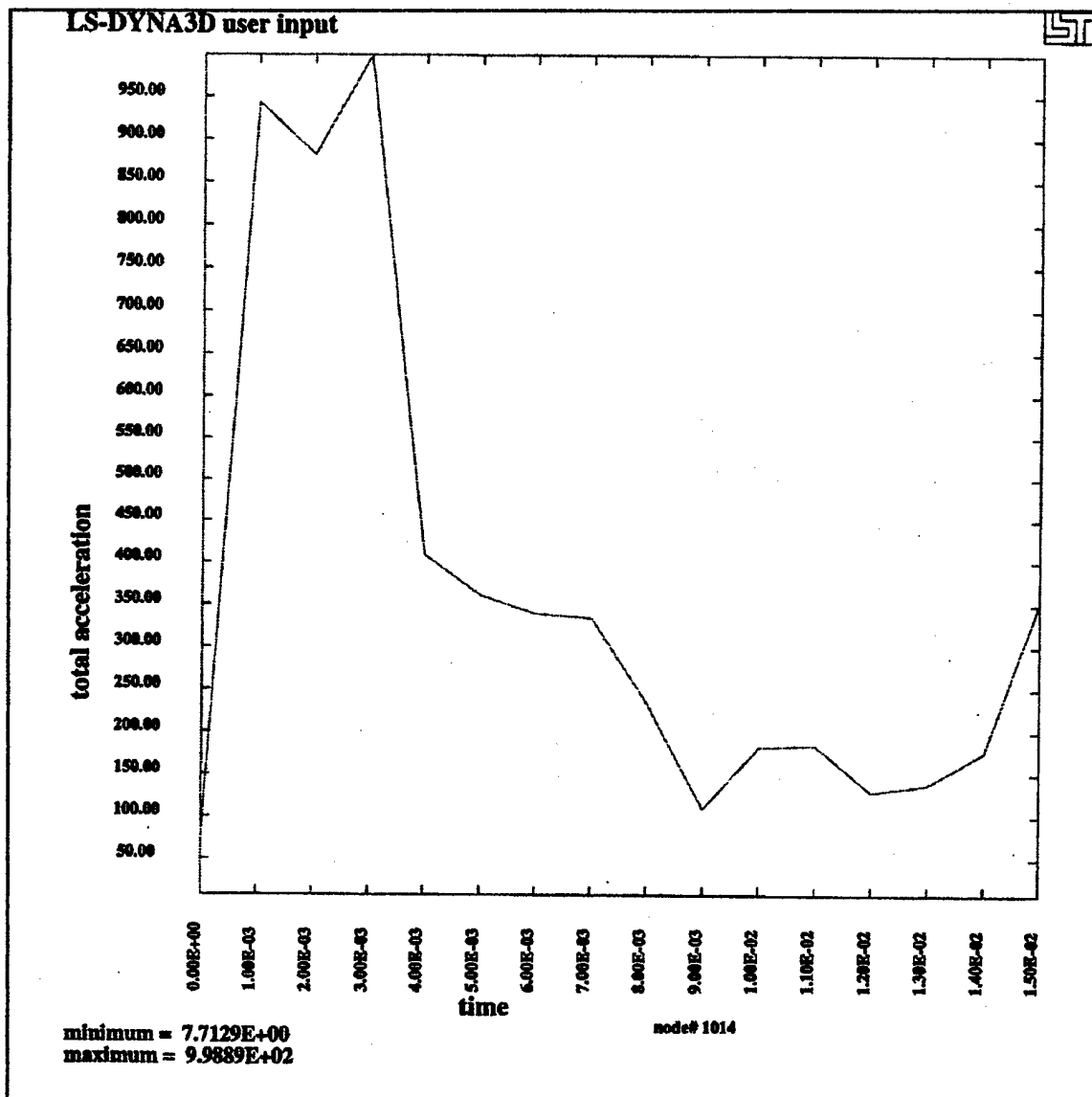


Figure 5.48. Acceleration profile used to calculate HIC for top impact case

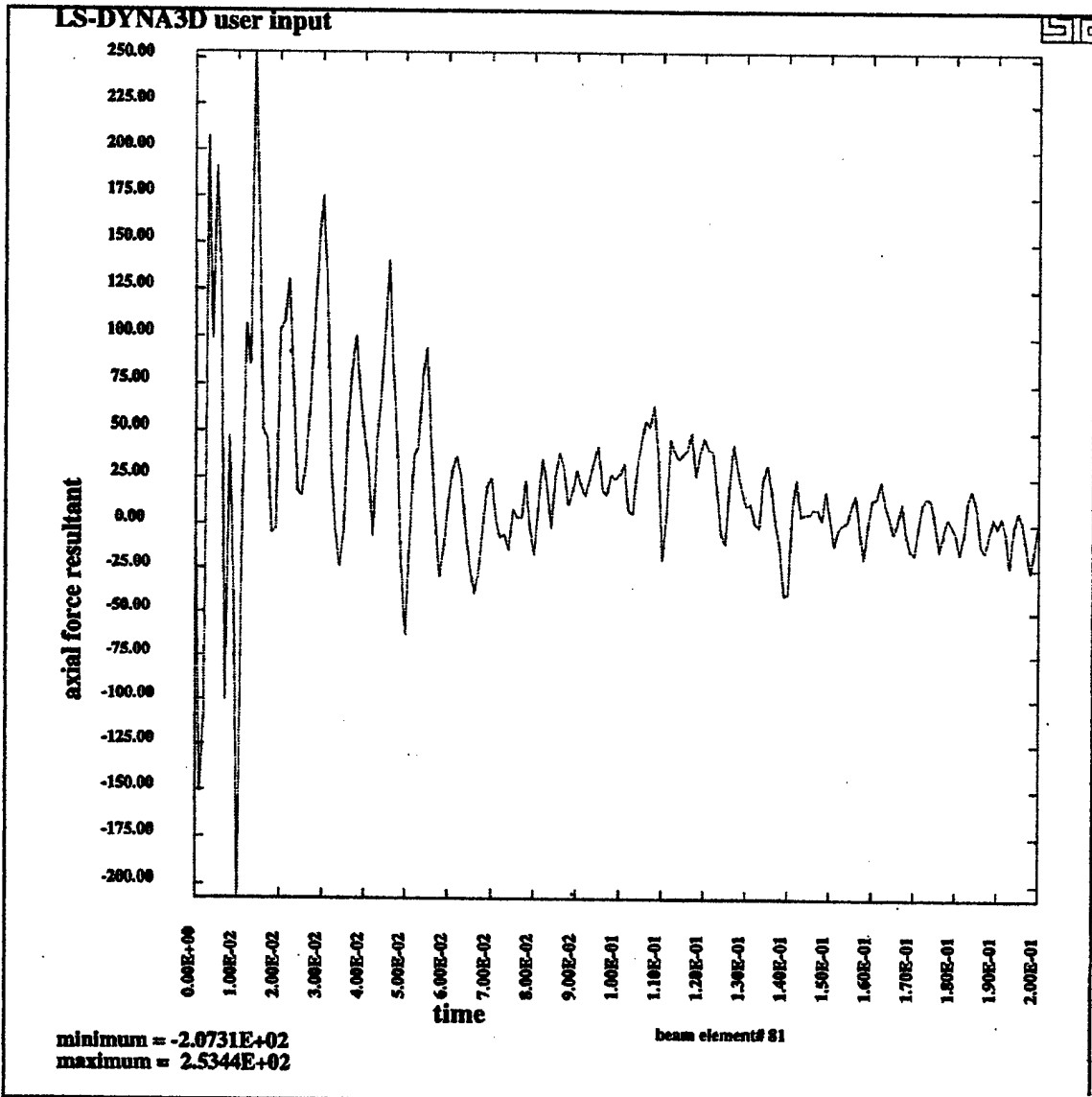


Figure 5.49. Axial force on occipital condyle during top impact

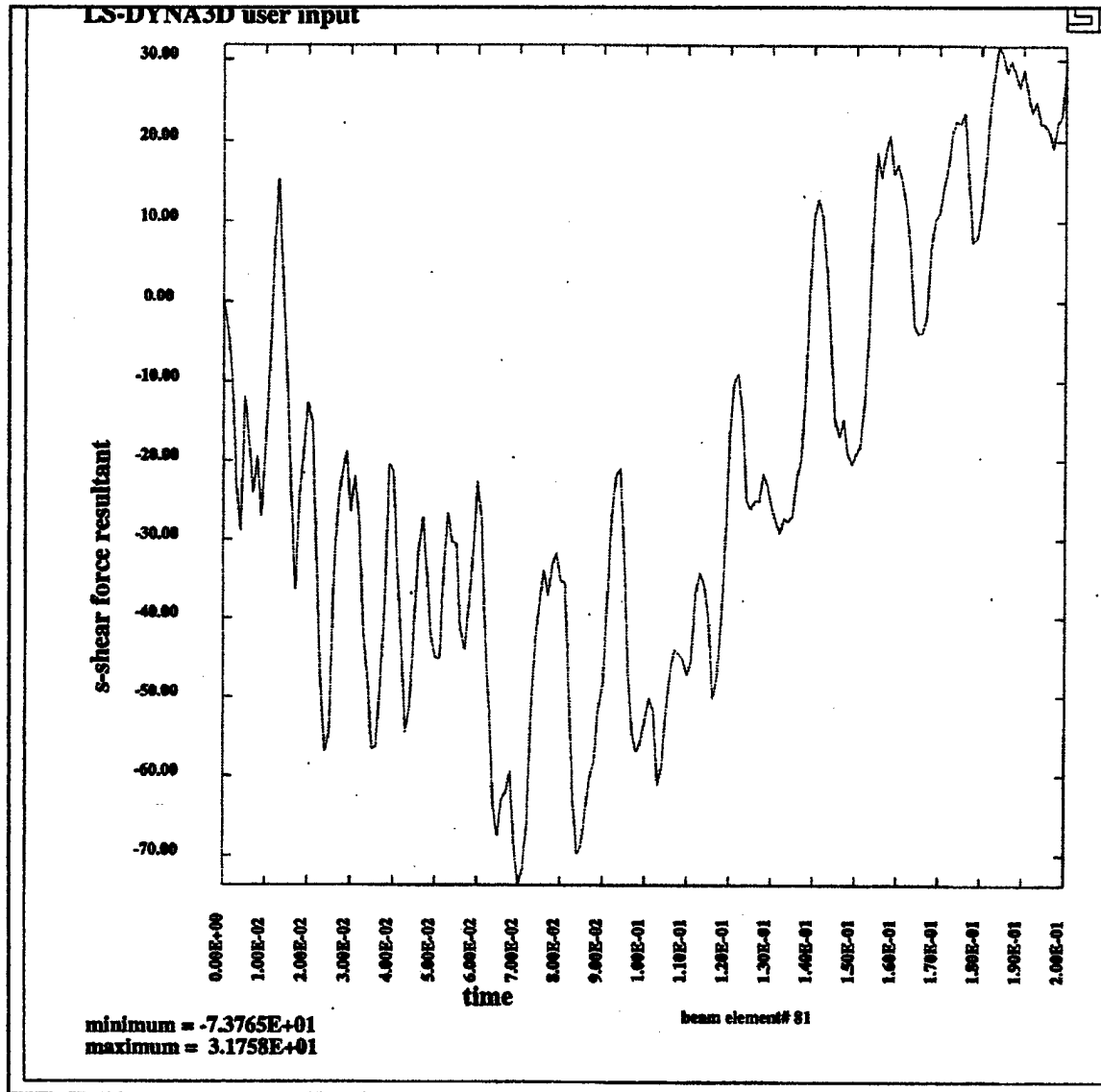


Figure 5.50. Shear force on occipital condyle during top impact

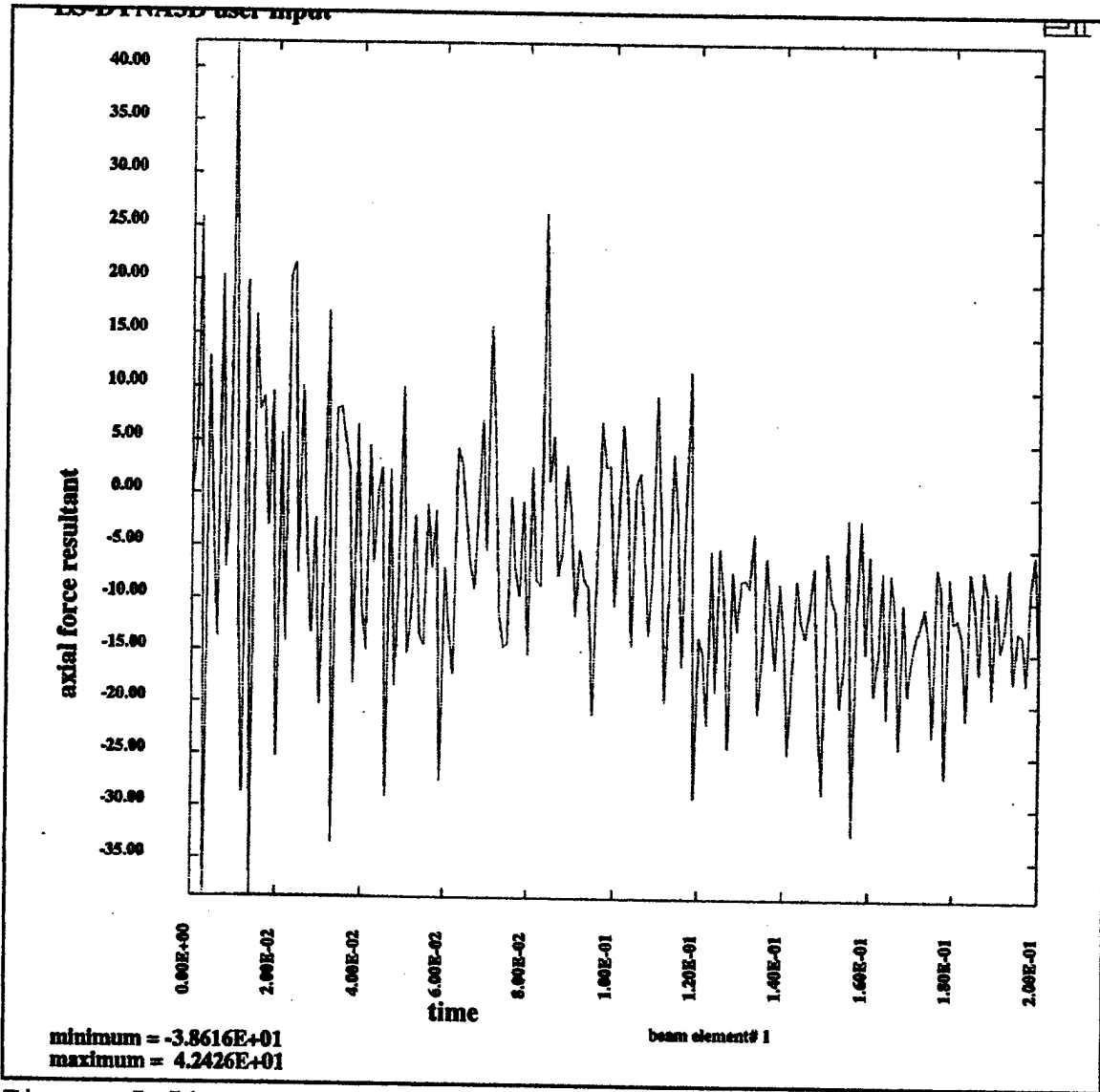


Figure 5.51. Axial force on C1 vertebra during top impact

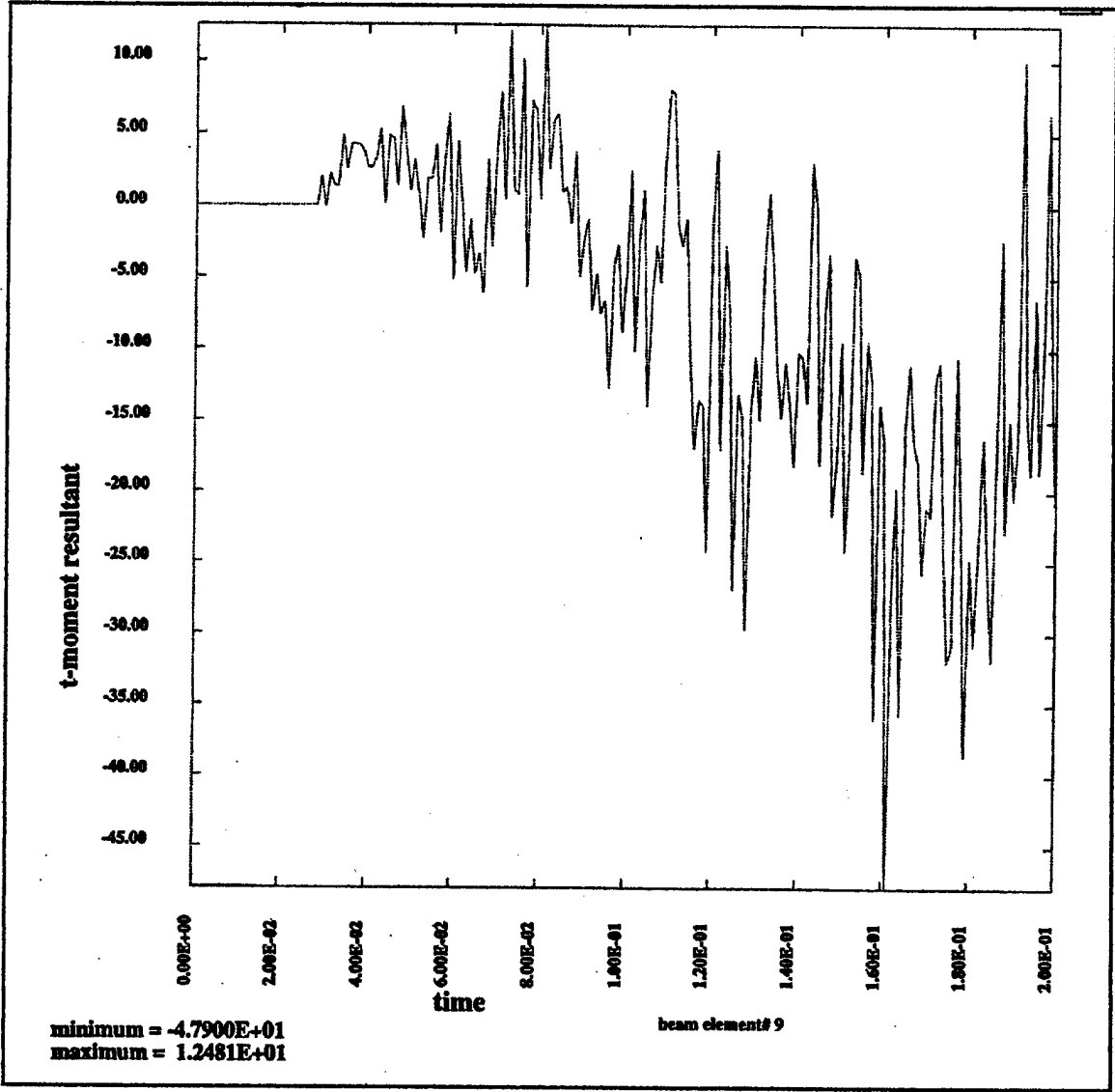


Figure 5.52. Bending moment on C5 during top impact

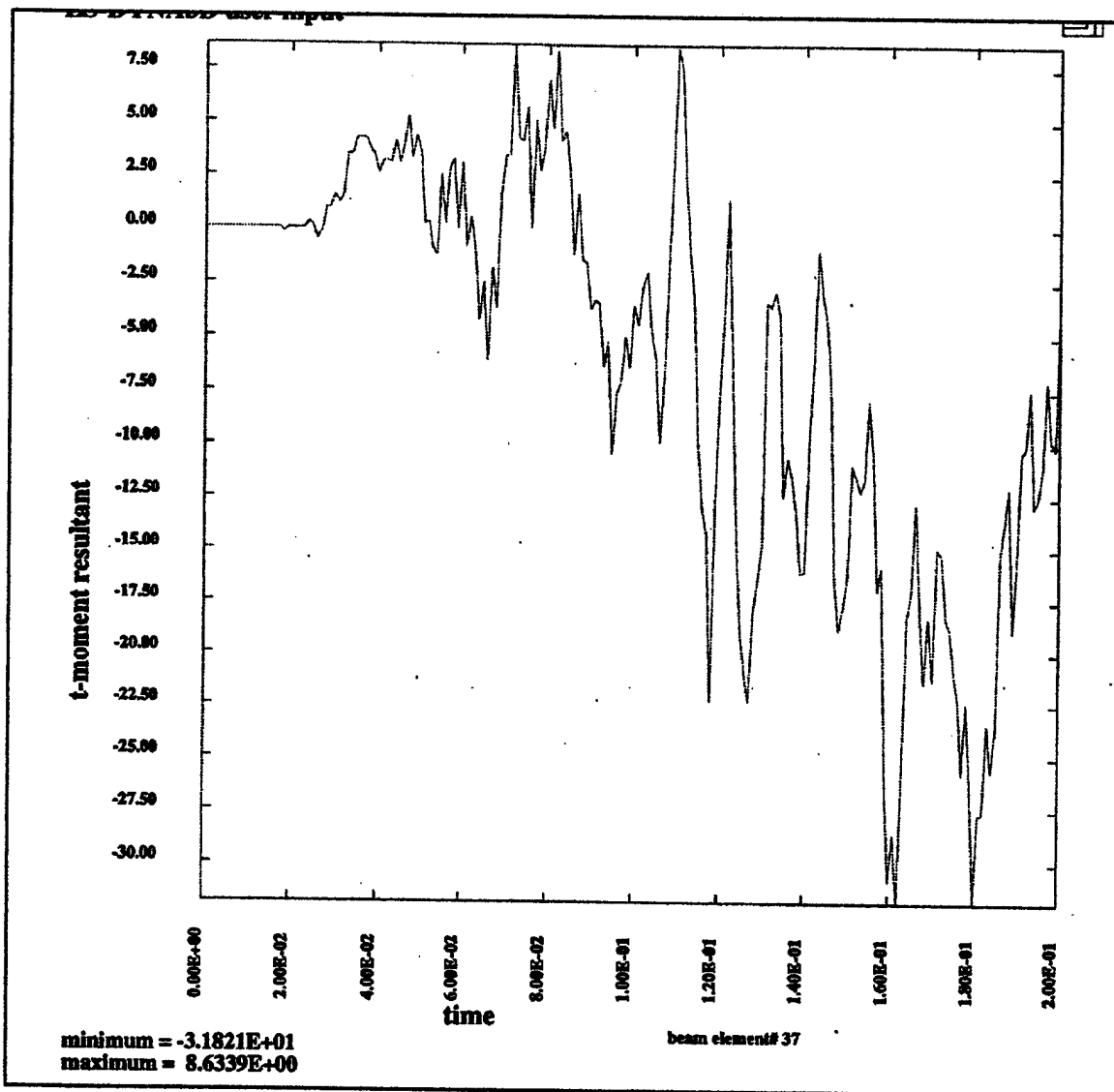


Figure 5.53. Bending moment on C4-C5 disc during top impact

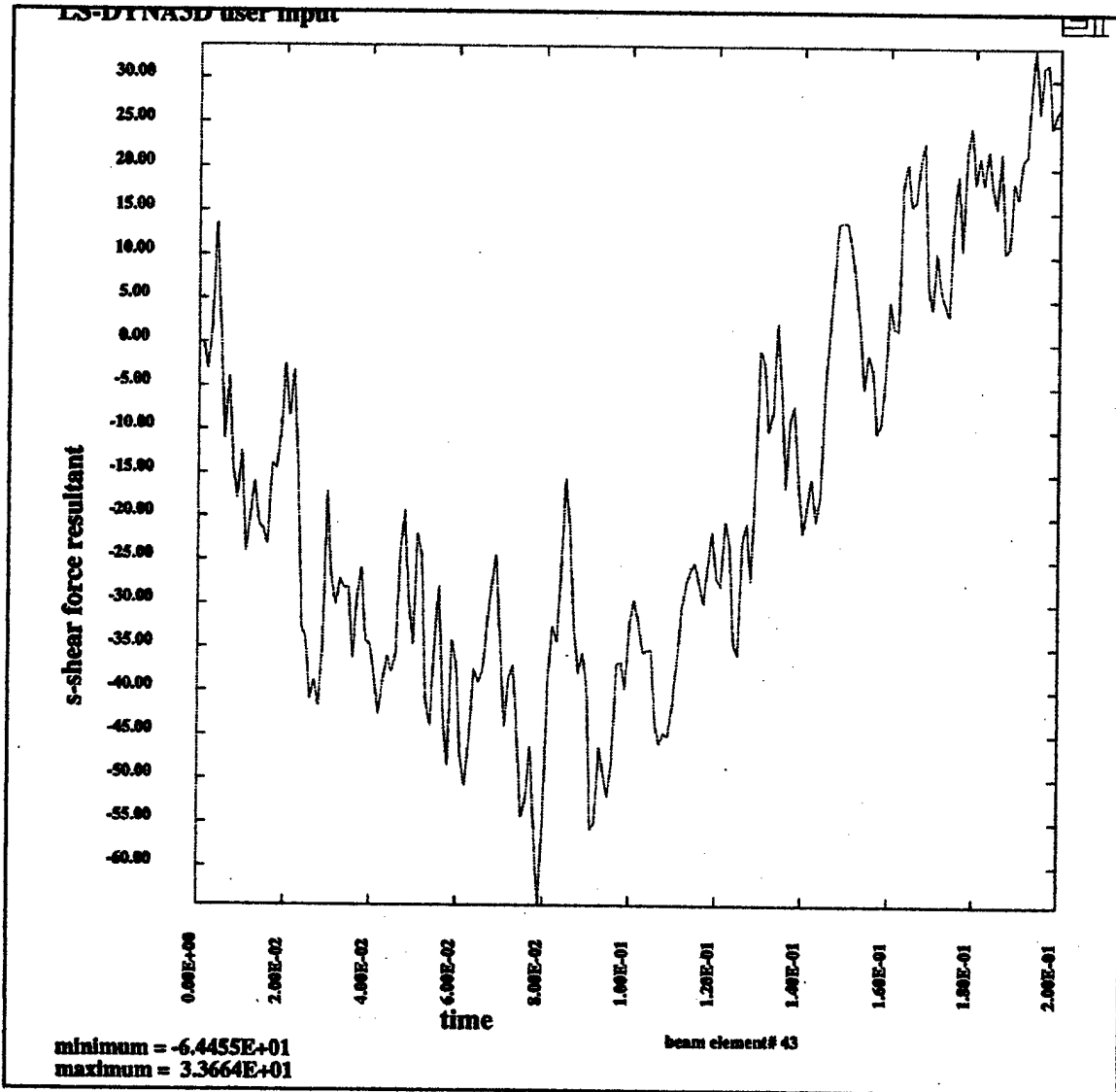


Figure 5.54. Shear force acting on facet joints of cervical spine during top impact

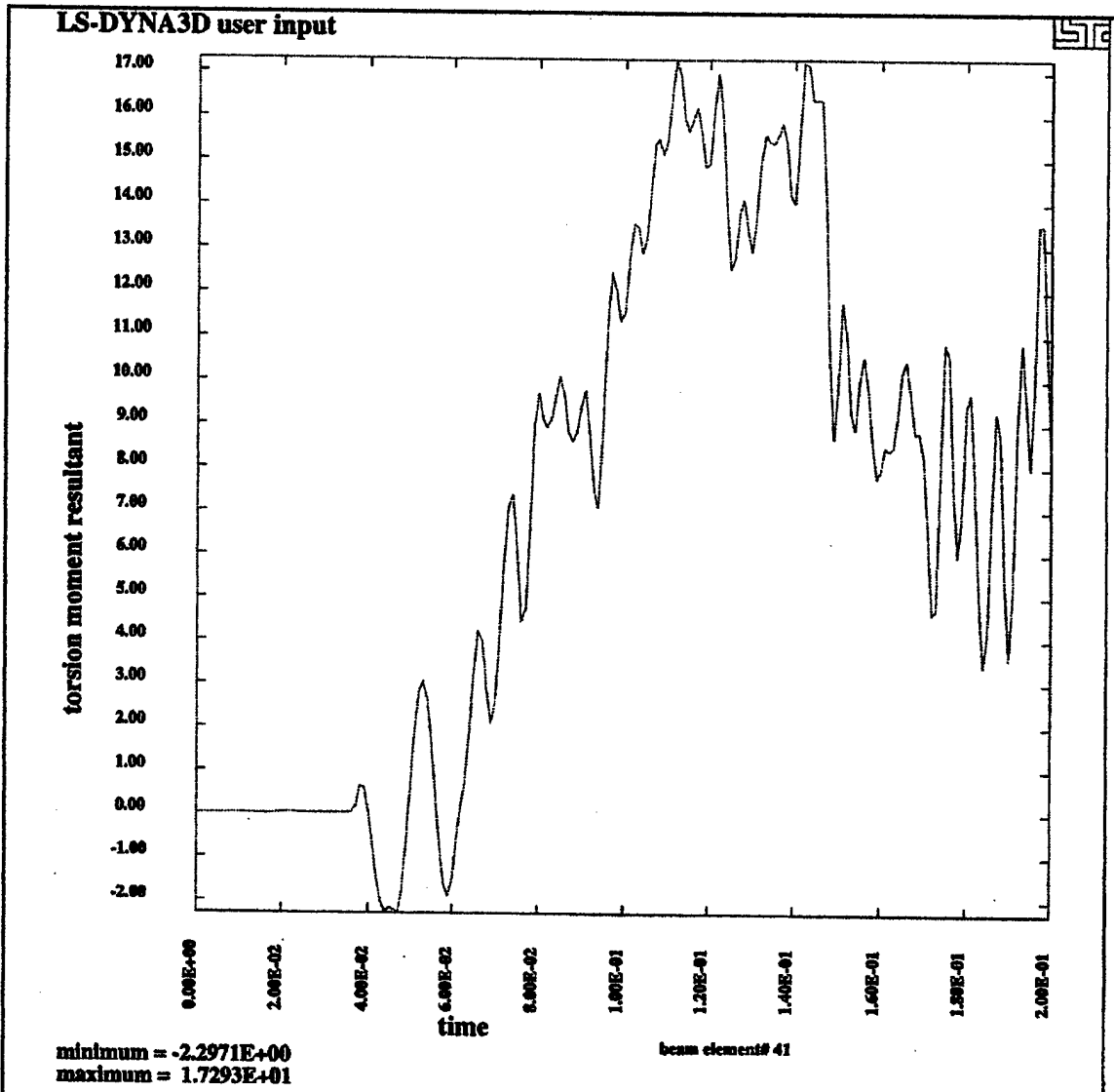


Figure 5.55. Torsion moment acting on facet joints of cervical spine during top impact

E. SIDE IMPACT

The next case to be explored is a fragment impact to the side of the helmet. Only one side is investigated due to the symmetry of the helmet. The position of the fragment relative to the helmet before impact is shown in Figure 5.56. The history of the stress field induced by the collision is shown in Figure 5.57 through Figure 5.60. The stress is a maximum right after impact of 1.47×10^6 Pa. This stress slowly decays but is still greater than 1.76×10^4 Pa after 200 ms.

Figure 5.61 shows the total acceleration of the center of gravity of the head for the first 15 ms after impact. The area under this curve was used to calculate an HIC value of 178.2. The maximum axial force acting on the occipital condyle, shown in Figure 5.62, is 227.1 N. Figure 5.63 shows the maximum shear force acting on the occipital condyle to be 81.8 N. The maximum lateral bending moment for the vertebra, shown in Figure 5.64, is 2.9 Nm and occurs at C4. The maximum bending moment for the vertebra, shown in Figure 5.65, is 37.4 Nm and occurs at C4. Figure 5.66 shows the maximum lateral bending moment for vertebral discs occurs at C4-C5. It is 4.3 Nm. Figure 5.65 shows the maximum bending moment for vertebral discs occurs at C4-C5. It is 30.8 Nm. The ability of the facet joints to resist shearing and torsional moments are shown in Figures 5.66 and 5.67. The shearing force is 61.5 N.

The torsional moment is 9.3 Nm.

The maximum vertebral moment exceeds the IARV value from Table 4.3. This value is exceeded by C4 and C5. Fractures of these vertebra are probable. These fractures are likely to occur at the smaller cross-section pedicles. If the fracture occurs at another location, it is likely due to a material defect in the bone resulting creating a stress concentration.

The critical value for the discs listed in Table 4.4 is exceeded by C3-C4, C4-C5, and C5-C6 with the maximum occurring at the C4-C5 level. This will probably result in severe disc injury. This injury may be in the form of a disc rupture, collapse around a nerve, or other injury.

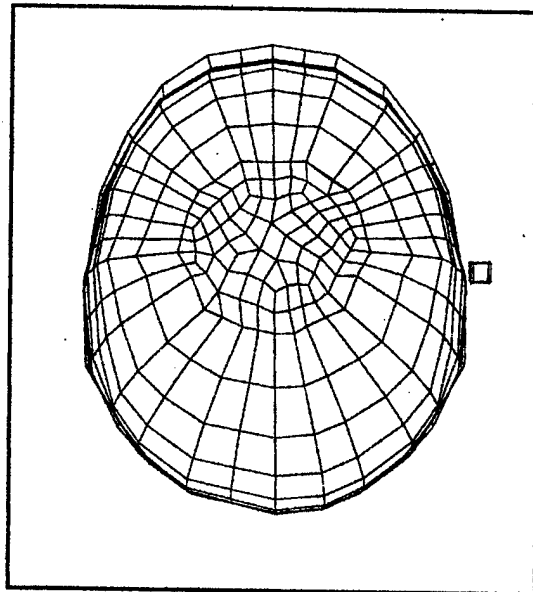


Figure 5.56. View of helmet before side impact

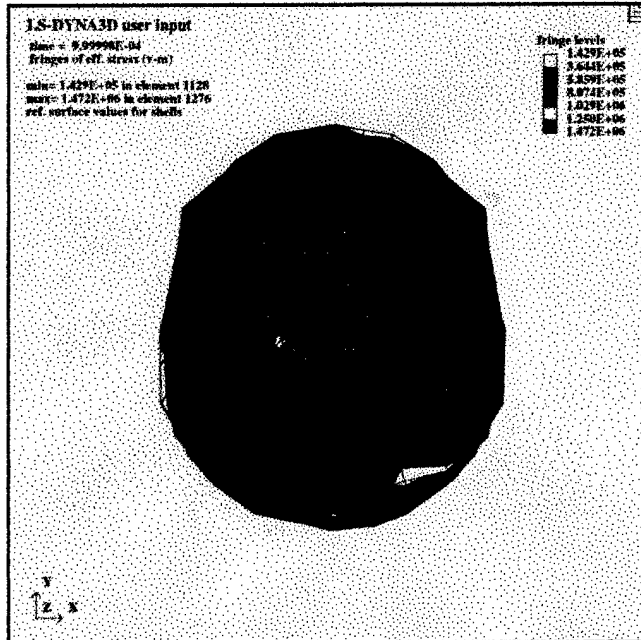


Figure 5.57. Von Mises stress induced in helmet 1 ms after side impact



Figure 5.58. Von Mises stress induced in helmet 10 ms after side impact

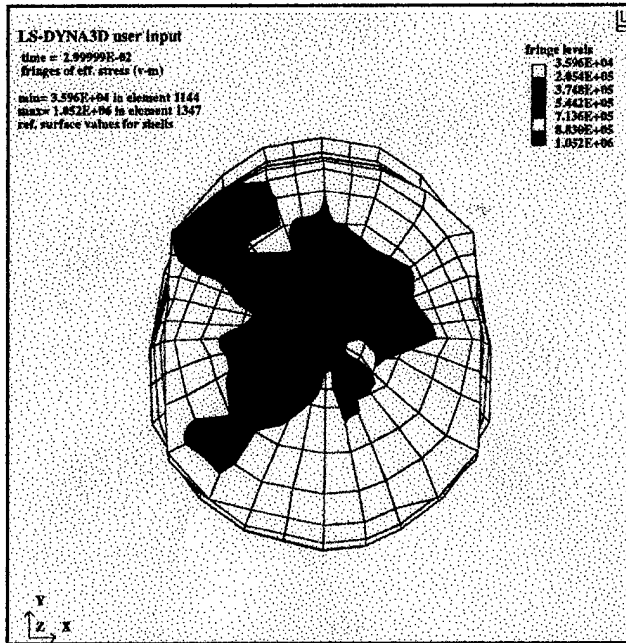


Figure 5.59. Von Mises stress induced in helmet 30 ms after side impact

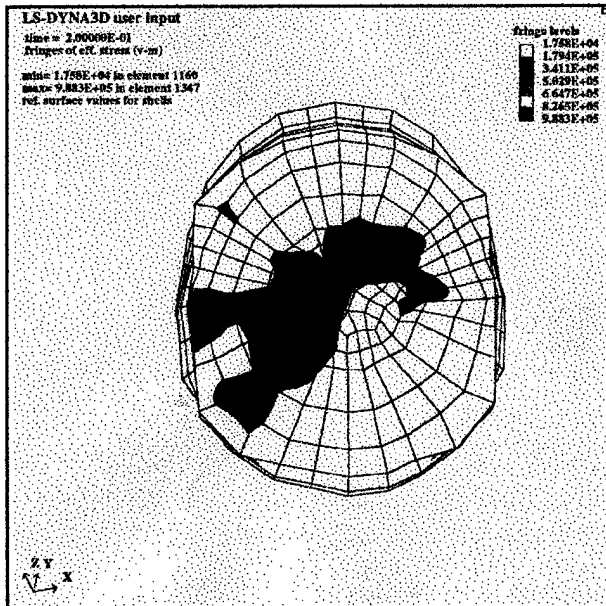


Figure 5.60. Von Mises stress induce in helmet 200 ms after side impact

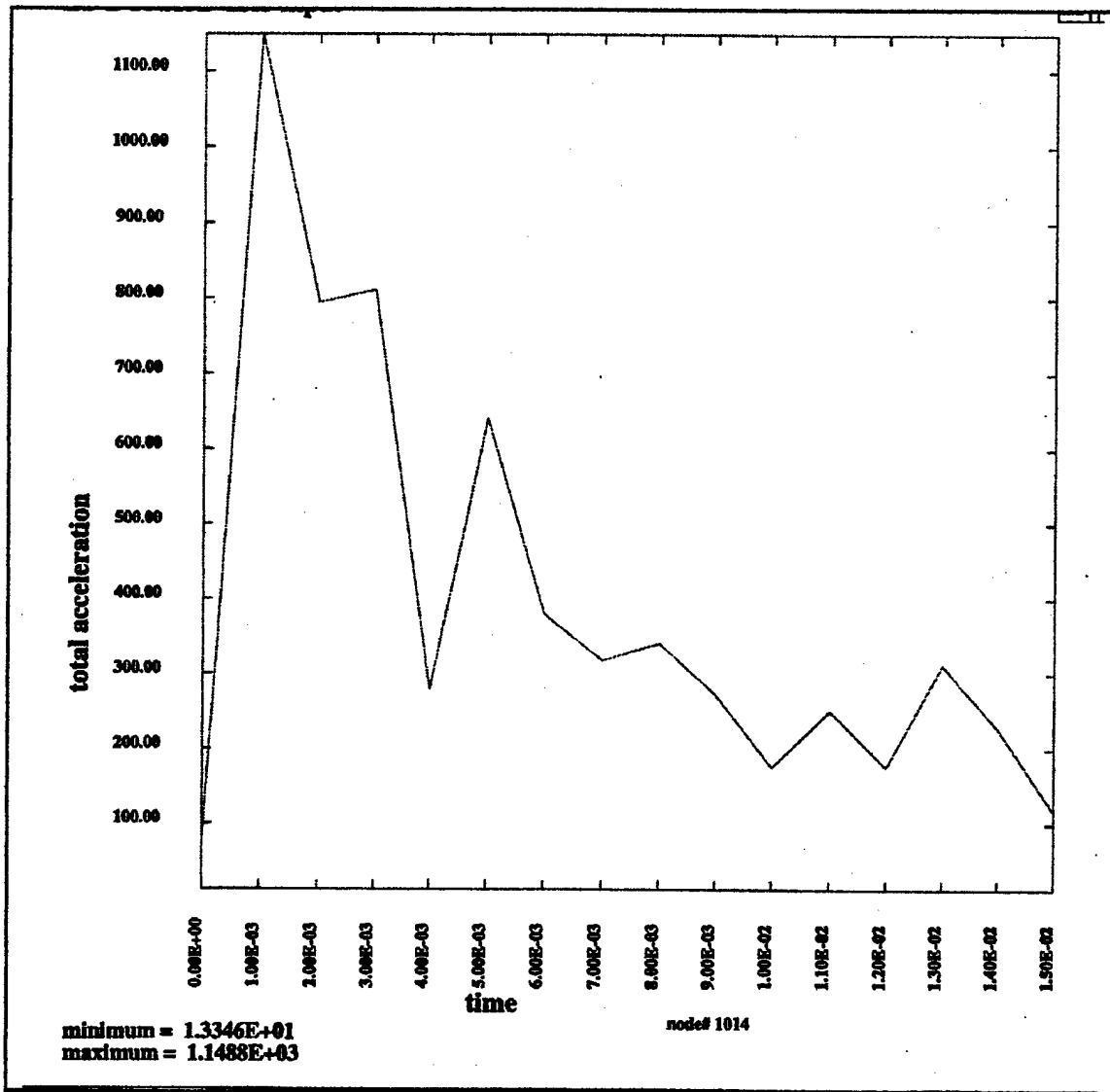


Figure 5.61. Acceleration profile used to calculate HIC for side impact case

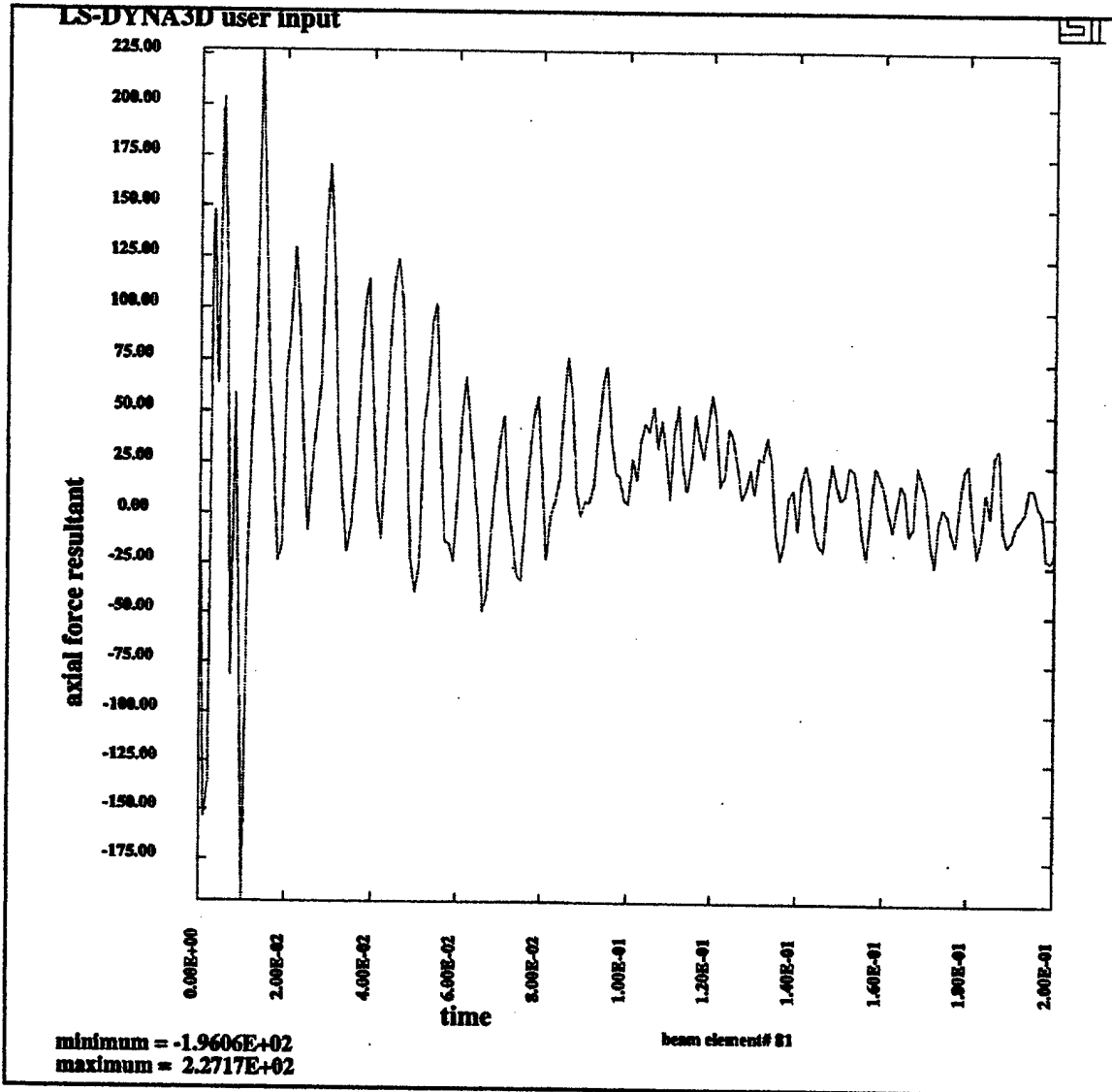


Figure 5.62. Axial force on occipital condyle during side impact

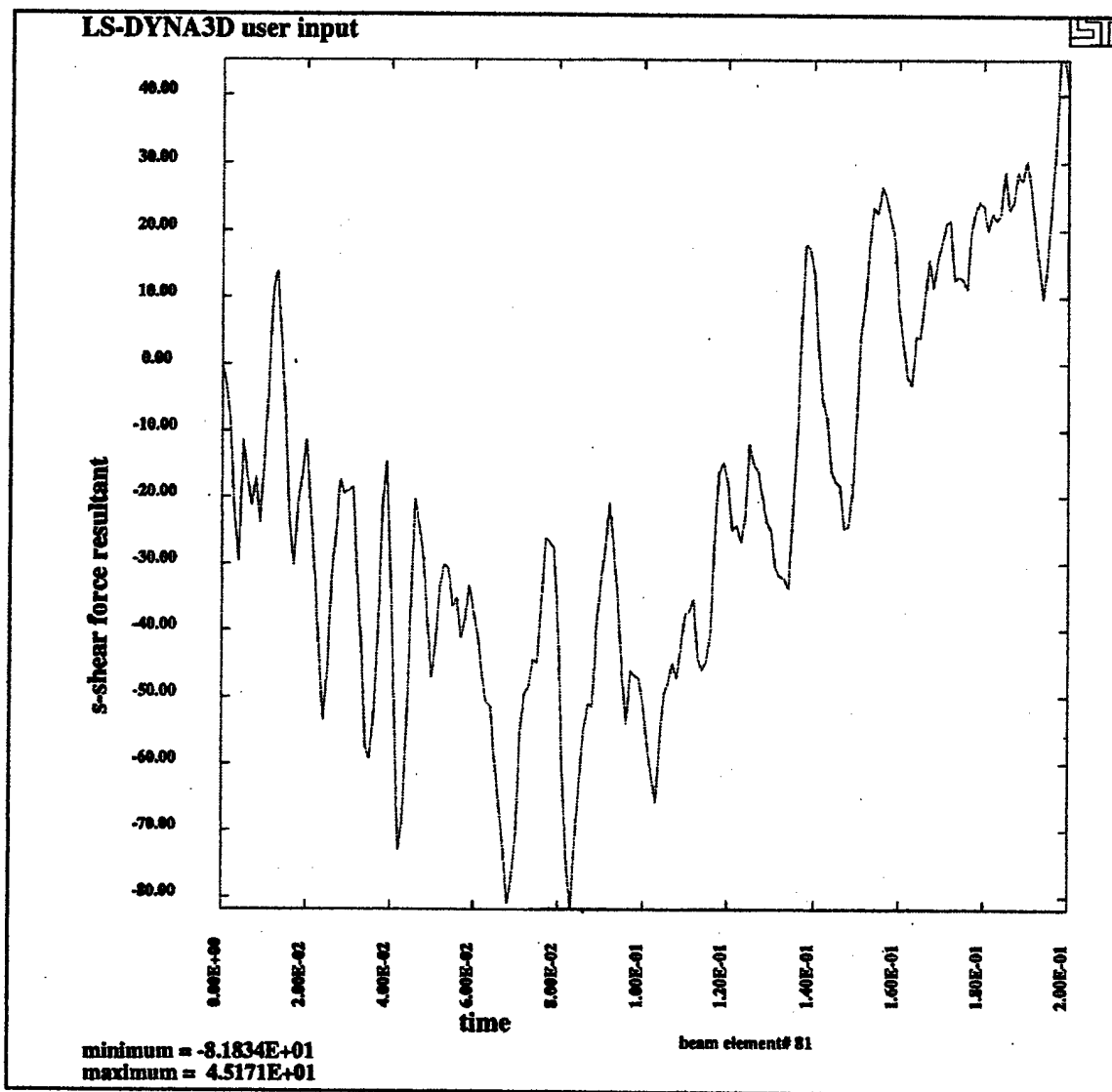


Figure 5.63. Shear force on occipital condyle during side impact

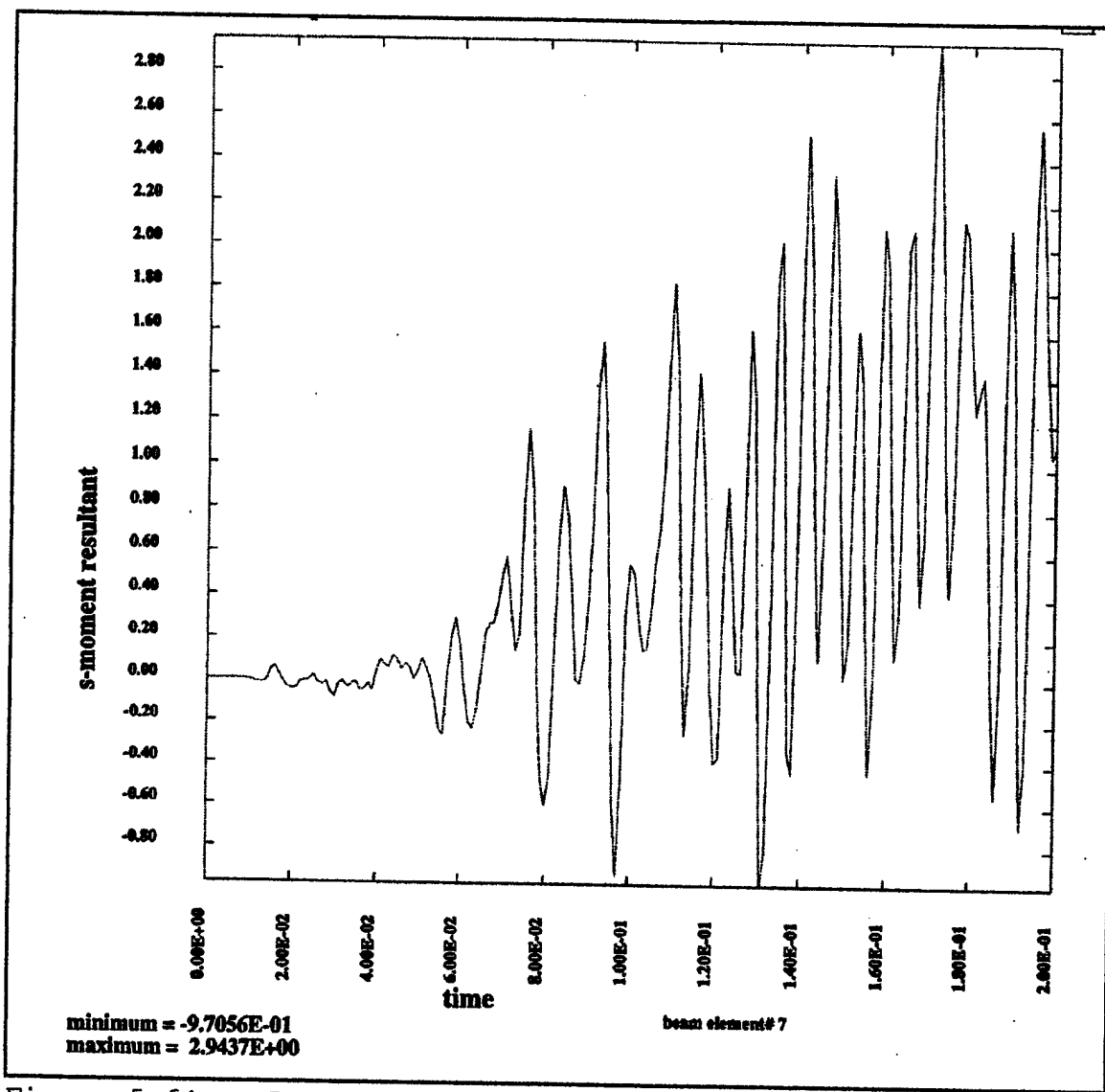


Figure 5.64. Lateral bending moment of C4 during side impact

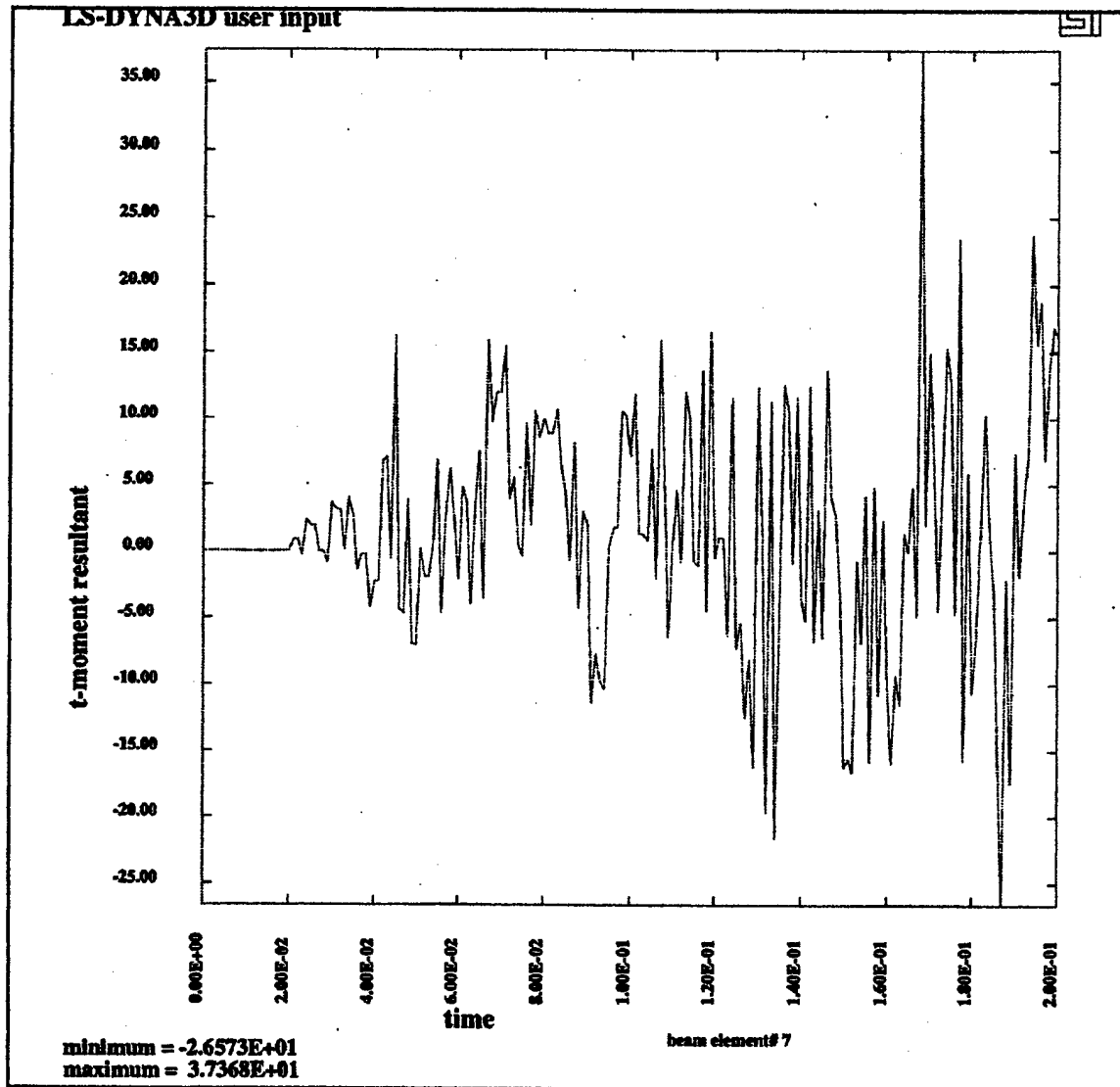


Figure 5.65. Bending moment of C7 vertebra during side impact

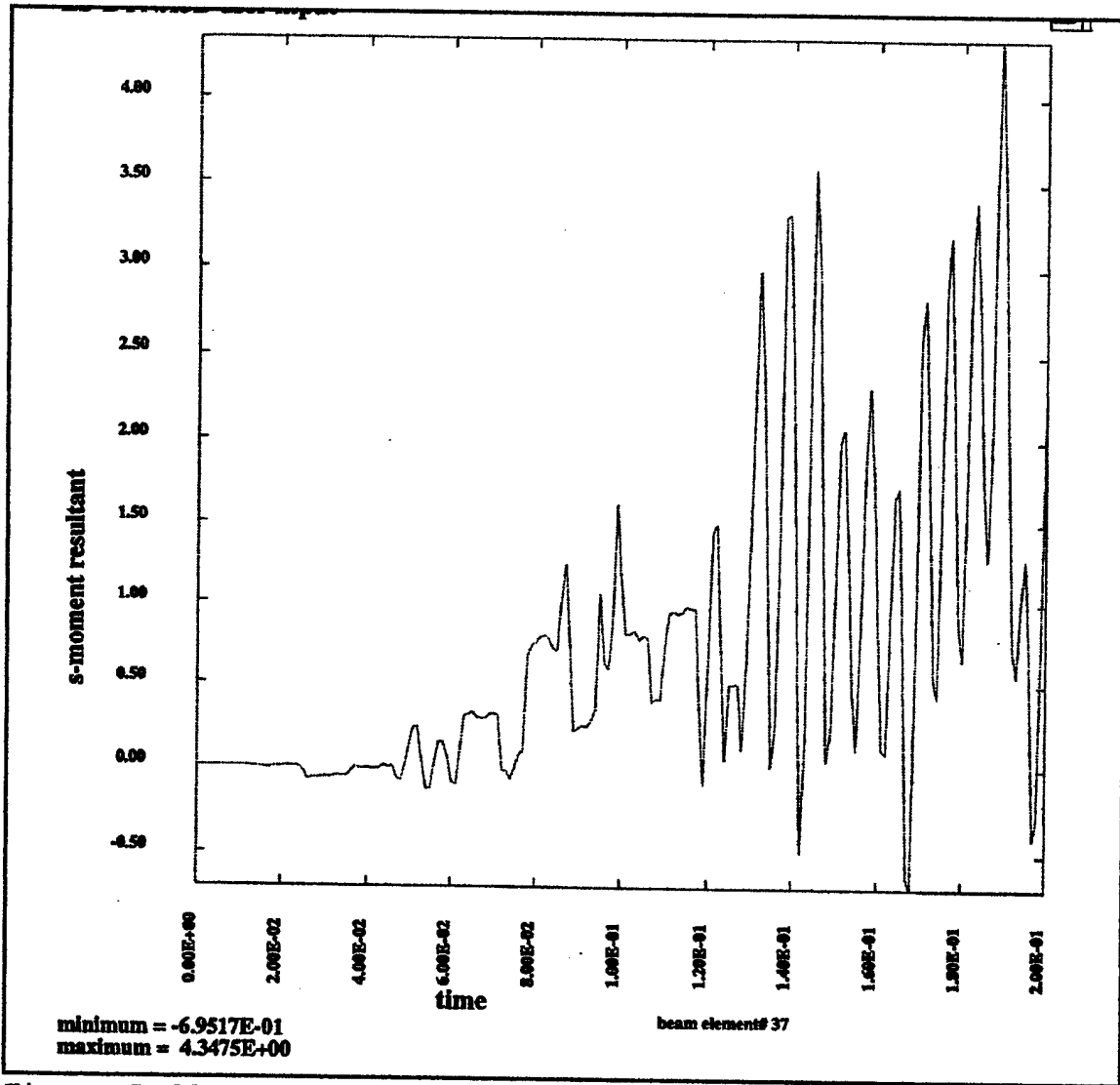


Figure 5.66. Lateral bending moment on C4-C5 disc during side impact

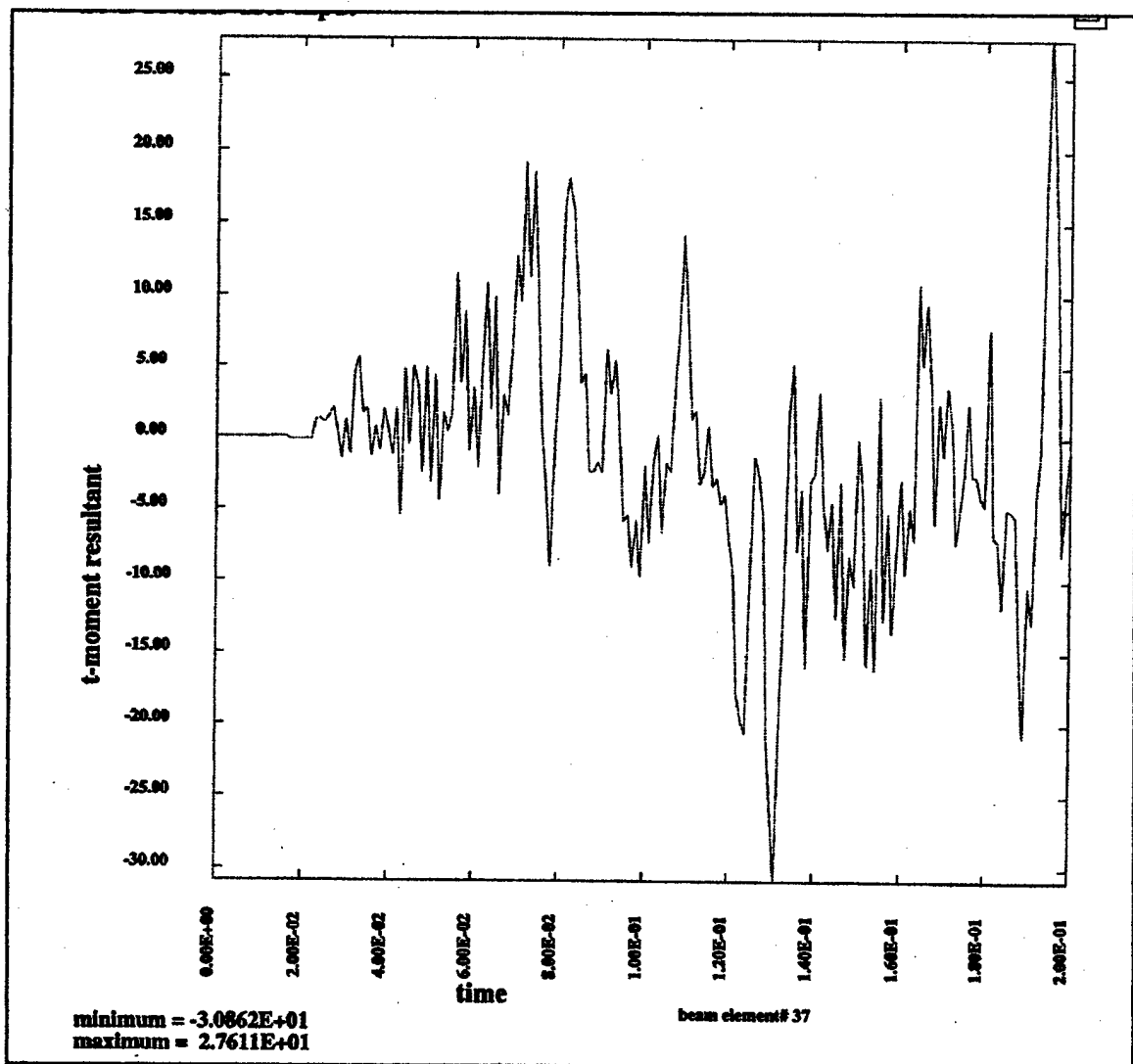


Figure 5.67. Bending moment on C4-C5 disc during side impact

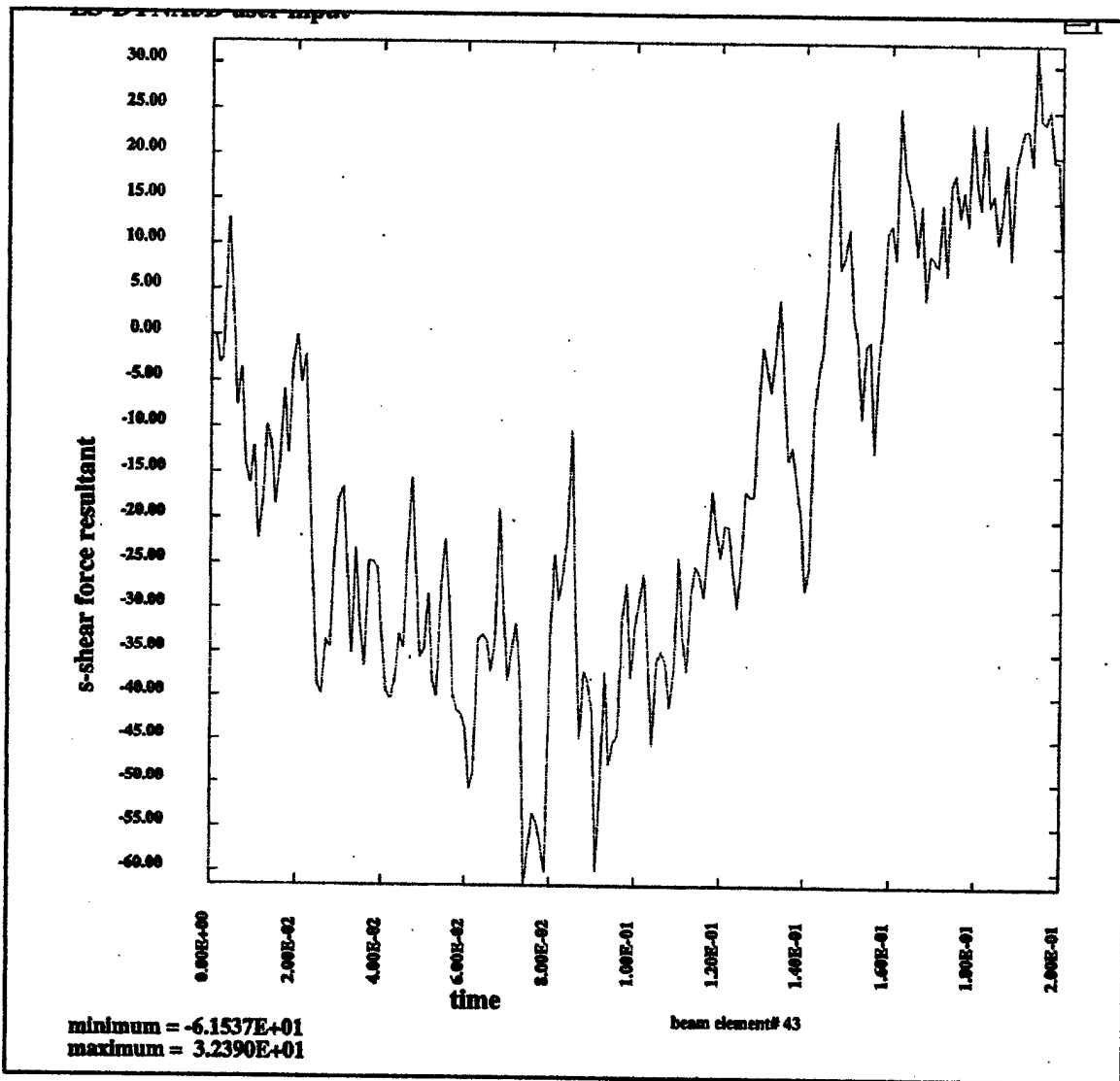


Figure 5.68. Shear force acting on facet joints of cervical spine during side impact

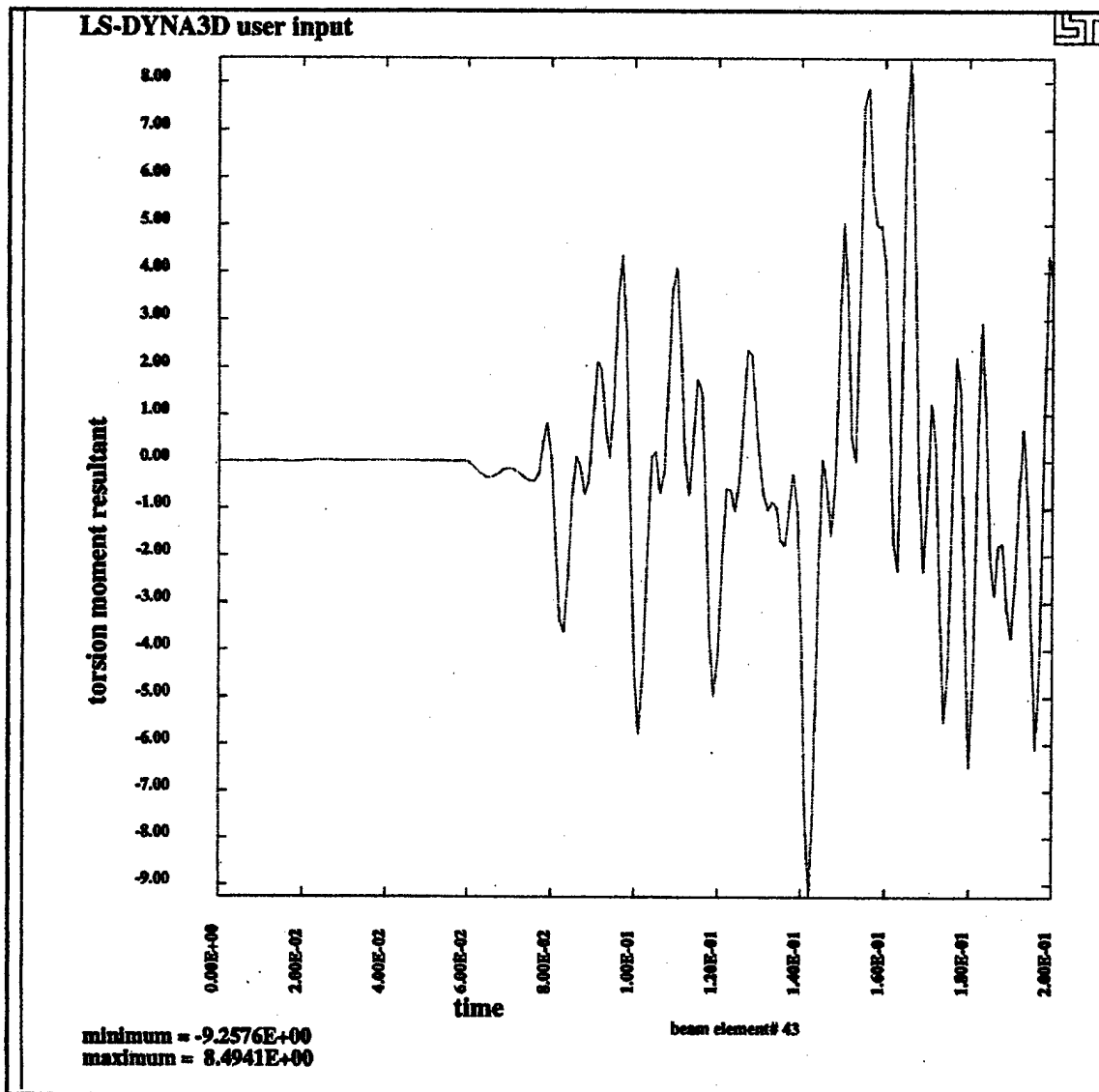


Figure 5.69. Torsion moment acting on facet joints of cervical spine during side impact

VI. CONCLUSIONS

This study investigated the biomechanical response of the head neck complex to impact loads incident on the PASTG ballistic helmet. A major difficulty in any biomechanical study is characterizing the proper parameters for the problem. The material properties of the body vary greatly among individuals. This prevents quantifying a universal injury threshold for a particular loading condition. Researchers have sought to work around this problem by relating findings to a potential or probability of injury. Examples of these findings can be seen in Tables 4.3 and 4.4. Most are related to a 50th percentile case. While these methods are an excellent way of characterizing the gross behavior of a large population, they cannot be used to specify results for individuals.

This model was validated based on the experimental findings of Ewing, 1978. The model was then used to study the effect of disc stiffness on injury potential in extension produced from a frontal impact. It was found that the disc stiffness was proportional to the injury potential. Flexion, compression, and lateral bending was examined with impacts to the rear, top, and side of the helmet respectively. Due to symmetry only one side of the helmet was examined. Table 6.1

reviews the maximum moments and HIC values calculated for each case. These can be seen graphically in Figures 6.1 through 6.4. Table 6.2 summarizes the injury potential of each case.

Table 6.1 Review of critical values found for each case

CASE	HIC	VERTEBRA	DISC BENDING MOMENT	FACET JOINT TORSION MOMENT
Critical Potential Values from Tables 4.3 and 4.4	1000	31 Nm Extension (E) 104 Nm Flexion (F) 31 Nm Lateral (L) 780 N Compressive (C)	4-11 Nm	4-11 Nm
Case 1	1.28	10.7 Nm (E)	1.12 Nm	8.78 Nm
Case 2	144.1	16.5 Nm (E)	10.7 Nm	11.5 Nm
Case 3	138.7	48.9 Nm (E)	40.1 Nm	12.5 Nm
Rear Impact	64	36.0 Nm (F)	28.9 Nm	13.3 Nm
Top Impact	143.1	42.4 N (C) 47.9 Nm (E)	31.8 Nm	17.3 Nm
Side Impact	178.2	2.9 Nm (L) 37.4 Nm (E)	4.3 Nm (L) 30.8 Nm (E)	9.3 Nm

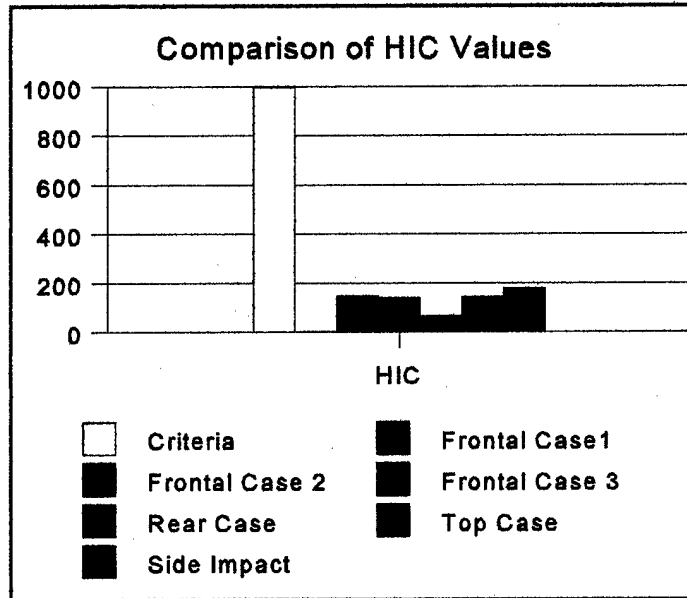


Figure 6.1. Comparison of HIC values for each test case

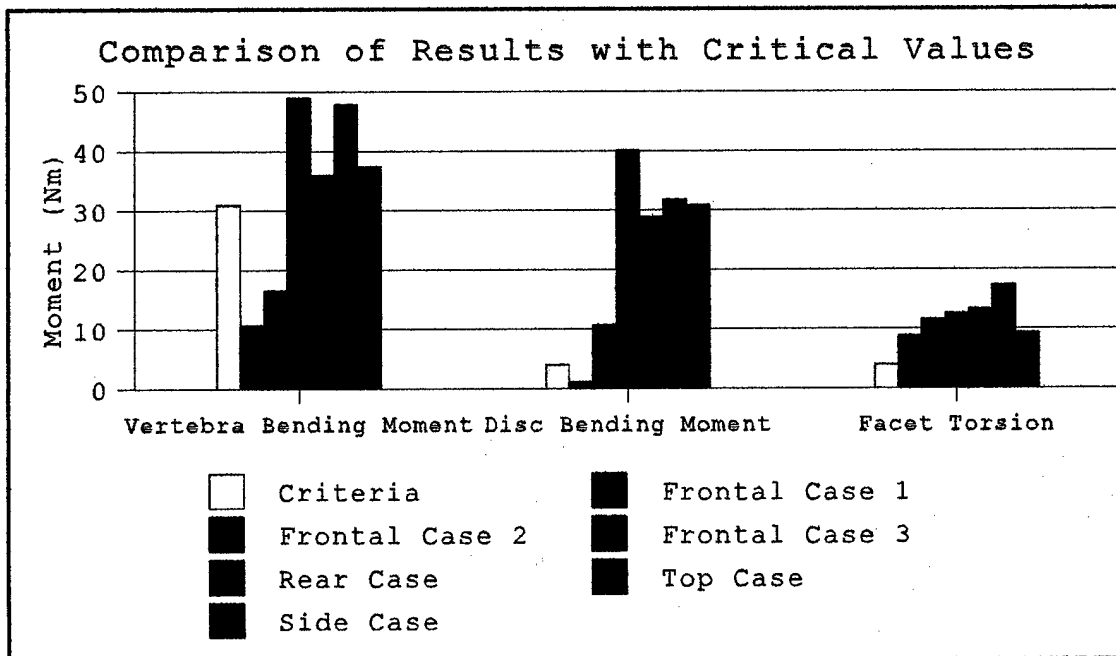


Figure 6.2. Comparison of results with critical values

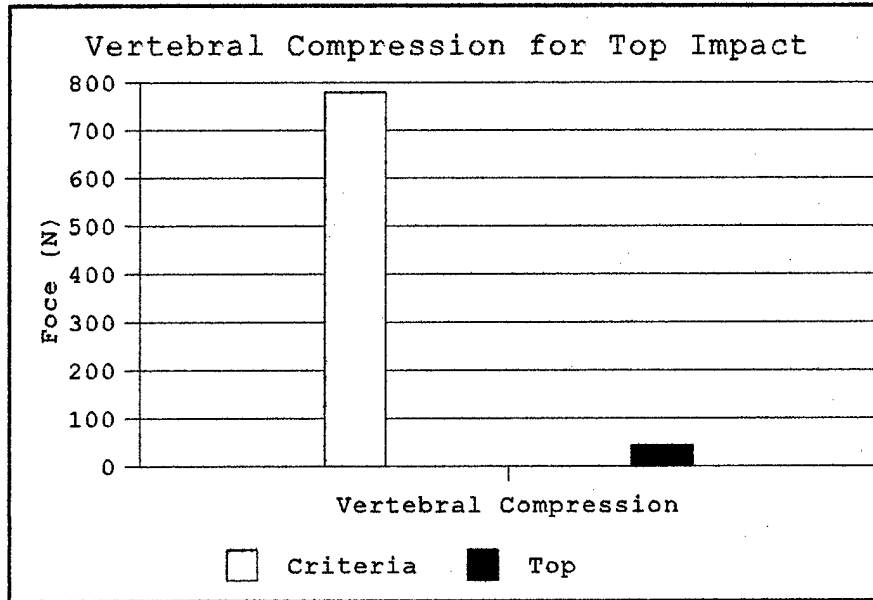


Figure 6.3. Comparison of vertebral compression for top impact case

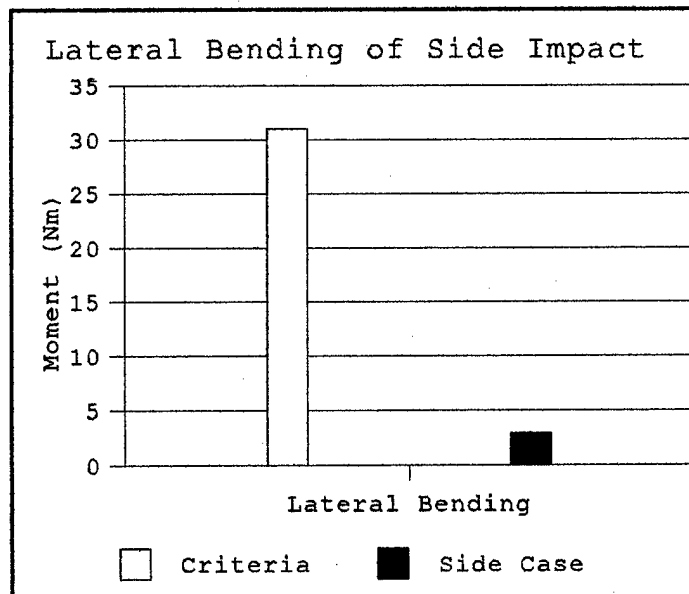


Figure 6.4. Comparison of vertebral lateral bending for side impact case

Table 6.2. Summary of injury potentials

CASE	POSSIBLE INJURIES
Extension: (frontal impact) Case 1	Minor injuries to include possible strains, pain, and possible loss of mobility, displacement of facet joint.
Case 2	Disc rupture, displacement of facet joint, increase in severity of minor injuries.
Case 3	Disc rupture, fracture of vertebral body, displacement of facet joints, other minor injuries
Flexion: (rear impact)	Disk rupture, displacement of facet joint, other minor injuries
Compression: (Combination Load from top impact)	None due to compression Disc rupture, fracture of vertebral body, displacement of facet joint, other minor injuries due to combination loading
Lateral Bending: (Combination Load from side impact)	None due to lateral bending Disc rupture, fracture of vertebral body, displacement of facet joint, other minor injuries due to combination loading

These injuries can create a myriad of problems in a battlefield environment. Any injury of the disc or vertebral body will translate not only to a loss of the individual for a significant period of treatment and recuperation, but a logistical burden as well. Cervical injuries also present a strong potential to cascade to other life threatening injuries without proper first aid and treatment. It is suggested that the type of injuries described in this study were not prevalent in previous conflicts, because the ballistic protection up to the time of the Vietnam war was not capable of stopping fragments with any significant energy.

It is recommended that follow on research examine concentrate on several areas:

- Effect of variation of bone stiffness on injury potential
- Experimental characterization of energy delivered to helmet
- Experimental characterization of energy transfer capabilities of helmet harness
- Effect of including muscle to model

APPENDIX. MATERIAL PROPERTIES OF PASTG HELMET

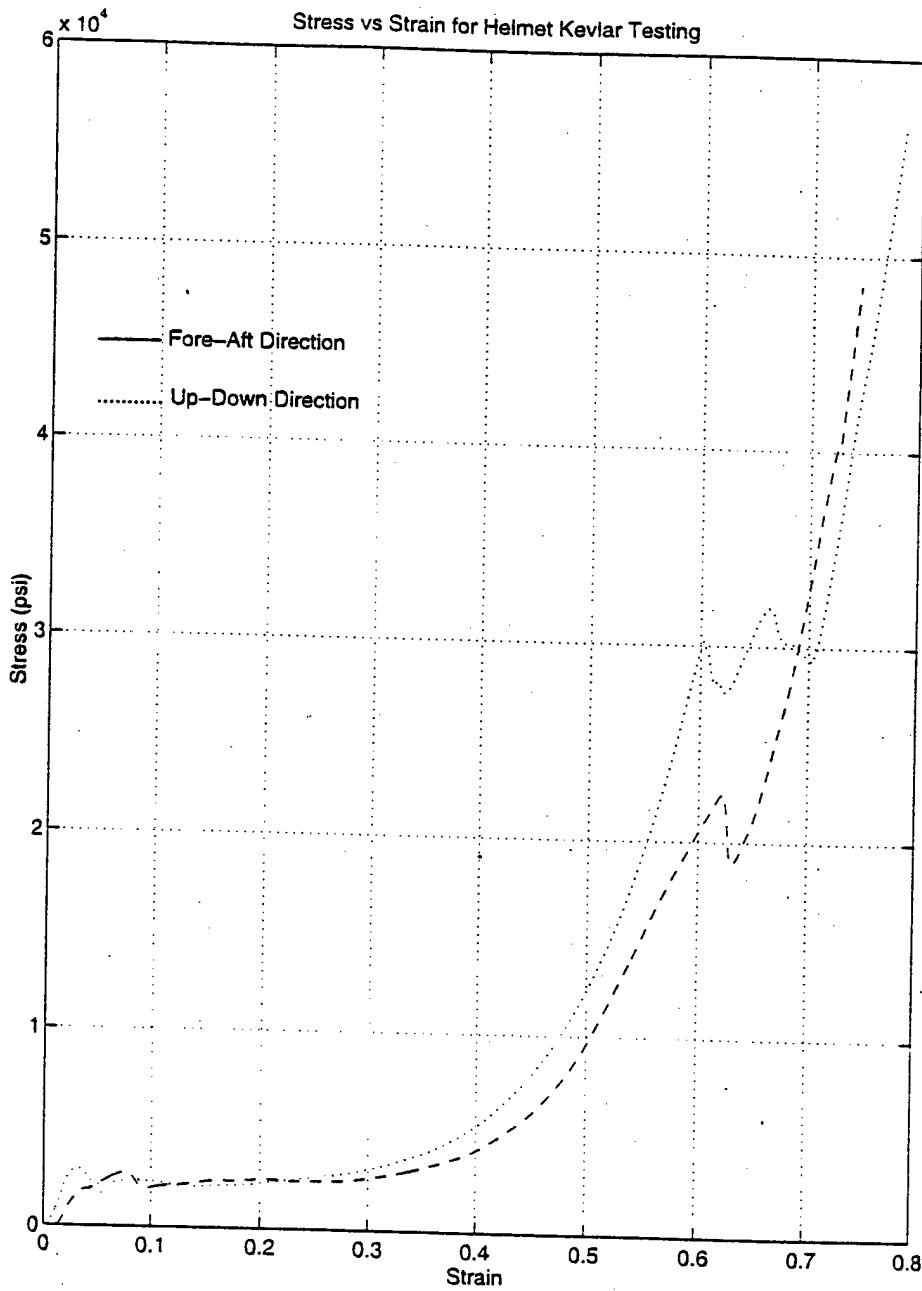


Figure A.1. Stress-strain curve for PASTG helmet

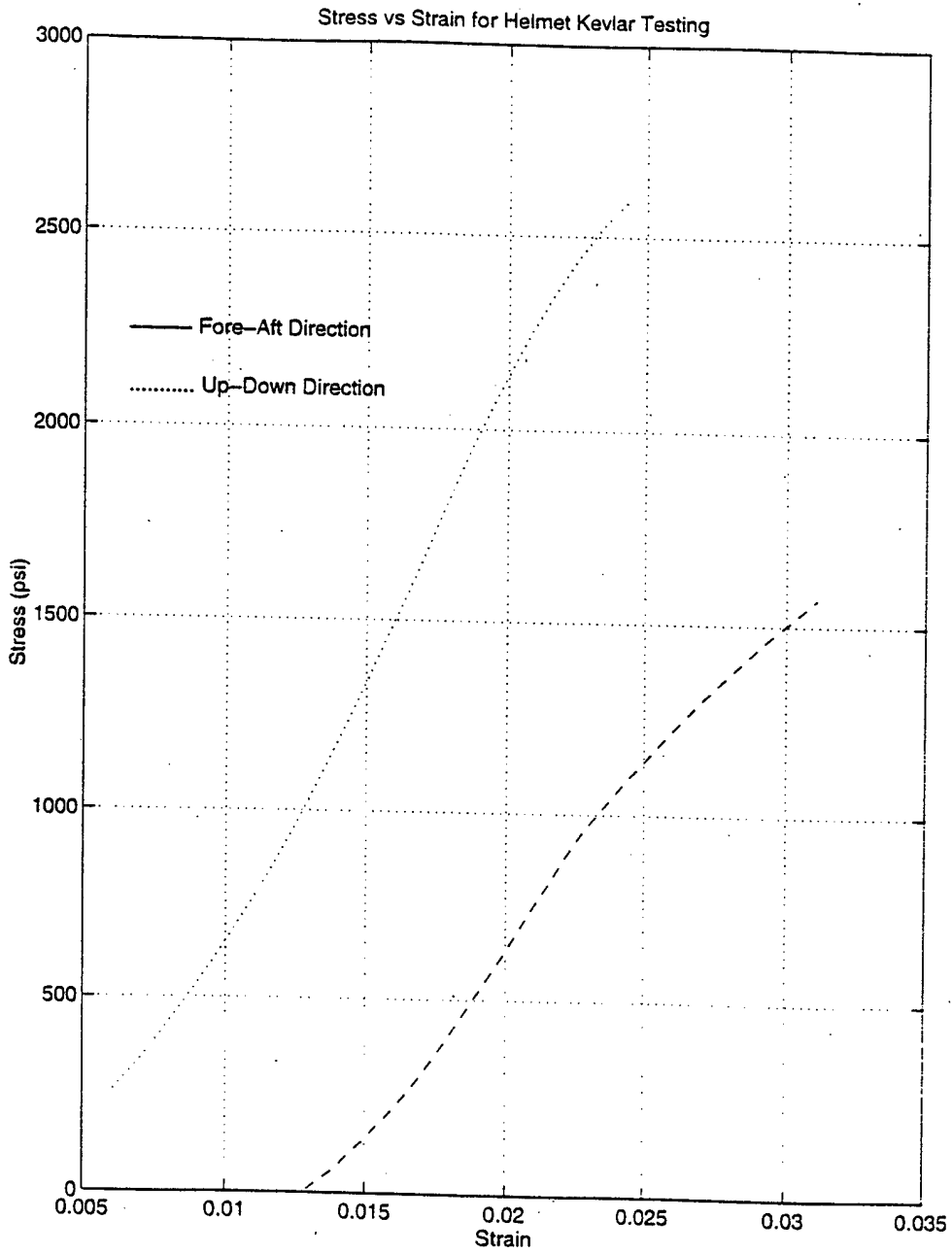


Figure A.2. View of linear region of stress-strain curve for PASTG helmet

LIST OF REFERENCES

Agard, "Anthropomorphic Dummies For Crash and Escape System Testing. Agard Ar-330", Advisory Group for Aerospace Research and Development, 1996

Berkeson, et al, "Mechanical Properties of Human Lumbar Spine Part II: Response in Compression and Shear: Influence of Gross Morphology", Journal of Biomechanical Engineering, Vol 101, no 2, 1979

Belytschko, et al, "Theory and Application of a 3D Model of Human Spine, Aviation, Space and Environmental Medicine", January 1978

Belytschko, T, et al, "AMRL-TR-76-10: A Model for Analytic Investigation of Three Dimensional Head Spine Dynamics", University of Illinois at Chicago, 1976

Belytschko, T, and Privitzer, E, "AMRL-TR-78-7: Refinement and Validation of a Three Dimensional Head-Spine Model", University of Illinois at Chicago, 1978

Berkeson, M H, et al, "Mechanical Properties of Human Lumbar Spine Motion Segments - Part II: Responses in Compression and Shear; Influence of Gross Morphology", Journal of Biomechanical Engineering, vol 101, no 2, 1979

Ewing, C, L, and Thomas, D J, "Human Head and Neck Response to Impact Acceleration", Naval Aerospace Medical Research Laboratory, Pensacola, FL, 1972

Goldsmith, W, et al, "Response of a Realistic Human Head/Neck Model to Impact", Journal of Biomechanical Engineering, vol 100, no 2, 1978

Huston, R L, and Sears, J, "Effect of Protective Helmet Mass on Head/Neck Dynamics", Transactions of the ASME, vol 103, no 2, 1981

Kallieris, D, et al, "Considerations for a Neck Injury Criterion", 35th STAPP Car Crash Conference, SAE, 1991

- Kleinberger, Michael, "Application of Finite Element Techniques to the Study of Cervical Spine Mechanics", 37th STAPP Car Crash Proceedings, 1993
- Li, Y, et al, " A Quasi Static analytical Sagittal Plane Model of the Cervical spine in Extension and Compression", 35th STAPP Car Crash Conference, SAE, 1991
- Mow, V C, and Hayes, W C, *Basic Orthopaedic Biomechanics*, Lippincott-Raven, 1997
- Nahum, A M, and Melvin, J W, *Accidental Injury: Biomechanics and Prevention*, Springer, 1993
- Nightingale, R, W, et al, "The Influence of End Condition on Human Cervical Spine Injury Mechanisms", 35th STAPP Car Crash Conference, SAE, 1991
- Patwardhan, A G, et al, "Kinematic Analysis and Simulation of Vertebral Motion Under Static Load - Part II: Simulation Study", Transactions of the ASME, vol 104, no 5, 1982
- Perry, C E, and Buhrman, J R, "Effect of Helmet Inertial Properties on the Biodynamics of the Head and Neck During +Gz Impact Accelerations", Safe Journal, Vol 26, Nov 1996
- Prasad, P, and King, A I, "An Experimentally Validated Dynamic Model of the Spine", Transactions of the ASME, vol 96, no 9, 1974
- Schultz, A B, et al, "Mechanical Properties of Human Lumbar Spine Motion Segments - Part I: Responses in Flexion, Extension, Lateral Bending, and Torsion", Journal of Biomechanical Engineering, vol 101, no 2, 1979
- Soni, A H, et al, "Kinematic Analysis and Simulation of Vertebral Motion under Static Load - Part I: Kinematic Analysis", Transactions of the ASME, vol 104, no 5, 1982
- Tencer, A F, and Mayer, T G, "Soft Tissue Strain and Facet Face Interaction in the Lumbar Intervertebral Joint - Part I: Input Data and Computational Technique, Journal of Biomechanical Engineering, vol 105, no 8, 1983
- Tencer, A F, and Johnson, K D, *Biomechanics in Orthopaedic Trauma: Bone Fracture and Fixation*, J B Lippincott Company, 1994

Williams, J L, and Belytschko, T B, "A Three Dimensional Model of the Human Cervical Spine for Impact Simulation", Journal of Biomechanical Engineering, vol 105, no 11, 1983

White, A A, and Panjabi, M M, *Clinical Biomechanics of the Spine*, Lippincott-Raven, 1990

Yoganadan, N, and Pintar, F A, "Inertial Loading of Human Cervical Spine", Journal of Biomechanical Engineering, Vol 119, No 8, 1997

INITIAL DISTRIBUTION LIST

	No. Copies
1. Defense Technical Information Center.....2 8725 John J. Kingman Rd., STE 0944 Ft. Belvoir, VA 22060-6218	2
2. Dudley Knox Library.....2 Naval Postgraduate School 411 Dyer Rd. Monterey, CA 93943-5101	2
3. Professor Young W. Kwon, Code ME/Kw.....2 Naval Postgraduate School 411 Dyer Rd. Monterey, CA 93943-5101	2
4. Naval/Mechanical Engineering Curricular Office.....1 Code 34 Naval Postgraduate School 411 Dyer Rd. Monterey, CA 93943-5101	1
5. LT Quinten M. King.....2 122 Warrington Rd. Toledo, OH 43612	2
6. LCDR Steve Parks.....1 Naval Surface Warfare Center Code 24 9500 MacArthur Blvd West Bethesda, MD 20817-5700	1
7. LCDR Marlene DeMaio.....1 National Naval Medical Center Dept of Orthopaedic Surgery 8901 Wisconsin Ave Bethesda, MD 20889-5000	1